The Role of the Mechanotransducer YAP/TAZ on Cell Volume Regulation

by

Nicolas Andres Perez Gonzalez

A dissertation submitted to the Johns Hopkins University in conformity with the requirements for the degree of Doctor of Philosophy

Baltimore, Maryland

February 2019

Abstract

For years, how mammalian cells control and regulate their size has remain poorly understood. This is in part due to difficulties on accurately quantifying cell volume in a high throughput manner. Many questions remain unanswered on how cells maintain their size uniformity throughout healthy tissue. In this thesis, by developing our own microdevice based on the fluorescence exclusion method, we have approached the subject of cell size from different perspectives with the unique goal to understand the mechanics of cell volume determination. We first developed a theoretical and experimental framework to study how cells adjust their volume to varying stiffness. We found that this relationship is non-trivial but can be predicted quantitatively from the distribution of active myosin throughout the cell cortex. Once we established the mechanics of cell volume determination, we pursued the metabolic pathway that could be related to cell size homeostasis. We quantified the activity of the mechanosensitive transcriptional regulators YAP (Yes-associated protein) and TAZ (transcriptional coactivator with PDZ-binding motif), widely known mechanotransducers of the Hippo pathway related to cell proliferation and organ size determination. Interestingly, we found that YAP/TAZ is positively correlated to the expression of active myosin as well as cell volume in all the conditions examined. To further prove the role of YAP/TAZ in cell volume regulation, we worked with CRISPR knockouts across the Hippo pathway and demonstrated that YAP and TAZ are novel regulators of single cell volume. We report that the role of YAP/TAZ in cell volume regulation must go beyond its influence on total cell cycle duration or the cell shape to explain the observed changes in volume. Moreover, in our context volume regulation by YAP/TAZ is independent of the mammalian target of rapamycin (mTOR), often perceived as the master regulator of cell volume. Instead, we find YAP/TAZ directly impacts the cell division volume. Based on the principle that YAP/TAZ is a mechanosensor, we find that inhibiting the assembly of myosin and cell tension slows cell cycle progression from G_1 to S. We pose the idea that YAP/TAZ and the Hippo pathway may be modulating the cell volume in combination with tension during a cell cycle checkpoint.

Thesis Advisors: Dr. Sean X. Sun and Dr. Denis Wirtz
Thesis Committee: Dr. Konstantinos Konstantopoulos, Dr. Yun Chen, Dr. Steven An,
Dr. Daniel Reich, Dr. Claire Hur

Acknowledgments

Acknowledgments are hard. They seek to give recognition to those that have made it possible for us to reach a particular milestone. As a scientist, to truly acknowledge every person involved in the process of making this dissertation, I would need to decouple events throughout my life and the reality is that I do not want to do so. I wonder: is it really the case that I want to thank only those involved directly in my project and life in Baltimore? How could you not acknowledge those who made it possible for you to be where you stand. Truth to be told, it was their hard work that brought me where I stand today.

While at Hopkins I slowly realized what I considered the true meaning of a PhD. I came seeking knowledge and technique and I found deep critical thinking. I came seeking for peers and colleagues and I found thinkers and challengers at every corner. More than ever I believe that the most important part of these last 4 and a half years is deeply embedded on the way I think about problems today, about possible solutions and the most logical approach, and I am thankful for taking this with me.

Because I believe that there have been so many people involved in making this possible, is that I find it hard to thank everyone, but I will do my best.

First, I want to thank those who have been by my side since the beginning of my education. To my friends that challenged me while in school and college. For the get togethers to study in high school and those long nights in college solving problems on numerical methods, on quantum mechanics and partial differential equations. Thank you. To those who were always there for a laugh or a beer. For sharing with me the good moments and the dark moments. To those who have always believed in each one of my projects and to those that in the darkness have always been a guiding light. While in college, I always dreamt of pursuing a PhD, and each one of my friends in the physics department was part of making it possible. Thank you, Gabriel Contreras and Karim Pichara, Alexis Ramirez, Pablo Cid, David Mero, Paul Leyton, studying in the library rooms with Susana Rojas, Arantxa Figueroa and Belen Cespedes! I don't think that this would be possible without any of you.

Contents

List of figures

List of tables

Chapter 1: Introduction

Consider the following problem: You want to build a house. A medium sized house. You have decided to make a very conservative and sturdy type of construction; therefore, you will build a thick foundation of concrete with brick walls on top. To get started, you proceed to collect materials, but at the store you realize that the options are overwhelming. There are all kinds of bricks that you could use. The variety is so large that the biggest brick is about six times the size of the smallest brick. To make it more difficult, the providers do not have a large enough quantity of any type of brick for you to build your house, so they offer to make a mix of all the bricks they have in stock. How could you possibly build your house?

During the second year of my PhD, my colleagues and me started discussing the problem of how cells regulate their volume. It was already a broadly recognized phenomenon that organs in our body have mechanisms to control their size. But how do they execute such control? When thinking about organ size, the problem is very similar to the problem of building a house. Instead of bricks, organs are composed of cells, and these cells just like the bricks we mentioned before are present in a wildly heterogeneous population. The problem was of particular interest for us since the volume of cells in the body seem to have a very stable coordination and is highly determined by its mechanics at equilibrium. Indeed, discussing a tight regulation of cell volume intrinsically means understanding the balance of forces at steady state in the cell.

1.1 The importance of cell volume regulation

A peculiar characteristic of the multicellular organisms is that differences in their size is primarily due to differences in their cell number rather than cell size (Conlon and Raff, 1999) highlighting once again that volume seems to be a highly controlled variable. Another layer of complexity on this issue is the curious feature that an organism like an animal is composed of a large number of cell types, such as fibroblasts in connective tissue, epithelial cells in the skin, neurons in the brain, red blood cells in the blood, etc. All of them varying vastly in size. Even though these cell types have different sizes between them, when focusing on one specific cell type in healthy tissue, they show regularity on cell size (Ginzberg et al., 2015). Due to its homogeneity is that dysregulation

of cell size has been reportedly related to disease or malfunction (Kozma and Thomas, 2002; Dannhauser et al., 2017). The fact that cells can so accurately remain within a range of cell size suggests the existence of mechanisms with which they control their growth and proliferation in a coordinated manner keeping a target size in homeostasis.

1.1 Cell volume regulation in yeast through time: what have we learned so far?

In order to understand cell volume regulation and the state of the art we first need to understand what have been the key milestones in the field. Already in the 1960s and 1970s there was a notion that cells could have mechanisms to keep a target volume in homeostasis. Some of this progress was done in budding and fission yeast (Johnston et al., 1977; Fantes and Nurse, 1977). Johnston et al. argued that such mechanism would prevent cells from becoming too small (from several divisions with decreased growth) or becoming too large. They performed two experiments. First, they arrested the cell cycle with temperature-sensitive mutants and quantified the effect of this arrest on growth. Second, they analyzed cell cycle on limited nutrient conditions. Johnston et al. found that growth rather than progression through DNA-division cycle is the rate limiting step in cell proliferation. Based on their results, their conclusion was that on yeast there must exist a critical volume that needs to be attained before continuing with the cell cycle. On the same year, Fantes and Nurse advocated for a similar hypothesis in fission yeast, *Schizosaccharomyces Pombe*. They changed the nutrient conditions in growing cells and studied growth rate and cell size (as measured by total protein content) and observed that smaller cells remained longer on the cell cycle (Fantes and Nurse, 1977). They argued that their results suggested the existence of a cell size requirement to start nuclear division. Most importantly, both of these seminal articles in cell volume regulation suggested the idea of a critical volume needed to be reached in order to progress through the cell cycle: this idea is commonly referred to as "sizer" model, given that it poses the hypothesis that cells have a mechanism to sense its own size. In parallel, Nurse and Thuriaux (1977) focused in a *wee1* mutant. They used a synchronous population under starvation to advocate for the idea of a critical size and found that in order to initiate DNA synthesis, cells needed to reach a critical size (as measured by protein content) therefore adding evidence for a growing body of literature in favor of a threshold point in the G1/S transition. Later, in 1996, Sveiczer et al. revisited the subject to further examine size control in *S. Pombe*. For this, they analyzed cell length and cell

2

cycle time in time-lapse movies on wild type *Schizosaccharomyces Pombe* and mutants. They studied cell size controls and found that when analyzing total extension (that is, division length minus birth length) through the cell cycle against birth length, there was a clear negative slope, indicating some compensation as a function of birth size. They showed with their analysis that smaller cells at birth extended more than larger cells therefore suggesting the existence of a target volume. Interestingly, they found that their behavior can be analyzed as a sizer only up to a defined point in the cell cycle. At that time, the growth rate is independent of size and cells keep on growing, now for a given amount of time. This is often referred as the "timer model", since growth progression seems to go on for a definite time independent of how big cells are. An interesting feature of this threshold volume in the G1/S transition is that it works as a regulation mechanism that would not enforce a hard checkpoint as it was later found. Di Talia et al. (2007) showed that when comparing small cells with larger cells, the first one buds at a smaller size than the budding size of larger cells (Di Talia et al., 2007).

1.2 Cell size regulation in bacteria: learning from yeast and what's beyond

Although the idea of the "sizer" model is attractive and elegant on its own, some research suggests different alternatives. In 2014, Campos et al. developed an assay to study bacterial size. They studied Escherichia Coli and Caulobacter Crescentus by performing time-lapse microscopy of an asynchronous population and monitored cell size over several generations. They measured bacterial elongation over entire cycles and showed that this is independent of cell length at birth. They concluded that cells grew the same amount between divisions regardless of their initial size. When they control how big they are, they do not sense their size but rather how much they have already grown (Campos et al, 2014). This model is often called in the literature as the "adder" model. This idea does not limit to bacterial systems, since it has already been explored on budding yeast, leading to an apparent contradiction with experiments mentioned before by Johnston et al. and Fantes and Nurse. Later Soifer et al. (2016) analyzed budding yeast and showed that although there seems to be a dependency on added volume in G1 and birth volume, the total amount of volume between budding events does not depend on budding size. By studying S. Cerevisae and measuring thousands of organisms, it was found that daughter cells add a constant amount of volume between two budding events (Soifer et al., 2016), therefore explaining the above-

3

mentioned contradiction and adding a new layer of complexity to cell volume regulation. Soifer et al. suggest that S. Cerevisae has two phases of control: first, there is a critical size checkpoint in the G1/S transition and after this, between budding events, organisms follow an "adder" model.

1.3 Mammalian cell volume regulation: current challenges and understanding

A question worth asking is if the work performed in bacteria and yeast can be replicated in mammalian cells. The difficulty on doing this lies on the challenges to measure cell size at the single cell level. In contrast with those organisms, mammalian cells are highly irregular in their morphology making the direct measurement of volume a hurdle. In recent years several methods have risen to address this problem. Some groups have focused on measuring cell density (Sung *et al*, 2013), buoyant cell mass (Son *et al*, 2012) or total protein content (Kafri *et al*, 2013) to address the question of size assuming the correlation between these variables holds true. Others have attempted to directly measure cell volume using the Fluorescence exclusion method (Bottier *et al.*, 2011; Cadart *et al.*, 2017; Perez Gonzalez *et al.*, 2018).

Regardless of the challenge of measuring volume accurately, many have attempted to understand how cells can keep their size with such regularity in similar ways to those used in bacteria and yeast. In the discussion about cell size, just like we have already mentioned, there are three main scenarios considered through the literature: (1) the "timer" model in which cells grow for a constant amount of time leading to larger cells growing more than smaller cells; (2) the "adder" model, in which a constant volume is added every cell cycle, leading to a steady state in the population and (3) the "sizer" model, in which there is a thresholding value of size at which cells progress through their cycle. Yet, results are confusing and contradictory with several studies suggesting some form of G1 length control as a function of cell size (Killander and Zetterberg, 1965a; Dolznig *et al.*,2004; Amir *et al*, 2014; Cadart *et al.*, 2018; Ginzberg *et al.*, 2018).

Killander and Zetterberg (1965a) reported seminal work on volume regulation based on the observation that fibroblasts entering S phase were more uniform in size than cells exiting mitosis. They reasoned that smaller cells should be maintained on G1 for longer periods to reach such critical size (Killander and Zetterberg, 1965a). Recent evidence points somewhere different.

Considering the difficulties on measuring cell size accurately, Varsano et al. (2017) took a practical approach. They developed microchannels that linearize mammalian cell growth. Given that the system is linear, cell size is easier to quantify than in regular conditions (Varsano et al., 2017) because there is only one dimension to quantify as in the work we have already discussed on bacteria and yeast. The authors used rat basophilic leukemia cells and RAW 264.7 macrophages, and presented G1 duration measurements against size at birth, which is commonly used to distinguish between "sizer" and "timer" models. In this type of dataset, a slope of -1 would advocate for a size checkpoint whereas a slope of 0 would point to independence between G1 duration and cell birth size. Their analysis showed a two-phase mechanism where both the "sizer" model and the "adder" model could be active depending on the birth size of cells (Varsano *et al*., 2017). Recently, Cadart et al (2018) used the fluorescence exclusion method to explore growth in single cells. They reported near-adder results, showing little to no correlation between the volume added during the cell cycle and their respective cell birth size. Ginzberg *et al.* (2018) have also suggested recently that cells regulate their growth with a compensatory mechanism increasing growth rates for small cells and decreasing them for larger cells, therefore guaranteeing a preserved target volume. They presented evidence advocating for the idea that cells both regulate their cell cycle length and growth rate to maintain the appropriate size. Briefly, Ginzberg et al generated mutations and used chemical treatments to alter cell cycle length. What they observed was that cells with longer cell cycles seemed to compensate by decreasing their growth rate, therefore maintaining their target volume. Conversely, cells with shorter cell cycles compensated by increasing their growth rate. On the same lines, it was recently shown via large-scale small molecule screening that the p38 MAPK pathway is involved in the coordination of cell size and cell cycle progression: in short, the authors proposed that p38 responds to changes in cell size to increase cell size uniformity.

1.4 On metabolic control of cell volume and its implications on homeostasis

An alternative view on cell volume regulation is related to the metabolism of the cell itself. This perspective is widely discussed in the literature given that it presents a straightforward path to unveil potential control mechanisms. By assigning a primary role to some proteins regarding size

determination it poses the idea that cell size can be modulated by changing growth rates, synthesis, degradation (Lloyd, 2013) and water flow (Koisuvalo *et al*., 2009).

It is this way that already several pathways and proteins have been implicated in cell volume control. The mTOR pathway, involved in protein translation, cell cycle progression and cellular proliferation, has been broadly recognized as a cell size modulator (Schmelzle and Hall, 2000; Lloyd, 2013). Insulin growth factor, IGF, usually associated to cell growth (Oldham and Hafen, 2003) has also been reportedly involved in size regulation (Edgar, 2006; Sun *et al*., 2006). This is has been attributed to an upregulation and downregulation of S6K activity, a downstream effector of mTOR (Edgar, 2006; Oldham and Hafen, 2003). Growth factor have also been related to size control: it is curious that deletion of insulin-like growth factor receptor (IGF-IR) leads to ~50% reduction in body size at birth in Drosophila and mice due to decreased cell number and cell size, confirming the role of IGF on cell size (Sun et al, 2006). An interesting part of this is that under limited conditions (no amino acids) IGF is not able to activate mTOR (Lloyd, 2013). Franklin and Johnson (1998) suggested Nerve Growth Factor (NGF) plays a role in cell size and treated neurons with it. They showed that size was preserved by decreasing the degradation rate of proteins. When NGF was removed, cells decreased in size, showing that it played an important role in keeping cell volume homeostasis and therefore proving the point that protein synthesis plays a role in it (Franklin and Johnson, 1998). Another interesting protein is Myc, a transcription factor that has been recently implicated in cell volume regulation. Through the study of Drosophila Melanogaster, Grewal et al. (2005), evidenced that Myc regulates ribosomal RNA synthesis leading to increased growth, which strengthens the hypothesis that macromolecular content regulation also impacts overall cell size (Saucedo and Edgar, 2002). As of now, the fact that the molecular basis of cell size regulation remains a challenge motivates the exploration of other actors involved.

Among all the proteins we mentioned before, the mTOR pathway has been broadly characterized as a master regulator of cell size by stimulating anabolism and inhibiting catabolism (Schmelzle and Hall, 2000; Lloyd, 2013). We are interested on this pathway because it has become a standard when talking about the molecular mechanisms of cell size regulation. Originally, Fingar et al. (2002) were interested on the effect of mTOR and phosphatidylinositol 3-kinase (PI3K) on

mammalian cell size. It had already been reported that PI3K affected cell number and cell size (Stocker and Hafen, 2000) and that Drosophila TOR (dTOR) produced varied cell size phenotypes (Montagne et al., 1999). Fingar et al. used rapamycin (an mTOR inhibitor) and reported that mTOR and PI3K dependent signals were necessary for cell to reach their volume (Fingar et al., 2002). Expression of S6K1 mutants that have rapamycin resistant activity partially rescued the original cell size further proving this point. They went further and performed overexpression of S6K1 and eIF4E increasing the cell size of this population. Based on their results they identified that S6K1 and 4EBP1 mediate mTOR dependent cell size regulation (Fingar et al., 2002). Another important fact of this path is that is can go modulate volume in both directions as it has already been shown that activation of the mTOR pathway also promotes additional growth (Edgar, 2006; Laplante and Sabatini, 2012). In particular, it has already been shown how constitutive activation of mTORC1 in beta-cells increases cell size, process that can be reversible with the use of rapamycin (Laplante and Sabatini, 2012). Another interesting thing about mTOR is that its control of size does not seem to be universal as if its regulatory behavior depended on other factors. In some tissue like muscle, mTOR has strong control of size, but in adult prostate or in post-natal granule neurons, it has very limited effect. (Kwon et al, 2003; Nardella et al, 2009).

Similarly to mTOR, the mammalian version of the Hippo pathway has been implicated in cell volume regulation (Dong et al., 2007; Saucedo and Edgar, 2007; Zhao et al., 2011; Yu et al., 2015) although traditionally the Hippo pathway has been perceived as an important pathway for control of organ size due to its role on proliferation (Tumaneng et al., 2012a). How these pathways truly affect this regulation still remains a mystery. Nevertheless, some research suggests that Hippo might be related to cell size itself: Tumaneng et al. showed a crosstalk between the Hippo pathway and mTOR pathway (Tumaneng et al., 2012b), and it has been shown by flow cytometry that Hippo pathway knockouts show a decrease in size (as measured by forward scattering). In this context, Myc has also been shown to have a dependency with a feedback mechanism with Yorkie in Drosophila (Neto-Silva et al, 2010).

With this literature review, what we are looking to motivate is that the analysis of cell volume regulation has several layers of complexity. In subsections 1-4 we motivated the observables of cell size and cell volume and how it has been used to understand how can cells keep

such tight uniformity. In subsection 5 we added a layer a complexity that underlies that observable of cell size. This means that the problem of cell volume can be approached from two different directions: on the one hand, we can understand volume itself and how it changes across the population; on the other hand, we can understand the proteins involved in keeping homeostasis.

1.5 On the alternative view of cells as mechanosensitive objects within the body and its implications to cell size regulation

Consider now a different approach. Cells are flexible and active objects that interact with the extracellular matrix but in a more fundamental level, cells comprise an internal compartment separated from an external compartment by a membrane and structural proteins underneath. In order to keep its status in equilibrium, cells maintain a pseudo steady state in which forces are balanced for each cell interacting with the matrix (Tao et al., 2017). Could it be that this interaction somehow plays a role in the determination of cell volume? Said balance is affected by many conditions. In particular, Engler et al. (2006) showed how different mechanical properties of the microenvironment can influence growth and differentiation. In their work, they showed that Naive Mesenchymal Stem cells (MSCs) commit to specific lineages based on the stiffness of the matrix they were cultured on. Moreover, they showed that the inhibition of nonmuscle myosin II blocks all stiffness directed differentiation illustrating how myosin is a key participant in the transduction of these signals (Engler et al., 2006). Studies like this one have led to a growing exploration on the impact of substrate stiffness in metabolism, growth, proliferation and other fields. Some have shown the influence of substrate stiffness on focal adhesion formation and cytoskeletal structure (Cukierman et al., 2001; Discher et al., 2005); others have shown its effects on metabolic pathways (Dupont et al., 2011; Elosegui-Artola et al., 2017; Mohri et al., 2017) and more recently the effect of substrate stiffness on cell volume (Fei Li et al., 2017). All of these recent studies help display the complex mechanical sensing cell have throughout the body and motivate a deeper understanding of mechanical sensing, stiffness and cell volume.

With the purpose of establishing said relationship between cell volume determination and its mechanical constraints it is necessary to first determine the problem at hand. In this view, a cell behaves like a balloon, separating an internal compartment from an external compartment. The

cell, separates these compartments with two elements: a semipermeable lipid membrane and a layer of structural proteins underneath. Most notably, below the bilipid layer, there is layer of myosin that exerts contractility, balancing locally the pressure difference (Tao and Sun, 2015) and therefore becoming crucial on cell shape determination (Smith et al., 2017). It is because of this layer that myosin has been broadly regarded as a key protein for contractility at the cortex. When treating this problem with a theoretical framework it is possible to understand that the local balance of forces can be used to determine the volume of a cell (Tao et al., 2017). Interestingly, the available evidence on this field is still limited, with some results pointing to an inverse relationship between cortical tension and volume (Guo et al, 2017) and two separate projects pointing towards a direct relationship between cortical tension and volume (Wang et al., 2018 and this thesis).

The most interesting but at the same time most complex part of this project is the intertwining between cell volume regulation and cortical tension. Here, we seek to establish a straightforward relationship between cell volume and cortical tension, which elevates the discussion of a cell size checkpoint to a new position. Part of our hypothesis is that volume corresponds to a global variable, difficult to measure for the cell by physical means, but tension is a local variable within the cell capable of efficiently transducing signals. This hypothesis shifts the weight from cell cycle regulation (or G1 length as it is usually presented in the field) and cell size regulation to a focus on tension regulation. There is already evidence of this potential relation, as it has been shown that tension is a better predictor of G1 length than other measurable geometrical properties of the cell (Uroz et al., 2018).

1.6 Construction of this thesis

This thesis is constructed partially following the research that I have performed along my colleagues during these five years at Johns Hopkins. It comprises two chapters that cover the work developed in two separate publications around the topic of cell volume regulation. The abovementioned chapters include a first chapter devoted to how volume is measured and the effect of stiffness in its regulation; we also describe the role that the mechanotransducer YAP/TAZ has in this context. The second chapter corresponds to the research that followed up to that on chapter two. Here we used the fluorescence exclusion method to uncover the role of the Hippo pathway in

cell volume regulation. These chapters are followed by a conclusion reviewing the work and a discussion on future directions.

The work shown in this thesis has been published on:

Perez Gonzalez, N., Tao, J., Rochman, N.D., Vig, D., Chiu, E., Wirtz, D. and Sun, S.X. Cell tension and mechanical regulation of cell volume. *Molecular biology of the cell*, *29*(21). (2018).

And on the Biorxiv as:

Perez Gonzalez, N.A., Rochman, N.D., Yao, K., Tao, J., Tran Le, M., Flanary, S., Sablich, L., Toler, B., Crentsil, E., Takaesu, F., Lambrus, B., Huang, J., Fu, V., Holland, A., An, S., Wirtz, D., Guan, K.L., Sun, S. YAP/TAZ as a Novel Regulator of cell volume, *Biorxiv* (2019).

Chapter 2: Cell Tension and Mechanical Regulation of Cell Volume

In the large scheme of things, this thesis is about cell volume regulation. As we have already established this is a rather complex and intricate issue to analyze due to the fact that this is a global variable of the cell. Typically, in a thermodynamics class, students learn that there are three key variables that characterize a system, Temperature, Pressure and Volume. In biology, the effect of Temperature changes on cells has been often characterized but the other two variables, Pressure and Volume have lagged behind and still remain poorly understood. This is largely due to the difficulties in assessing both of these quantities at a population level and further at the single cell level. In the following chapters I seek to demonstrate how the fluorescence exclusion method is an extremely useful way to understand cell volume at the single cell level.

2.1 Introduction

What determines the physical volume of a cell? Despite the fundamental importance of this question, and decades of experimental studies on growth dynamics in mammalian cells (Killander and Zetterberg, 1965; Fox and Pardee, 1970; Yen *et al.*, 1975; Brooks and Shields, 1985; Hola and Riley, 1987; Conlon and Raff, 2003; Godin *et al.*, 2010; Son *et al.*, 2012), the mechanisms behind cell volume regulation are not well understood (Ginzberg *et al.*, 2015). It is known that different cell types from the same organism can have dramatically different volumes (Ginzberg *et al.*, 2015), but how cells sense and control growth/division rates under different conditions is not clear. From genetic studies, several pathways have been implicated in cell volume control. The mTOR signaling pathway is known to regulate cell size by stimulating anabolism and inhibiting catabolism (Schmelzle and Hall, 2000; Lloyd, 2013). Similarly, the mammalian version of the Hippo pathway and its downstream effector YAP/TAZ are important in controlling tissue and organ size and have been implicated in cell volume regulation (Dong *et al.*, 2007; Saucedo and Edgar, 2007; Zhao *et al.*, 2011; Yu *et al.*, 2015). While studies have suggested that there is a cell size checkpoint within the cell cycle at transition from G1 to S, which determines the added cell volume (Ginzberg *et al.*, 2015; Varsano *et al.*, 2017), exactly how and what signaling pathways are connected with the size checkpoint is still unclear.

Working from a different perspective, cells are active mechanical objects that form adhesions with the extracellular matrix and balance forces in the cytoplasm with the extracellular environment (Tao *et al.*, 2017). Mechanical properties of the microenvironment have been shown to influence cell growth– and cycle–related phenomena including differentiation (Engler *et al.*, 2006) and may impact cell volume as well. Indeed, YAP/TAZ has been shown to be sensitive to mechanical forces and the stiffness of the environment (Dupont *et al.*, 2011; Codelia *et al.*, 2014; Low *et al.*, 2014; Piccolo *et al.*, 2014; Elosegui-Artola *et al.*, 2016), which suggests that the mechanical state of the cell could influence cell growth and volume. In this paper, we explore how cytoskeletal tension is related to cell volume and how substrate stiffness influences cell size through the measurement of single cell volumes for several different cell types. We show that how cells distribute their tension over different regions of the cell surface can explain the observed cell volume under different conditions. Moreover, we explore how single cell tension (reported by the amount of phosphorylated myosin light chain [pMLC], similarly to previous work; Fernandez-Gonzalez and Zallen, 2009; Elliott *et al.*, 2015) is related to YAP/TAZ nuclear localization and discover that the amount of nuclear YAP/TAZ, which is also the active form, is correlated with the amount of myosin in the apical region of the adherent cell. This is consistent with suggestions that YAP is sensitive to cytoskeletal tension (Dupont *et al.*, 2011; Elosegui-Artola *et al.*, 2016). The level of nuclear YAP/TAZ also in- creases with increasing cell volume, suggesting that as the cell grows, it increases myosin activity to maintain force balance, and the change in the myosin level can serve as a signal for YAP/TAZ activity, which influences the observed cell size.

Several methods have been used to measure cell volume (Hurley, 1970; Tzur *et al.*, 2009; Sung *et al.*, 2013; Cadart *et al.*, 2017). Here we are interested in a high-throughput measurement of live cell volume for single adherent cells. We use the fluorescence exclusion method (Bottier *et al.*, 2011; Cadart *et al.*, 2017) to quantify cell volume. The fluorescence exclusion method was able to reveal that mitotic cells swell before cytokinesis (Son *et al.*, 2015; Zlotek-Zlotkiewicz *et al.*, 2015). We simultaneously measure cell volume, cell adhesion area, and cell shape factor for three different cell types on substrates varying in stiffness from 3 kPa to GPa (glass). The results show that the mean cell volume depends on the substrate stiffness, but that dependence varies across different cell types. For all cells, the measured volume is strongly correlated with cell adhesion area, but the slope of this correlation depends on the adhesion shape and the substrate

stiffness. For the same adhesion area, more elongated cells have a smaller volume than more circular cells. This result can be explained by a mechanical model of the cell where cortical tension developed by myosin is proportional to the mean curvature of the cell surface. In addition, from quantitative immunofluorescence measurements, we find that the total pMLC content and the spatial distribution of pMLC can predict cell volume. Using the measured pMLC levels as inputs, our mechanical model can be used to predict cell volume across all cell types on all substrates.

Cytoskeletal tension and substrate stiffness have been shown to influence the nuclear localization of YAP/TAZ (Dupont *et al.*, 2011; Codelia *et al.*, 2014; Low *et al.*, 2014; Piccolo *et al.*, 2014; Elosegui-Artola *et al.*, 2016), which in turn influences cell proliferation and growth (Shen and Stanger, 2015). The nuclear portion of YAP/TAZ is a cofactor with TEAD and regulates the transcription of a large group of proteins (Zhao *et al.*, 2008). To explore how cell tension is related to YAP/TAZ nuclear localization, we performed quantitative immunofluorescence measurements. While the results show dependence on cell type, for the terminally differentiated cells tested, we observed that the average cell volume is positively correlated with the level of nuclear YAP/TAZ. But the nuclear-to-cytoplasmic ratio of YAP/TAZ is not a predictor of cell volume. The nuclear YAP/TAZ level is also positively correlated with the amount of apical pMLC, a read- out of apical cell tension. In mesenchymal stem cells (MSCs), the behavior of YAP and tension is more complex, but the correlation between nuclear YAP/TAZ and apical pMLC persists. These results suggest that cell tension can potentially serve as a checkpoint signal that allows the cell to sense its volume and control the cell cycle progression in late G1.

2.2 Experimental Procedures

2.2.1 *Cell Culture*

NIH 3T3 fibroblasts were a gift from D. Wirtz (Johns Hopkins University, Baltimore, MD), neonatal foreskin fibroblasts (NuFF) were a gift from S. Gerecht (Johns Hopkins University, Baltimore, MD) and mouse Mesenchymal Stem Cells were a gift from Xu Cao Lab (Johns Hopkins Medical School, Baltimore, MD). The cells were cultured in Dulbecco's modified Eagle's media (Corning) supplemented with 10% fetal bovine serum (FBS; Sigma) and 1% antibiotics solution [penicillin (10,000 units/mL) + streptomycin (10,000 µg/mL); Gibco] at 37 °C and 5% CO_2. Both

the 3T3s and NuFFs were tested for mycoplasma contamination and kept for a maximum of 3 months.

2.2.2 *Micro-fluidic device fabrication.*

Silicon molds were fabricated using standard photolithography procedures. Masks were designed using AutoCAD and ordered from FineLineImaging. Molds where made by following manufacturer's instruction for SU8-3000 photoresist. Two layers of photoresist were spin coated on a silicon wafer (IWS) at 500 rpm for 7 seconds with acceleration of 100 rpm/s and 2000 rpm for 30 seconds with acceleration of 300 rpm/s respectively. After a soft bake of 4 minutes at 95 °C UV light was used to etch the desired patterns from negative photoresist to yield feature heights that were approximately 15 µm. The length of the abovementioned channels is 16.88 mm and the width is 1.46 mm.

A 10:1 ratio of PDMS Sylgard 184 silicone elastomer and curing agent were vigorously stirred, vacuum degassed, poured onto each silicon wafer and cured in an oven at 80 °C for 45 minutes. Razor blades were then use to cut the devices into the proper dimensions, inlet and outlet ports were punched using a blunt-tipped 21 Gauge needle (McMaster Carr, 76165A679). The devices were then sonicated in 100% EtOH for 15 min, rinsed with water and dried using a compressed air gun.

50 mm glass bottom petri-dishes (FlouroDish Cell Culture Dish, World Precision Instruments) were rinsed with water and then dried using a compressed air gun. The petri-dishes and PMDS devices were then exposed to oxygen plasma for 1 minute for bonding. Finally, the bonded devices were placed in an oven at 80 °C for 45 minutes to further ensure enhance bonding.

2.2.3 *Synchronization and stiffness experiments.*

Cells were treated with 2 or 5 µg/mL of aphidicolin (Sigma-Aldrich, A0781) for 24 hrs to synchronize them in the G1 phase of cell cycle (Mittnacht *et al*, 1991). The optimal concentration and incubation period were determined using standard flow cytometry techniques (Fig. S8). To serum-starve cells, the media within the chambers were removed and the chambers were rinsed

with 1X PBS 3 times. Serum-free media supplemented with 1% Pen/Strep was then injected into the chambers and left on the cells for 24 hrs.

For stiffness experiments, silicone elastomer was prepared by mixing a 1:1 weight ratio of CY52- 276A and CY52-276B (Dow Corning Toray) for 3 kPa (Style et al. 2014), a 0.9:1 weight ratio of CY52- 276A and CY52-276B for 12.6 kPa (Berget et al. 2016), a 1:1 weight ratio of QGel 920A and QGel 920B (Quantum Silicones) for 0.4 kPa (Gutierrez et al. 2011). In all cases the elastomer was vacuum degassed for ~5 min to eliminate bubbles, the polymer was then spin-coated onto the micro-well of the dish at 1,000 rpm for 60 s. The dish was cured overnight and resulted in a ~50 μm thick layer of silicone. The devices were then rinsed with water, dried using compressed air, plasma treated and bonded to the cell volume PDMS devices. The final devices were again placed in an 80 °C for 45 minutes to enhance the bonding.

2.2.4 *Cell Volume Measurements*

Micro-fluidic chambers were exposed to 30s oxygen plasma before being incubated with 50 μg/mL of type I rat-tail collagen (Corning; 354236) for 1 hr at 37 °C. The chambers were washed with 1X PBS before approximately 50,000 cells were injected into them. The dishes were then immersed in media to prevent evaporation. The cells were allowed to adhere for 12-18 hrs in the incubator at 37 °C with 5% CO_2 and 90% relative humidity. On the day of the experiment, 0.5 μg/mL of Alexa Fluor 555 Dextran (MW 70 kD; ThermoFisher) dissolved in media was injected into the chambers and the devices were imaged within 1-2 hrs after injection.

The cells were imaged using a Zeiss Axio Observer inverted, wide-field microscope using a 20x air, 0.8 numerical aperture (NA) objective equipped with an Axiocam 560 mono charged-coupled device (CCD) camera. The microscope was equipped with a CO_2 Module S (Zeiss) and TempModule S (Zeiss) stage-top incubator (Pecon) that was set to 37 °C with 5% CO_2 for long-time imaging. Differential interference contrast (DIC) microscopy was used to accurately capture the cell area and shape and Epifluorescent microscopy was used to measure volume. Individual cells were traced using the following algorithm.

Cell contours were segmented from the DIC and epifluorescence (Volume) channels. First, a rough contour is generated from a smoothed copy of the Epi channel where pixels darker than the background intensity are identified. Next a measure of the local contrast of the DIC channel (here high contrast regions are identified) is used to expand the contour to include small features (small lamellipodia etc.) which have low contrast in the Volume channel and may be missed. This expanded contour is used to identify the cell boundary. Inner and outer annuli are created by dilating this contour 10 and 25 pixels away from the cell (shown as green and red lines in Figure S1 (a)). The mean fluorescence intensity of the pixels between inner and outer annulus, or mean background intensity, $I_{annulus}$, is related to the total channel height. The volume boundary, shown as purple line in Figure S1(a), is created by dilating the cell contour 20 pixels away from the cell. The local fluorescence intensity enclosed by the volume boundary, I_V, corresponds to the local height above the cell (h_2, shown in Figure 2.1(a)). The volume of the cell is then calculated as follows:

$$V = \text{Channel Height} \sum\nolimits_{\text{pixels within volume boundary}} \left(1 - \frac{I_V}{I_{Annulus}}\right) \delta A$$

Every experiment on cell volume was repeated at least three times with three technical repeats corresponding to the three individual channels in the microdevice. Experiments in glass gave at least 50 single cell measurements. Softer substrates yielded smaller datasets per measurement. The sample size for volume measurements was kept over 100 single cells except for 3T3s in 0.4 kPa. This was done in order to get a normal distribution for each complete dataset".

2.2.5 *Immunofluorescence*

Immunofluorescence was carried out as described as in (Aifuwa et al, 2015). Briefly, cells were seeded at either single cell density (12,000 cells/cm^2 for 3T3s, 7,500 cells/cm2 for NuFFs) or confluent density (75,000 cells/cm^2 for 3T3s, 60,000 cells/cm^2 for NuFFs) for 12-18 hrs and then fixed with 4% paraformaldehyde (100503-917, VWR) for 10 minutes. Samples were then rinsed 3 times with 1X PBS. 0.1% Triton X (T8787, Sigma Aldrich) dissolved in PBS is then added for 10 minutes, washed 3 times with 1X PBS and then the fixed cells are blocked with 1% bovine serum albumin (A7906, Sigma Aldrich) for 1 hour at room temperature. Primary antibodies are incubated overnight in 1% BSA. Antibodies used included: YAP 63.7 (1:100; ms; SC-101199), Phospho-Myosin Light Chain 2 Thr18/Ser19 (1:100; rb; Cell Signaling Technology #3674), Anti-

CD105 (1:100, rb, Abcam ab21224), Anti-Cd90/Thy1 (1:100, rb, Abcam ab 133350). The next day the dishes are rinsed 3 times with 1X PBS and incubated for 2 hrs in secondary antibodies with the following secondary antibodies Mouse Alexa Fluor 488, Rabbit 568, and DNA was stained using 20 µg/mL of Hoechst 33342.

Wide-field microscopy using the set-up described above was used to measure the total pMLC, YAP/TAZ, and DNA content of the cells. To obtain spatial information about pMLC we used a Zeiss LSM 800 confocal microscope equipped with a 63X oil-immersion, 1.2 (NA) objective. A 567nm laser was used to image the stained cells. Images were acquired with a resolution of 1024 x 1024, which gives a field of view of 10485.76 µm^2. We imaged the cells with confocal image stocks of total thickness of 20 µm to cover the entire height of the cells. Confocal image slices were spaced 2 µm apart and the pinhole size was 1 µm.

For each fluorescence image, we subtract the pixel intensities with mean background intensity. A binary mask is generated based on the pixel intensities of fluorescence image (for the pixel intensities within the cell region is much higher than the intensities of anywhere else), where pixels within the cell/nucleus region are marked with "1" and pixels outside the cell/nucleus are marked with "0". By multiplying the binary mask with actual florescence image, we can identify all the pixel values that is within the cell/nucleus. The total intensities within cell/nucleus boundary is calculated by summing up all the intensity values. The cell and nucleus boundary is then traced by Matlab routine "bwboundaries". Every traced region with total area of 1,500 pixels square or less is considered as debris or cell fragments, and, therefore, is ignored.

We utilized the pMLC channel to generate the binary mask for the cell. The traced boundary is then dilated 15 pixels away from the cell, to capture all the scattered light from epifluorescence image. The binary mask for the cell nucleus is generated based on Hoechst channel. No dilation is made on nucleus mask, to avoid overestimation of total nucleus YAP. We multiply the nucleus mask with every cell mask, to exclude all the nuclei from other cells within the same field of view. The traced boundary is shown in Fig. S1 (b).

For confocal z stacks, the basal layer of the cell is identified when clear stress fibers are seen (as example shown in Fig. S4 (b)). All stacks that are below the basal layer are neglected. We identified the first apical slide when the stress fibers disappear. The traced boundary of every apical slides is dilated 5 pixels (~ 1 micrometer) inside the cell, to mark the inner boundary of cortical layer (marked with pink line, Fig. S4 (c)). Cortical pMLC of one apical slide is calculated by subtracting the total PMLC intensities that within the inner boundary from the total pMLC intensity. Fig. S4(c) shows pMLC are mainly cortical, except for basal layer, where clear stress fibers can be seen. Therefore, the pMLC within the cell cytoplasm is very minimal compared to cortical pMLC.

Every experiment was repeated two times with two technical repeats on every experiment. In addition, each technical repeat consisted of at least 100 single cell measurements. The sample size for qIF aimed for at least 200 single cells with exception of two experiments on 0.4 kPa for 3T3s and NuFFs for which we obtained 80 cells and 178 cells respectively. This dataset size was targeted in order to get a normal distribution for each complete dataset. Finally, no single cells were excluded during the analysis of these datasets. The only cells excluded we those forming clusters.

2.2.6 *Y27632 Treatment*

Cells were treated with the ROCK inhibitor Y27632 (stem cell technologies,129830-38-2) to decrease expression of pMLC, a downstream protein of the Rho/ROCK pathway. Y27632 was diluted from stock in PBS and it was used at a final concentration of 100 μM. For treatment, media was replaced with fresh media and Y27632 at the final concentration for 2 hours. Then the cells were flown into the microfluidic device for volume measurement.

2.3 Theoretical Model: Mechanical Model of the Cell

A simple mechanical model was used to predict cell shapes and volumes in the main text. Under static conditions where all forces are balanced, the hydrostatic pressure difference across the cell membrane, ΔP, is balanced by membrane tension, T, and active myosin contraction, σ_a, in the cell cortex. Mathematically, this force balance can be written as:

$$H^{-1} = \frac{2(\sigma_a h + T)}{\Delta P} \quad (1)$$

where H is the local mean curvature of cell surface; h is cortical thickness, which is around 0.5 to 1 μm. The inverse of local mean curvature, H^{-1}, is the local radius of curvature, the integration of which over the cell apical surface will give the overall cell volume. This force balance condition is of the form of the classic Young-Laplace equation, which was discussed in our pervious theoretical work (Tao, et. al. 2015). If the cell is not subjected to any external mechanical forces, nor to sudden osmotic shocks, the cell membrane tension, T, remains very small when compared to $\sigma_a h$ and, therefore, can be neglected. The active myosin contraction, σ_a, depends on the concentration of phosphorylated myosin, which is reported by the light intensity of phosphorylated myosin light chain (pMLC) from the quantitative immunofluorescence experiments described in the main text. We quantified the total pMLC level in the cell, which includes the contribution from apical tension $\int \sigma_a h$ (Fig. 3, main text). In addition, from the confocal experiments, image intensity at different z-planes was used to report variation of $\sigma_a h$ across the apical surface. The observed cell adhesion size and shape is utilized as one of the two boundary conditions used to solve for the cell shape in Eq. (1). The force balance condition also implies cell shape and volume can be predicted if we know the myosin activity, pressure difference across the membrane, and the substrate adhesion size and shape. Details on how to calculate H^{-1} are included in Perez et al (2018).

2.4 Results

2.4.1 *Cell volume is heterogeneous and depends on substrate stiffness*

To quantify cell volume in different physical and biochemical environments, we use the fluorescence exclusion method to simultaneously measure single-cell volume, adhesion area, and cell shape for three different fibroblastic cell types (Figure 2.1a). We compare common mouse fibroblasts (3T3) with human-isolated fibroblasts (NuFF) and mouse-isolated mesenchymal stem cells (MSC). 3T3 fibroblasts are from the standard NIH line. NuFFs are neonatal foreskin fibroblasts obtained from Global Stem (Rockville, MD) at passage 9 and used up to passage 28. MSCs were isolated from bone marrow of 6 week–old mice.
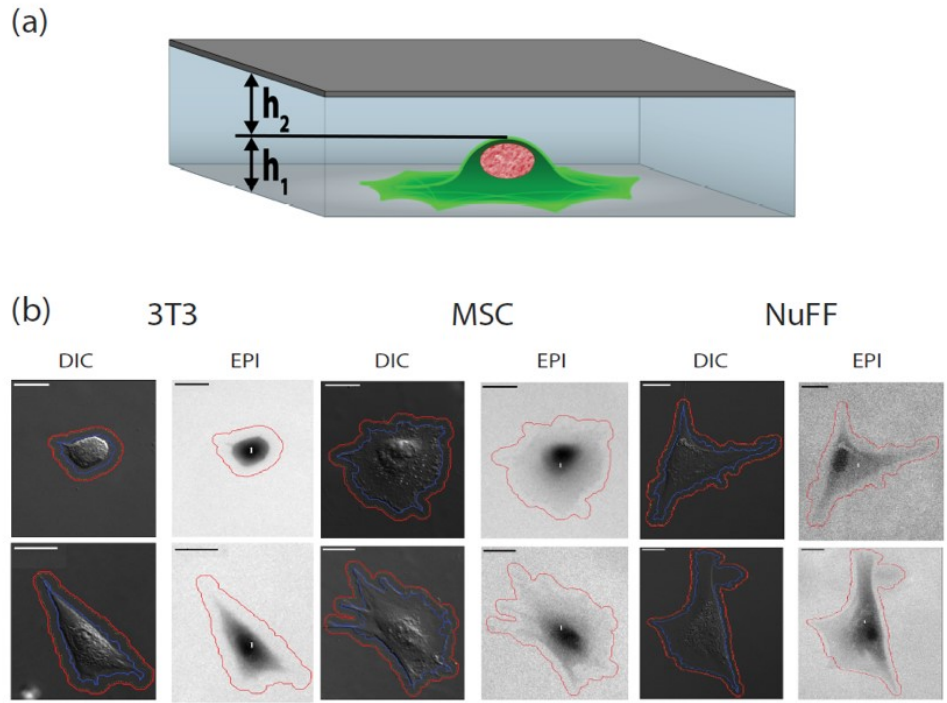
Figure 2.1. Cell volume measurement by Fluorescence Exclusion method. (a) Diagram of microfluidic device used to perform volume measurements at the single cell level. The channel height is 15 μm. (b) Sample images of 3T3s, NuFFs and MSCs area included showing the DIC channel in the left and the associated fluorescent channel on the right. Scale bar is 10 μm.

Volume measurements were performed for cells at low density and on substrates of 3-kPa PDMS, 12.6-kPa PDMS, and glass (gigapascals). We also tried 0.4-kPa PDMS substrates, but found them to be too soft to form stable microfluidic channels for volume measurement. In addition, we measured cell volume during cell cycle arrest achieved through serum starvation or treatment with aphidicolin on glass substrates. The resultant cell volume measurements displayed in Figure 2.2a and Figure 2.3a, show several striking features. Individual cell volume in each condition always shows significant heterogeneity, with a high proportion of smaller cells (Figure 2.2). This is in accord with previous results using a different method of measurement (Tzur *et al.*, 2009). This heterogeneity is partly explained by the fact that cells are in different stages of the cell cycle, and cells divide symmetrically, producing two daughter cells, so that there are more young cells than old cells. The shape of the volume distributions can be roughly explained theoretically from cell aging dynamics (Stukalin *et al.*, 2013). The average cell volume varies significantly across cell types, the largest line tested being the MSCs. The average cell volume also depends on the

substrate stiffness. In particular, the 12.6-kPa substrate always shows a significant deviation, indicating unusual behavior at intermediate stiffness. For 3T3s and MSCs, the average cell volume at 12.6 kPa is 32 and 50% higher than on 3 kPa and glass, respectively. For NuFFs, it is 40 and 15% less than on glass and 3 kPa, respectively (Figure 2.3). The sharp variation around intermediate stiffness is surprising, but parallels previous work that showed a similar change in cell adhesion shape (Rehfeldt *et al.*, 2012) and traction force (Han *et al.*, 2012) at intermediate stiffness.
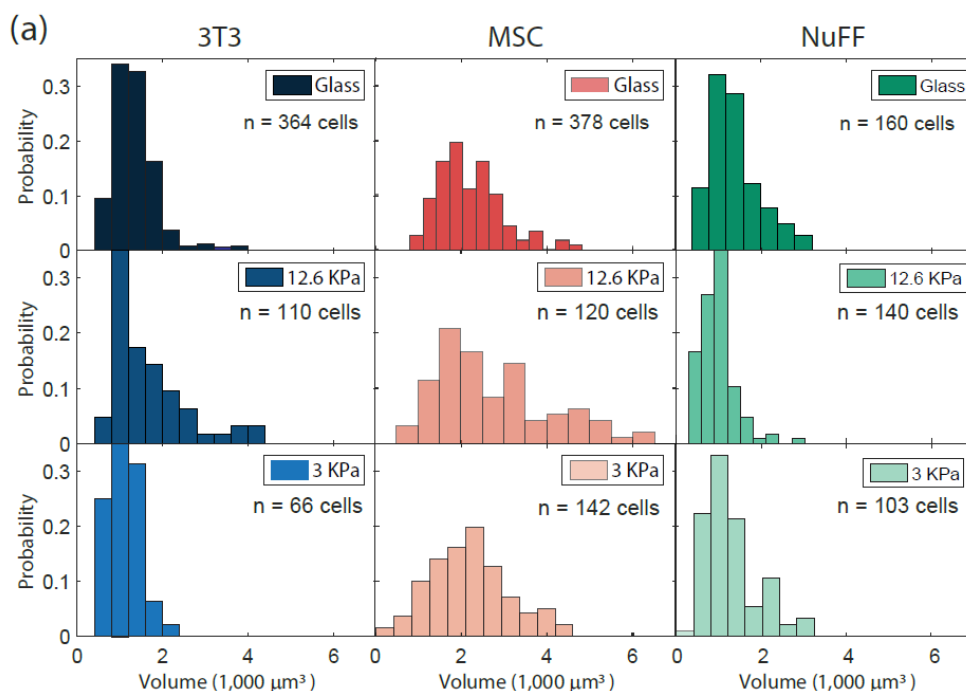
Figure 2.2. Cell volume is heterogeneous and depends on substrate stiffness. (a) Histograms of cell volume on 3 kPa, 12.6 kPa and glass substrate are shown for 3T3, MSCs and NuFFs. The wide range for the volume values shows intrinsic variation within the population as well as volume changes due to the cell cycle. Distribution is skewed to the left, evidencing that there are more young cells than older cells.

The overall trend of these results is in agreement with results previously published (Wang *et al.*, 2018) on the MCF7 cell line, and is somewhat different from confocal microscopy results for cells on polyacrylamide gels (Guo *et al.*, 2017), presumably due to the difference in substrate material and coating) Cell cycle arrest using serum starvation and aphidicolin produced significant changes in average cell volume as well (Figure 2.3a). Cells after serum starvation can be smaller, while aphidicolin-treated cells can be significantly larger. Aphidicolin inhibits DNA polymerase and

arrests cells in late G1 and early S (Krokan *et al.*, 1981). From DNA staining measurements, we observe that these cells all have a single copy of DNA (unpublished data), suggesting that they have stopped copying their DNA (Supplemental Figure S8, a–c), but perhaps continue to accumulate cell mass.
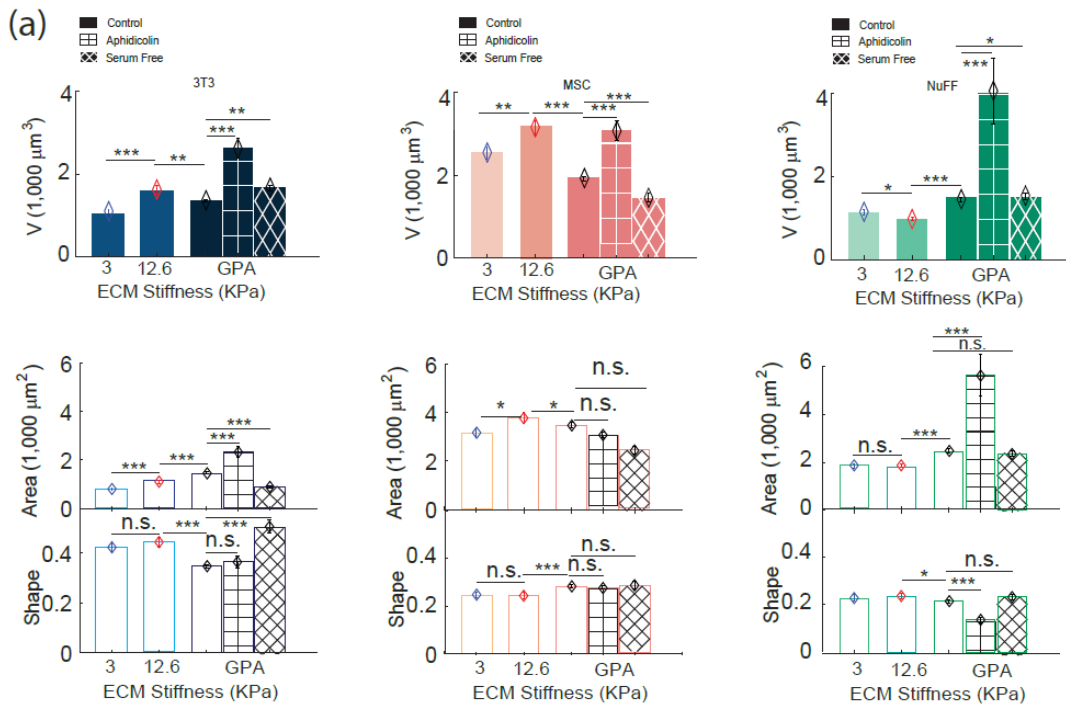
Figure 2.3. Cell volume depends on substrate stiffness and cell cycle distribution. (a) Average cell volume for 3 kPa, 12.6 kPa, glass (GPa), serum starvation and aphidicolin treatment for 3T3s, MSCs and NuFFs. At 12.6 kPa, 3T3s and MSCs are larger while NuFFs are smaller. Serum starvation generally decreases cell volume while aphidicolin treatment generally increases cell volume. The average cell adhesion area and adhesion shape are also shown. The shape factor has been defined as $S = 4\pi(Adhered\ area)/perimeter^2$. Distributions of adhesion areas and shapes are shown in Supplemental Figure S2. Statistical significance: p: *** $p<10^{-6}$; ** $p<0.001$; * $p<0.01$; n.s. $p>0.05$. Number of cells: for 3T3s: N=66 on 3kPa, N=110 on 12.6 kPa and N=364 on collagen-coated glass; for MSCs: N = 142 on 3 kPa, N=120 on 12.6 kPa, and N=378 on collagen-coated glass; for NuFFs: N=103 on 3 kPa, N=140 on 12.6 kPa, and N = 160 on collagen-coated glass.)

Cell two-dimensional (2D) adhesion area is often used as a proxy for cell volume. Because we simultaneously measure cell area, cell shape, and cell volume, we can examine the correlation between cell area and volume. Indeed, under all conditions, the cell area is positively correlated with the cell volume (Figure 2.4a); however, the slope of the area–volume correlation varies among different conditions. Moreover, the area–volume correlation depends on the 2D adhesion shape factor, defined as $S = 4\pi\, Adhered\ area/perimeter^2$.
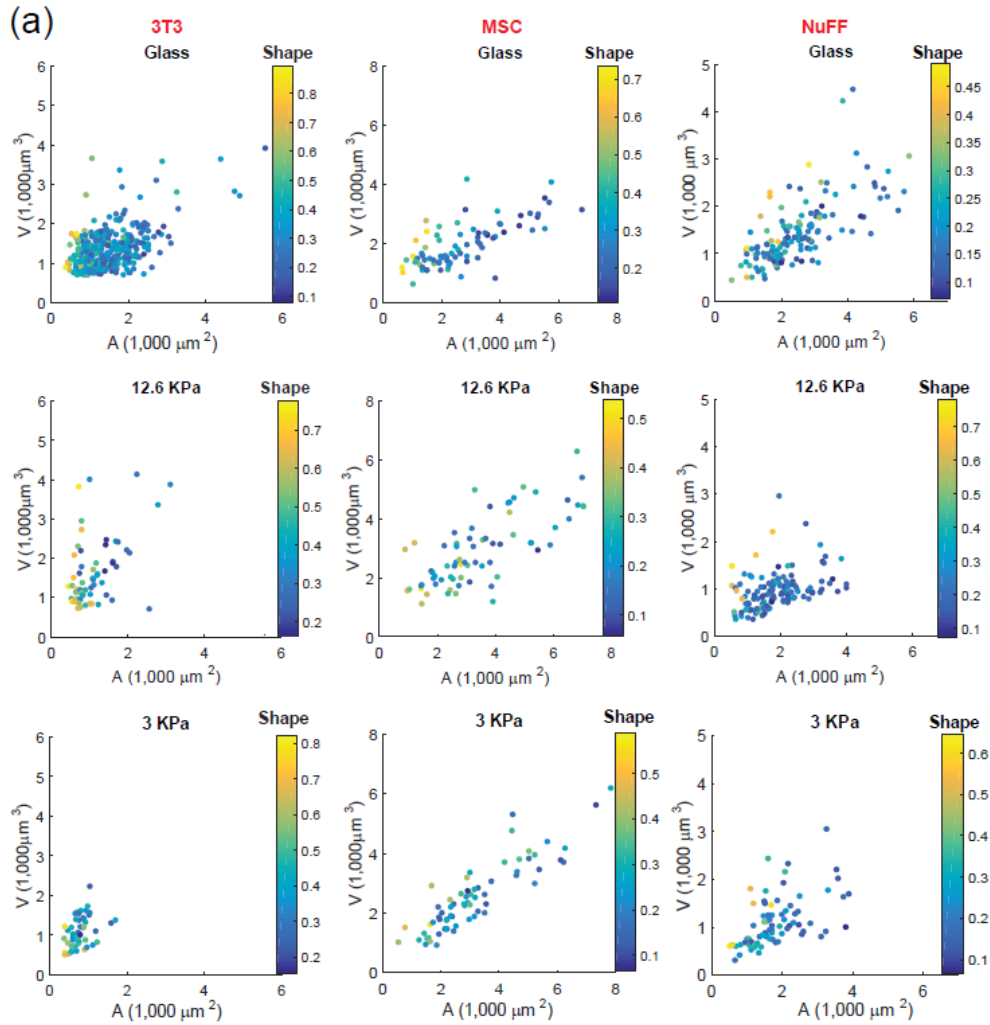
Figure 2.4. Cell volume in relation to cell adhesion and cell shape. (a) Cell volume is shown versus cell adhesion area for 3T3s, MSCs, and NuFFs on different substrates. Each point represents a cell, with the additional information of shape factor, S. Area is well correlated with volume, but data are heterogeneous. Moreover, the slope of the correlation depends on substrate stiffness. For the same area, more circular cells have a larger volume.

Cells with circular adhesions ($S \sim 1$) are consistently larger in volume for a given area (Figure 2.4a and Figure 2.5b), although there is significant noise. While cells with small adhesion areas do tend to have smaller volumes, adhesion area does not uniquely determine cell volume. For example, NuFFs generally have a larger spread area than 3T3s, but they have similar volumes. Supplemental Figure S2 also shows additional data for serum starvation and aphidicolin conditions, dis- playing volume distributions as well as cell area versus volume, and cell area distributions for all conditions.
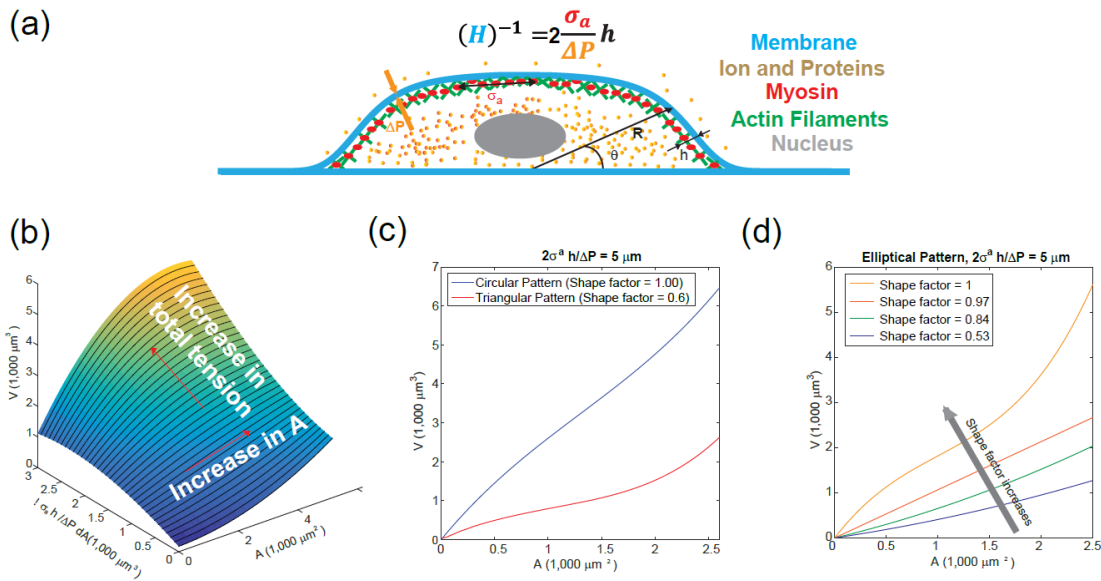
Figure 2.5. Theoretical dependency of volume on other factors. (a) Cartoon depicting an adherent cell. The volume is defined by the apical surface (which is determined numerically establishing force balance at the cortex). (b) Model predictions of cell volume with increasing adhesion area and total active myosin contraction. This figure assumes circular adhesion areas for the predicted volume. (c) Volume versus area for two different adhesion shapes. (d) Shape dependency on elliptical pattern illustrating that for the same cortical contraction σ_a, more circular looking cells are larger in size. This predicted behavior is consistent with data shown in (a).

2.4.2 *Cortical contractility and tension distribution can predict cell volume*

To further understand the connection between cell area and volume, we turn to a theoretical model of cell volume based on cell cortical-tension balance. When cells adhere to a flat substrate (Figure 2.5a), the cell volume is defined by the geometric shape of the apical cell surface. The cortex of mammalian cells consists of an actomyosin network that dynamically adjusts to the hydrostatic pressure difference between the inside and outside of the cell (Tao and Sun, 2015; Tao *et al.*, 2017).

The hydrostatic pressure difference, ΔP, arises from the slight osmotic imbalance between the cytoplasm and the extracellular medium. The pressure difference is balanced by the fluidized actomyosin cortex (Tao and Sun, 2015; Tao *et al.*, 2017),

$$\Delta P = 2(\sigma_a h + T)H$$

Where (σ_a) is the mechanical stress in the cortex, representing mostly myosin activity; h is the cortical thickness; T is the mem- brane tension; and H is the mean curvature of the cell surface. For a given pressure difference, cells can actively adjust cortical tension by activating different amounts of myosin contraction through the Rho signaling pathway (Krokan *et al.*, 1981; Zhao *et al.*, 2007; He *et al.*, 2018). In most situations, $T \ll \sigma_a h$, and the relationship is simplified to

$$H^{-1} = \frac{2\sigma_a h}{\Delta P} \tag{1}$$

Where

$$\frac{2\sigma_a h}{\Delta P} \equiv \lambda$$

has dimensions of length. H is a geometric property of the cell and is related to the apical cell shape $R(\theta)$ (Figure 2.5a and Supplemental Figure S3). Equation 1 is consistent with single cell measurements of cortical myosin distribution in Elliott *et al.* (2015). If the cell adhesion size, shape, and λ are known, then the volume of the cell can be computed (Perez et al, 2018 and Supplemental Figure S3). Theoretical results predict that for the same level of λ, the volume is a monotonically increasing function of the adhesion area (Figure 2.5, b and c). Moreover, for the same adhesion area, increasing λ also increases cell volume. The slope of the area–volume curve also depends on S: for the same λ, an elongated cell has a smaller volume (Figure 2.5, c and d). The data show that rounder cells ($S > 0.5$) are indeed larger than more elongated cells ($S < 0.5$) for the same adhesion area (Figure 2.4a). The model can be implemented for arbitrary adhesion shapes, and the computed three-dimensional (3D) cell shapes can be compared with reconstructed 3D shapes of cells obtained from confocal z-stack images (Figure 2.6).
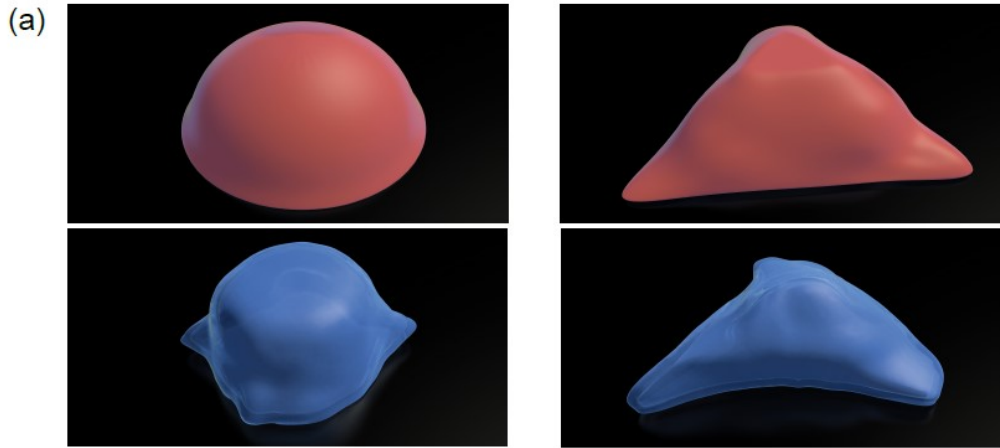
Figure 2.6. Three dimensional reconstructions: Theory versus data. (a) Model prediction (red) are compared with representative 3D reconstructions from confocal z-stacks (blue), for the same adhesion shape.
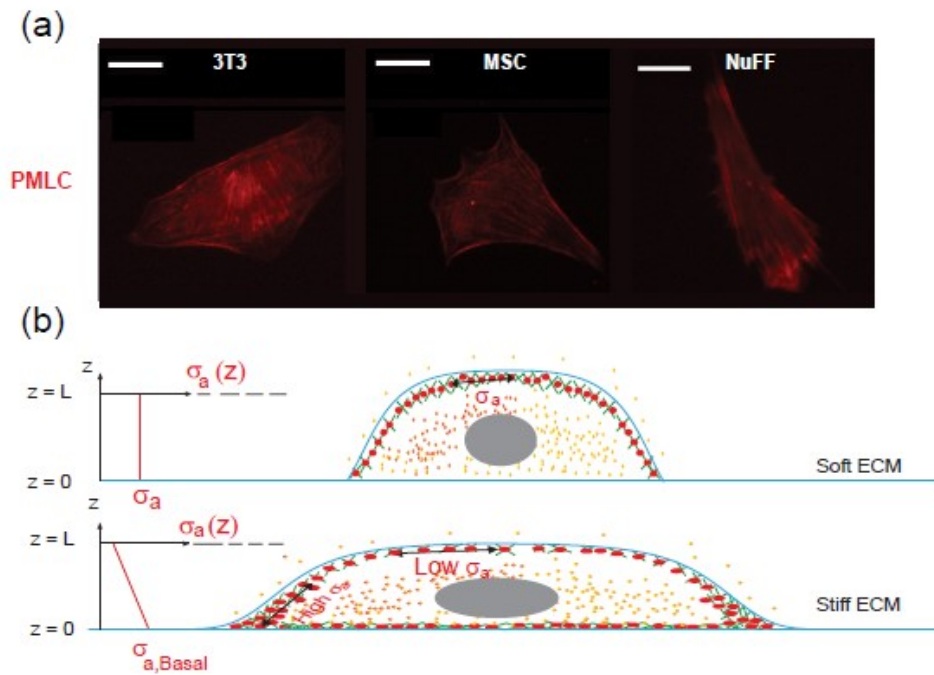
Figure 2.7. Spatial distribution of pMLC changes cell to cell. (a) Sample immunofluorescent image of pMLC of 3T3s, NuFFs and MSCs. These images are postprocessed for quantification of total pMLC. Confocal Z-stacks were also used to measure relative amount of pMLC at each z level. (b) In stiffer substrate and thinner cells, there is a higher concentration of pMLC near the basal surface. For rounder cells, the apical pMLC distribution is more equally distributed. Cartoons depict on the left how sigma can have different concentrations through the z axis.

In live cells, we expect cortical tension and λ to vary spatially across the cell cortex, as seen, for example, in Elliott *et al.* (2015). The spatial distribution of λ impacts the cell volume. From our mathematical model, if λ is concentrated near the basal surface of the cell, then the cell volume is smaller (Supplemental Figure S3). If λ is uniformly distributed in the apical cell surface, then the volume is larger (Supplemental Figure S3).
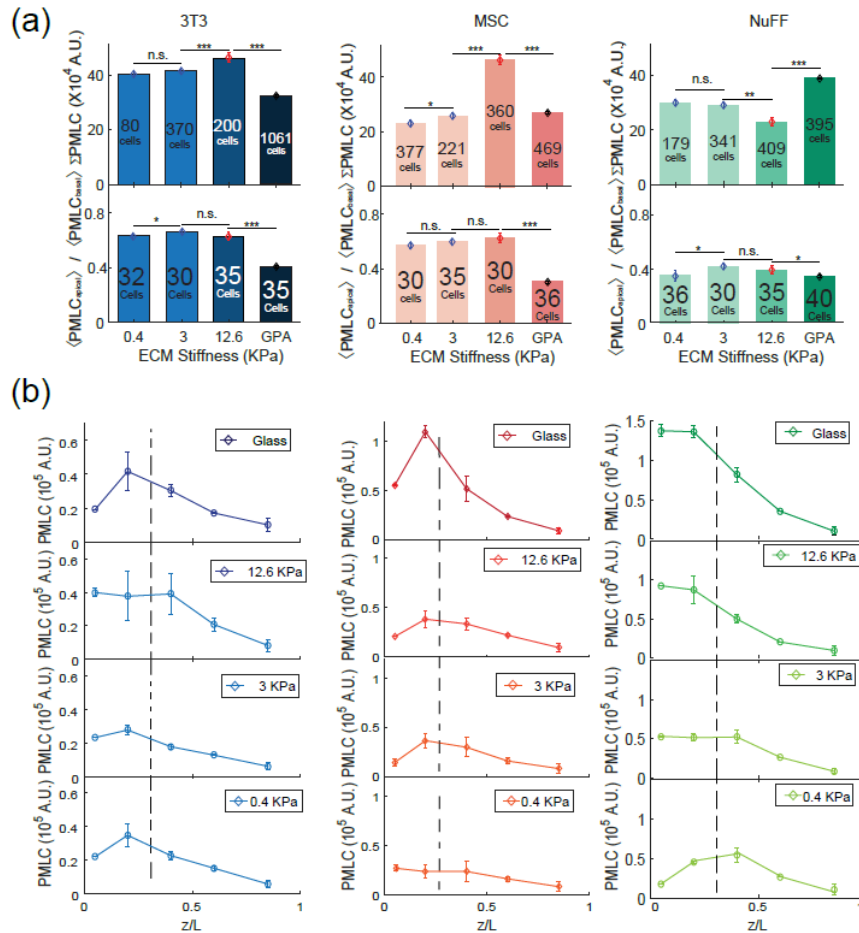
Figure 2.8. Spatial distribution of pMLC from quantitative immunofluorescence. (a) Top row shows average total pMLC (quantified as the total fluorescent signal inside the cell area in epifluorescent images) per condition. Bottom row shows the relative ratio of apical versus basal pMLC (pMLC$_{apical}$ / pMLC$_{basal}$) as measured from confocal zstacks. Average values change for stiffness as well as cell types. (b) Spatial distribution of pMLC throughout the z axis is presented as an average for each condition and cell type. As a general rule, the concentration of pMLC tends to be higher at the bottom of the cell though it can be notices how when substrates are soft, the ratio between apical and basal pMLC decreases. Notice the dashed line represents the cut from apical to basal region (this is defined as 1 μm above the region with stress fibers).

To obtain insights from data, we used immunofluorescence and imaged the distribution of phosphorylated myosin light chain (pMLC) using confocal z-stacks. The level of pMLC is a measure of active myosin assemblies in the cell and is a direct measure of σ_a. We also expect pMLC to reflect the level of λ, since ΔP is likely to be spatially uniform and is governed by cell osmotic control. Figure 2.7 and Figure 2.8 show the measured vertical distribution of pMLC from confocal measurements for all stiffness conditions.

On the average, pMLC is more concentrated near the basal surface on stiffer substrates, and more uniformly distributed across the apical cell surface on softer substrates (Figure 2.8, a and b), in accordance with previous measurements (Han *et al.*, 2012). This trend is reflected by the apical versus basal pMLC ratio, $pMLC_{apical}$ /$pMLC_{basal}$, where $pMLC_{apical}$ is defined as mean intensity above the dotted line in Figure 2.8b and $pMLC_{basal}$ is defined as the mean intensity below the dotted line (Figure 2.8b). The dotted line separates the basal layer of the cell from the apical region and is defined as the z-position 1 μm above the z-position that displays basal stress fibers. Cells distribute pMLC differently on different substrates, mostly due to integrin engagement and focal adhesion formation (Geiger *et al.*, 2009). It is known that integrins and focal adhesions nucleate actomyosin bundles in stress fibers (Tojkander *et al.*, 2012).

Our mechanical model predicts that the cell volume generally increases with increasing $pMLC_{apical}$ /$pMLC_{basal}$ (Figure 2.9a). This is because greater $pMLC_{apical}$ corresponds to a more hemispherical cell with a greater mean height. Indeed, we can fully explain all average cell volume data under all conditions across three different cell types by measuring the total level of pMLC (measured from epifluorescence) and the pMLC distribution (reported by the apical-to-basal ratio) (Figure 2.9a). To connect measured pMLC intensities with λ, a single fitting parameter is used for each cell type (Supplemental Material and Figure 2.9b). Moreover, treating cells with the ROCK inhibitor Y27632 decreases the overall pMLC level observed in all three cell types, and we observe a corresponding de- crease in cell volume (Supplemental Figure S5). For cells with the same adhesion area, cells exposed to Y27632 showed consistently smaller cell volumes. Therefore, cortical tension and tension distribution can predict cell volume, based on the cortical force–balance condition.
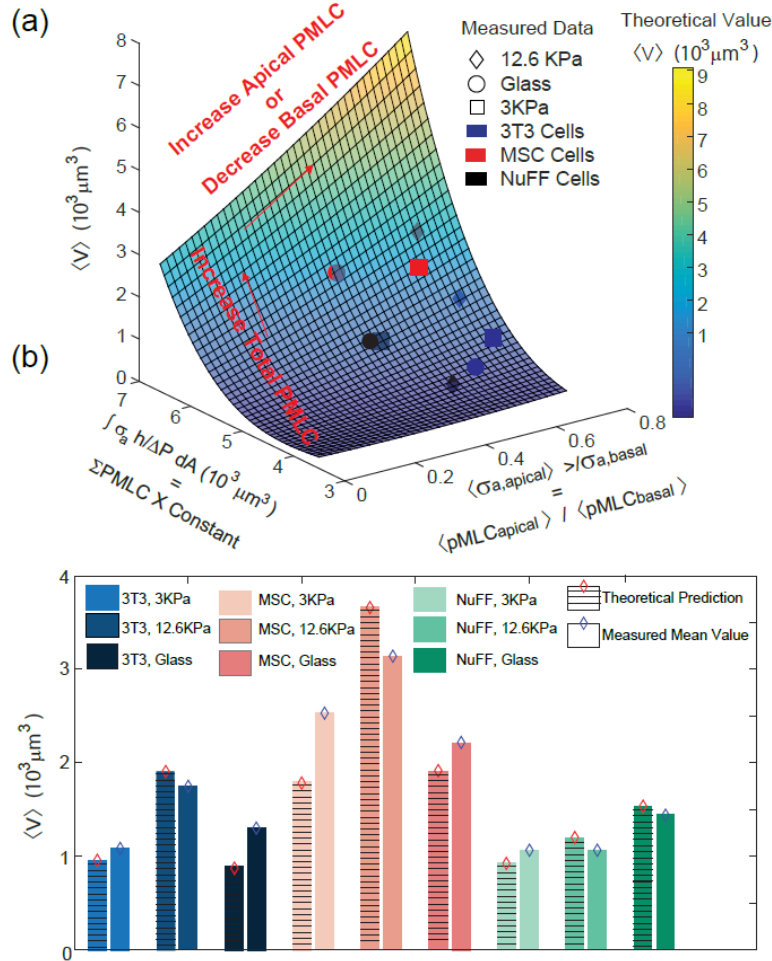
Figure 2.9. Theoretical predictions versus measured data. (a) Estimated volume considering a range of values for the total pMLC and its distribution. The values considered where those to fit the experimental range. In each one of our cell types the volume has been scaled to the volume measured in glass, and a single fitting parameter has been used to relate total pMLC with integrated $\lambda = \int (\sigma_a h / \Delta P)\, dA$. (b) Each one of the predictions for volume are explicitly compared.

2.4.3 *Cell tension, growth, and connections to the Hippo signaling pathway*

We have shown that cell cortical tension and the spatial distribution of pMLC can explain observed cell volumes on different substrates. However, it is not clear how the cell regulates growth and volume increase over the cell cycle and determine the cell volume at division. One possibility is that as cortical tension adjusts to increasing cell mass, the mechanical cue from increasing cortical tension can be a signal for regulating cell growth and division. YAP and its paralogue TAZ are downstream effectors of the Hippo pathway and have been shown to respond to the stiffness of the

substrate (Dupont *et al.*, 2011). To examine the relationship between cell tension as measured by pMLC and YAP/TAZ, we performed quantitative immunofluorescence measurements, stained YAP/TAZ, pMLC, and DNA for all three cell types under all conditions, and quantified single-cell YAP/TAZ and pMLC levels using widefield epifluorescence (Figure 2.10). The antibody used stained for both YAP and TAZ, and therefore, from here on, YAP refers to both YAP and TAZ. Qualitatively, NuFFs and 3T3s show predominantly nuclear localization of YAP (Supplemental Figure S6g) under all conditions; however, the total amount of nuclear YAP, denoted as ΣYAP_n, did show a significant correlation with the average cell volume under all conditions (Figure 2.10b). The mean cytoplasmic YAP intensity was not observed to vary significantly between conditions, though there was consider- able cell–cell heterogeneity. For this reason, we did not find the YAP nuclear/cytoplasmic ratio to be a useful measure of activity in these cell lines. Note that the cell volume as a function of the substrate stiffness shows opposing trends in NuFFs and 3T3s. Cells have highest volume on 12.6 kPa for 3T3s, but lowest volume on 12.6 kPa for NuFFs. Nevertheless, for both cell types, higher cell volume corresponds to higher levels of nuclear YAP. Both cell types show the highest cell volume and the highest level of nuclear YAP with aphidicolin treatment (Supplemental Figure S8, g–i).

Moreover, the total level of pMLC is correlated with total nu- clear YAP, both at the individual cell level (Figure 2.10, a and b) and at the population average level across all conditions (Figure 2.10b). Here, 3T3s show a continuous rise in nuclear YAP level with in- creasing pMLC, but the nuclear YAP level saturates in NuFFs with increasing pMLC, suggesting that other factors may be at play in controlling nuclear YAP in NuFFs that are absent in the standard 3T3s.
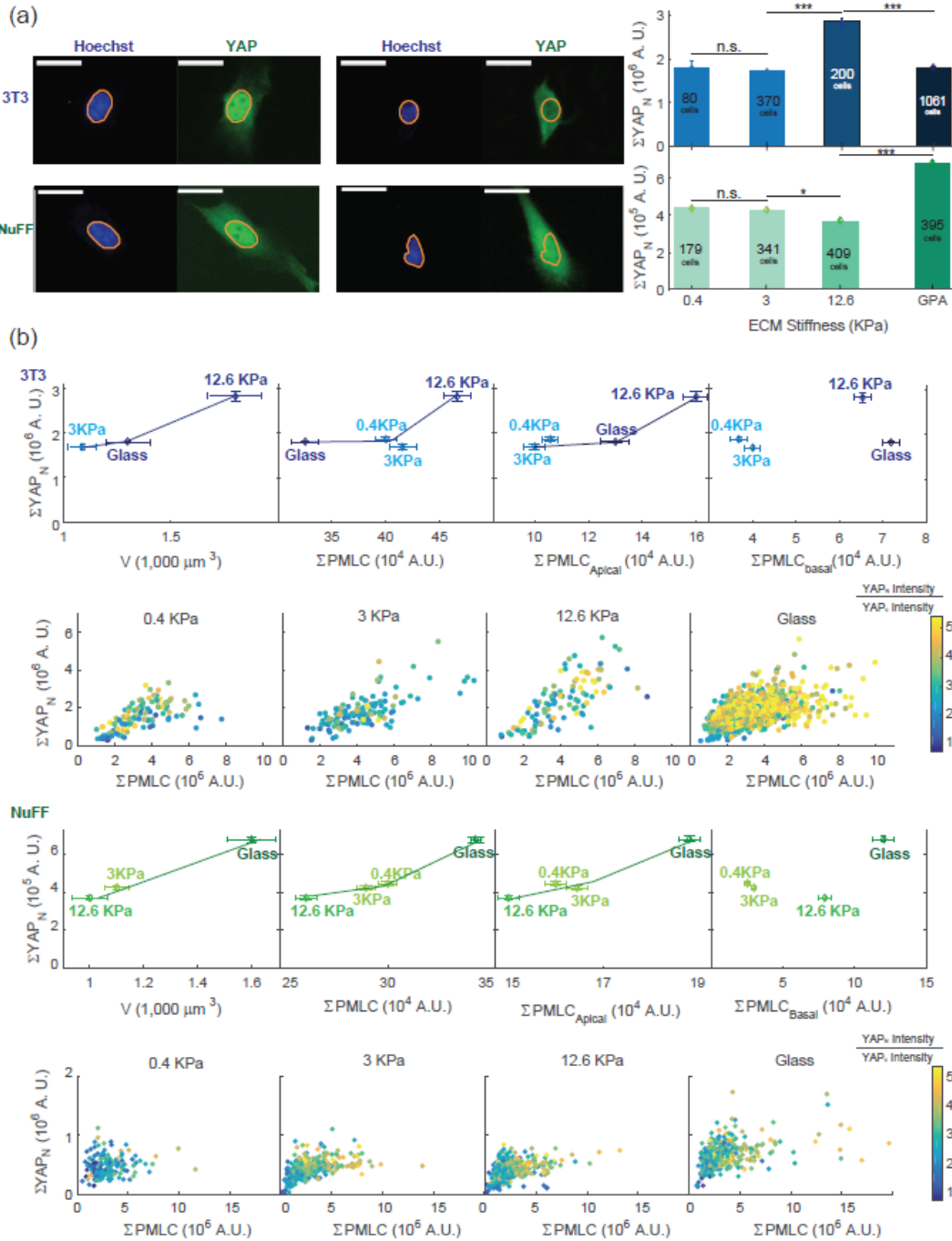
Figure 2.10. Cell Volume is correlated with nuclear YAP/TAZ level in 3T3s and NuFFs. (a) Immunofluorescence widefield images with YAP in green and DNA in blue. The DNA channel is used to mask the nuclear region. The total nuclear YAP (ΣYAP_N) is obtained from epifluorescence images for different stiffnesses. (b) The total average nuclear YAP is plotted vs. the average measured cell volume, average total pMLC level, and apical and basal pMLC levels. The individual cell data are also plotted in panels below and color-coded by the nuclear YAP

intensity/cytoplasmic YAP intensity ratio. At both the single-cell and ensemble levels, higher nuclear YAP is correlated with higher total pMLC. Higher nuclear YAP is also correlated with larger cell volume and higher apical pMLC, even though NuFFs and 3T3s display opposing trends as functions of substrate stiffness. Nuclear YAP is not correlated with basal pMLC. For NuFFs, nuclear YAP seems to plateau at large ΣpMLC, suggesting that nuclear YAP level reaches a maximum even as pMLC level is increasing. This suggests that there is another signal limiting nuclear YAP levels in NuFFs. Note that in both 3T3s and NuFFs, the nuclear-to-cytoplasmic YAP concentration ratios are generally higher than 1. Visually, nearly all cells appear to have significant nuclear YAP. (Scale bar = 10 μm. All error bars represent standard error. Statistical significance: ***$p < 10^{-6}$; *$p < 0.01$; n.s.: $p > 0.05$. Number of cells for epifluorescence imaging: for 3T3s: $N = 80$ on 0.4 kPa, $N = 370$ on 3 kPa, $N = 200$ on 12.6 kPa, and $N = 1061$ on collagen-coated glass; for NuFFs: $N = 179$ on 0.4 kPa, $N = 341$ on 3 kPa, $N = 409$ on 12.6 kPa, and $N = 395$ on collagen-coated glass.)

From confocal images, it is possible to estimate the relative proportion of pMLC above the basal surface (apical surface) versus the pMLC in the basal surface of the cell (Figures 2.8, a and b, and 2.10b). Because it is the apical surface of the cell that determines the cell volume, we compute the total apical pMLC by summing apical intensities from Figure 2.8b. We observe that the level of apical pMLC is correlated with nuclear YAP for all conditions, whereas basal pMLC is not correlated with nuclear YAP (Figures 2.10b and 2.12b). These results directly implicate apical pMLC, and not total pMLC, as a possible signal for nuclear translocation of YAP. We speculate that this could be because apical and basal pMLC (associated with adhesions) may be biochemically distinct to serve different signaling functions in the cell.

2.4.4 *MSCs show bifurcated cell tension dependence*

In fully differentiated cells, we observed that apical pMLC is correlated with the level of nuclear YAP. Under conditions where cell volume is higher, the average nuclear YAP level is also higher. When we examine the same type of data for MSCs, these relationships no longer hold (Figure 2.11 and Figure 2.12). While on the average the cell volume is correlated with nuclear YAP, nuclear YAP is no longer positively correlated with pMLC or apical pMLC. When we examine single-cell data, we discover that depending on the stiffness of the substrate, the correlation between total nuclear YAP and pMLC bifurcates, showing two distinct branches. As substrate stiffness increases, there appear to be more cells in the lower branch with lower nuclear YAP. The upper branch generally contains cells with lower nuclear-to-cytoplasmic YAP–intensity (N/C) ratio and higher overall YAP expression. The lower branch contains cells with higher N/C ratio, but lower

overall YAP as well as lower nuclear YAP (Figure 2.11, b and c; Figure 2.12a). The relative proportion of cells in the upper branch decreases with increasing stiffness, which is consistent with the results of Dupont *et al.* (2011). Interestingly, only a single branch is observed in the cell area versus volume correlation (Figure 2.4a). We hypothesize that the two branches in the nuclear YAP/pMLC correlation represent two phenotypes of MSCs, although more than 99% of our MSC population stained positively for both stem markers: CD90 and CD105 (Supplemental Figure S7). Clearly, these cells are not distinguishable through the use of these common differentiation markers. Stem cells might be sensitive to their neighboring cell identity (Smith *et al.*, 2015) and cell density; it is possible that cell phenotype is influenced by the local environment.
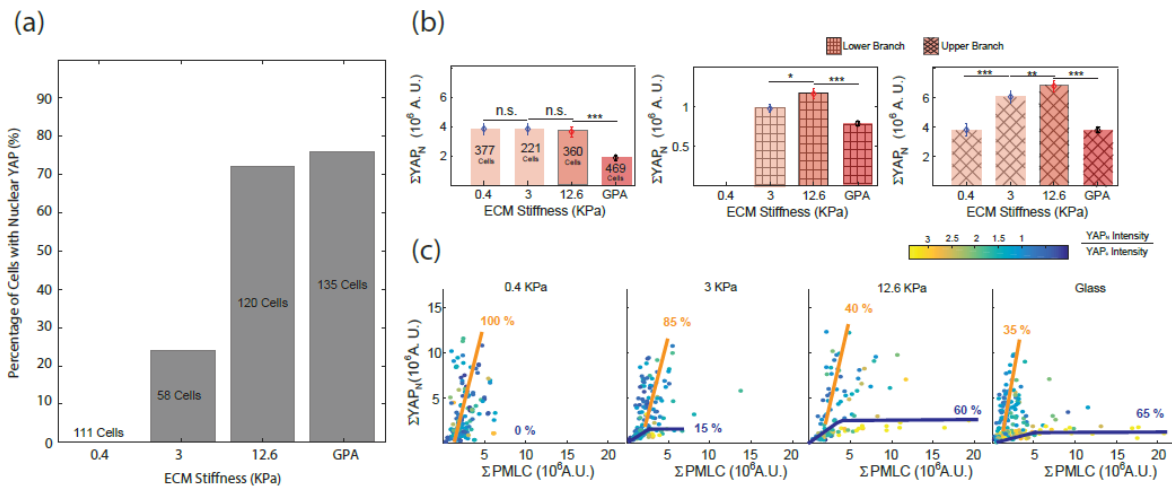
Figure 2.11. MSCs show bifurcated behavior in YAP nuclear localization and pMLC level. (a) Percentage of MSCs showing nuclear YAP localization. With increasing stiffness, more cells contain nuclear YAP, in agreement with Dupont *et al.* (2011). (b) The measured total amount of nuclear YAP, ΣYAP_N, decreases with increasing stiffness. (c) Closer examination of single-cell nuclear YAP and pMLC data shows bifurcated behavior on different substrates. On stiffer substrates there are two branches. The upper branch has high overall YAP expression, but low nuclear-to-cytoplasmic (N/C) YAP intensity ratio. The lower branch has lower overall YAP expression, but high N/C. The proportion of the upper branch cells decreases with increasing stiffness. Thus, on softer substrates, it appears that most cells have a lower N/C YAP ratio. On stiffer substrates, there are more cells with high nuclear N/C YAP ratio. (All error bars represent standard error. Statistical significance: ***$p < 10^{-6}$; **$p < 0.001$; *$p < 0.01$; n.s.: $p > 0.05$. Number of cells: $N = 377$ on 0.4 kPa, $N = 221$ on 3 kPa, $N = 360$ on 12.6 kPa, and $N = 469$ on collagen- coated glass.)

To check whether cell tension and YAP relationships still hold for the observed branches, we examined the nuclear YAP and pMLC correlations for the separate branches, while assuming that their average cell volumes are similar. We included only cells that are distinct in either branch, and exclude cells that have low nuclear YAP and low pMLC near the origin. The upper/lower branch is de- fined by cells with ΣYAP_n higher/lower than the plateau drawn in Figure 2.11b, c. We find that for individual branches, the correlations between ΣYAP_n, cell volume, and apical pMLC are again preserved (Figure 2.12b).
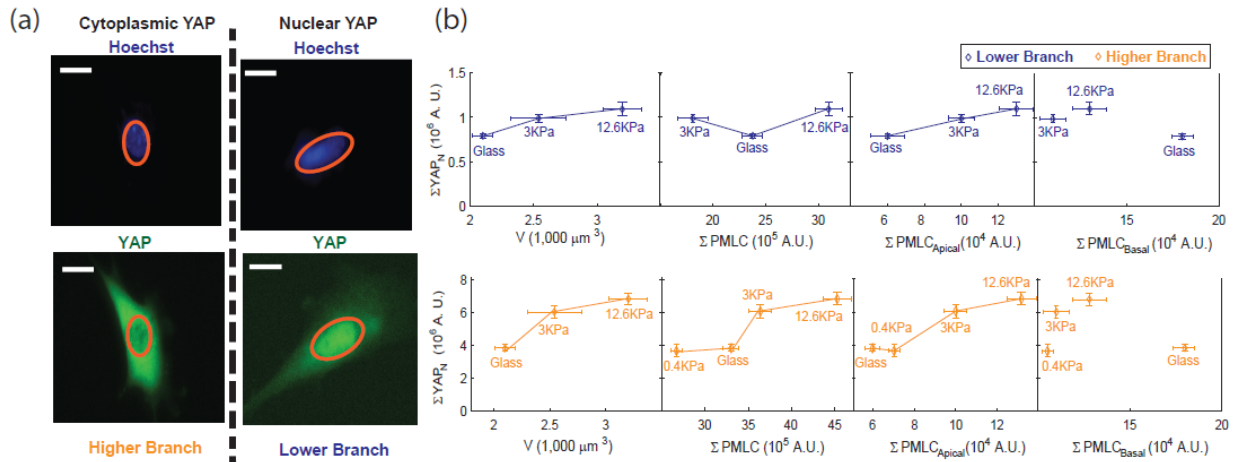
Figure 2.12. MSCs bifurcation can be split. (a) Representative images of MSCs with nuclear YAP localization and cytoplasmic YAP localization. (b) When the total nuclear YAP is plotted vs. volume, pMLC, and apical pMLC, the positive correlation between nuclear YAP and these variables is recovered, similarly to 3T3s and NuFFs. These two branches correspond to the split made in figure 11. Cells in these separate branches are both positive for MSC markers CD90 and CD105 (Supplemental Figure S7). These results suggest that these are two branches that may not be distinguished by typical MSC differentiation markers. (All error bars represent standard error. Statistical significance: ***$p < 10^{-6}$; **$p < 0.001$; *$p < 0.01$; n.s.: $p > 0.05$.

If YAP plays a role in cell cycle and growth regulation, then the level of myosin can potentially influence YAP phosphorylation and allow the cell to sense its own size. Indeed, our data are suggestive of a size checkpoint between G1 and S that is determined by cell tension. Figure 2.13 and Figure 2.14 show the same nuclear YAP and pMLC correlation, but now labeled by cell DNA content. Nuclear YAP level rises with increasing pMLC at different rates on different-stiffness substrates, but the maximal YAP_n is reached at the same level of pMLC (Figure 2.13 and Figure 2.14). However, there is diversity in this behavior. For 3T3s, nu- clear YAP seems to continue to

increase in S/G2 together with pMLC and the rate of YAP_n increase depends on the substrate. In NuFFs, YAP_n still increases with pMLC in G1 and stops rising at the same level of pMLC, but there are some cells in G1 with high pMLC at the level of the YAP_n plateau. The plateau value varies with substrate stiffness. The G1 cells with high pMLC are likely very high in volume. For MSCs in the lower branch, the behavior is similar to that of NuFFs, showing a stiffness-dependent YAP_n plateau. MSCs in the upper branch are entirely different. They have high YAP expression, but no obvious checkpoint based on tension between G1 and S or distinguishing YAP levels between G1 and S. Recent work on confluent epithelial cells also suggests that cell tension influences the cell cycle (Uroz *et al.*, 2018), consistent with the tension checkpoint idea presented here.
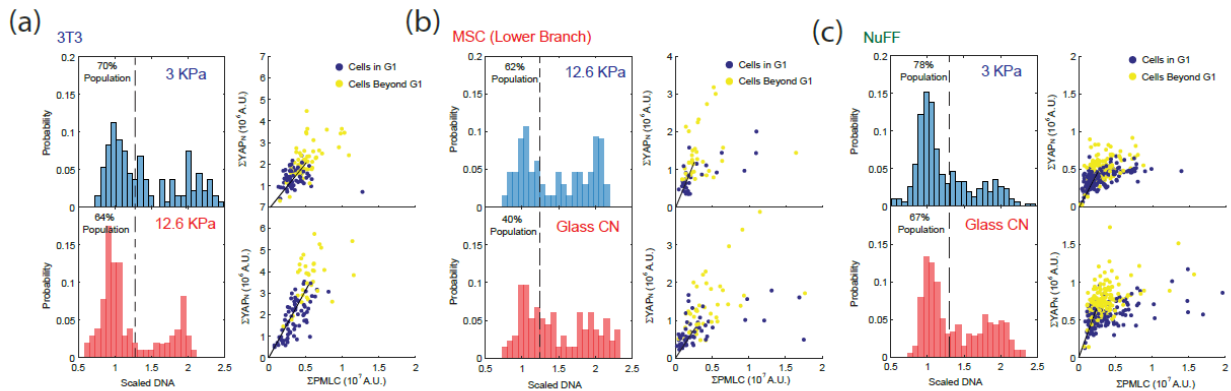
Figure 2.13. Nuclear YAP and pMLC relation suggests a late G1 checkpoint based on cell tension. (a) Two stiffness conditions with the greatest difference in average cell volume are selected for 3T3s, MSCs, and NuFFs. The DNA histogram (left) is shown together with the total nuclear YAP vs. the total cell pMLC level (right). Cells are colored by their DNA content, with G1 cells identified as cells with DNA content below the dashed line in the DNA histogram (1.25 in the scaled DNA level). Cells beyond G1 have higher levels of nuclear YAP and pMLC. The rate of nuclear YAP and pMLC increase, however, varies with condition and cell type.
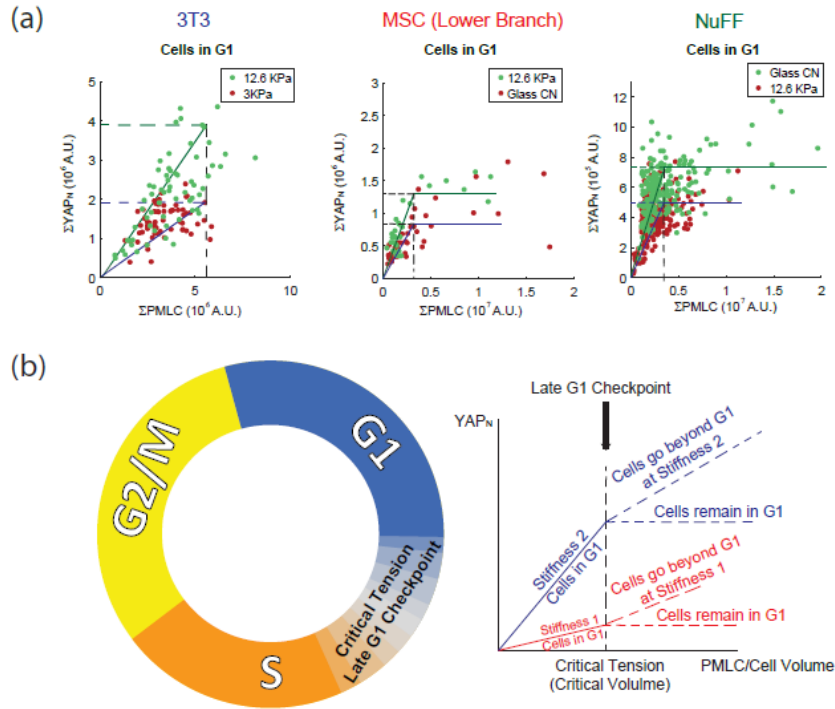
Figure 2.14. Similar levels of pMLC at the single cell level fit G1 tension checkpoint theory. (b). When cells in G1 under different conditions are compared, we observe that nuclear YAP rises with pMLC in G1 until a critical pMLC level is reached, suggesting a checkpoint based on cell tension. For 3T3s, cells proceed to S after the critical level of pMLC and nuclear YAP continues to rise with pMLC. For NuFFs and the MSC lower-branch populations, cells in G1 can continue to increase in pMLC and cell size, but the nuclear YAP level plateaus after the critical level of pMLC. (c) G1–S transition checkpoint based on cell tension. Nuclear YAP increases with increasing pMLC until a common critical tension level is reached, at which the cell transitions from G1 to S. If cells continue to grow in G1, nuclear YAP does not increase after the critical tension, but plateaus. These cells are presumably arrested in G1.

2.5 Discussion

Cell volume is a fundamental property of living cells, and understanding how cells control their growth and volume has implications for development and wound healing as well as a variety of diseases. By performing quantitative immunofluorescence and single-cell volume measurements, we discovered that cell volume depends on cell adhesion area and substrate stiffness. This dependence may be explained by how cells balance forces at the cell surfaces. At an upstream level, cells can sense mechanical force changes in the cell membrane through tension-sensitive ion channels and the Rho pathway. When the cytoplasmic pressure, ΔP, increases (e.g., from import of organic molecules and ions to make more proteins), the cell also increases water content and

increasingly activates RhoA and myosin contraction as more proteins are synthesized through the cell cycle. As a result of this regulatory system, as the cell grows, more active myosin is developed in the cortex. The spatial distribution of myosin depends on additional factors such as integrin engagement and substrate stiffness, but the overall active myosin content must increase with increasing cell size. We find that the level of apical myosin, or myosin not engaged with integrin adhesions and stress fibers, is directly related to the nuclear YAP level, which also explains why β-integrin influences YAP nuclear localization (Elosegui- Artola *et al.*, 2016).

In addition to the proposed mechanism of a tension-based cell cycle checkpoint, we find that cell volume under different conditions can be explained quantitatively from a theoretical model of 3D cell shape. We also discover that synchronization using serum starvation and aphidicolin have opposite effects on cell volume. The heterogeneous distribution of cell volume can be understood by considering the distribution of cells through the cell cycle. The cell cycle distribution is not uniform, but concentrated near younger cells. Because expression levels of many proteins depend on the cell cycle, this result suggests that cell cycle–averaged expression-level changes would depend heavily on the relative duration of each cell cycle phase (Wang *et al.*, 2018). Any perturbations that influence the cell cycle would indirectly influence the expression of many types of proteins. The YAP and the Hippo pathways have been proposed to influence the cell cycle (Shen and Stanger, 2015). Quantitative single-cell measurement would reveal how mechanical tension and the Hippo pathway can regulate cell growth and proliferation in a variety of conditions.

Chapter 3: YAP/TAZ as a novel regulator of cell volume

The relationship we established in chapter 2 between stiffness and cell volume determination highlights the underlying physical principles that dominate morphological features of the cell. Indeed, it is the balance of forces in all levels within the cell that determine its shape. In the last part of chapter 2, we explored the relationship between our tension reporter pMLC, volume and the mechanotransducer YAP/TAZ and discovered that in all conditions, YAP/TAZ was well correlated with cell volume. To break the correlation, we took a step further and sought to determine if YAP/TAZ expression does determine cell volume and how, which is the core of this chapter.

3.1 Introduction

The question of cell size is at the core of how organisms coordinate cell growth and proliferation. The importance of cell volume is not limited to growth, development and tissue homeostasis, its dysregulation has been broadly used as a biophysical marker for disease (Kozma and Thomas, 2002; Dannhauser et al, 2017). At a basic level, with an increase in cell size, the surface to volume ratio shrinks, potentially altering the ratio of membrane-bound components to cytoplasmic components, thus fundamentally changing both inter and intra-cellular signaling dynamics.

Recently substantial progress has been made towards understanding cell volume regulation largely enabled by the development of more quantitative single cell tools to directly measure single cell volume in normal culture (Sakaue-Sawano, 2008; Varsano, 2017; Cadart et al, 2018). To study cell volume in a high throughput manner, we use the fluorescence exclusion method developed by Bottier et al. and others (Cadart et al, 2017; Bottier et al, 2011; Perez Gonzalez, Rochman, Tao et al, 2018), as it is already been used to reveal that mitotic cells swell before cytokinesis (Zlotek-Zlotkiewict et al, 2015) and that some types of cells reveal a near-adder type of behavior regarding cell volume homeostasis (Cadart et al, 2018).

In previous work, we demonstrated a relationship between cell volume, cell apical cortical tension as measured by phosphorylated myosin light chain (pMLC), and YAP/TAZ activity (Perez Gonzalez, Rochman, Tao et al, 2018). We reported mean YAP/TAZ activity is a good predictor of mean cell volume across different cell lines and substrates. Here, we demonstrate using single cell volume measurements that YAP/TAZ plays an important role in cell volume regulation. The relationship between the Hippo pathway and morphological changes in the cell has already been hinted at in the literature, largely relying on flow cytometry and visual inspection (Pouffle et al, 2018). In this work, we measure cell volume of human embryonic kidney cells across a group of CRISPR knockout cell lines from the Hippo pathway and demonstrate that the role of YAP/TAZ in cell volume regulation must not be limited to its influence on total cell cycle duration and cell shape nor through its connection with mTOR. We implicate YAP/TAZ in the regulation of cell division volume and motivate the possibility that the Hippo pathway may be involved in modulating cell tension, and thus cell volume, throughout G1/S cell cycle checkpoint.

3.2 Experimental Procedures

3.2.1 *Cell Culture*

HEK 293A were a gift from Kun-Liang Guan (UCSD, San Diego, California), CRISPR KOs on the Hippo pathway were provided by Dr. Guan. LATS1/2 was generated as detailed on Meng et al. (2015) whereas the YAP KO, TAZ KO and YAP/TAZ dKO was generated as detailed Plouffe et al. (2018). The cells were cultured in Dulbecco's modified Eagle's media (Corning) supplemented with 10% fetal bovine serum (FBS; Sigma) and 1% antibiotics solution [penicillin (10,000 units/mL) + streptomycin (10,000 µg/mL); Gibco] at 37 °C and 5% CO_2.

3.2.2 *Cell Size Measurements*

Cells were sized and counted with a Coulter Counter (Multisizer 3, Beckman Coulter, Fullerton, CA) using an orifice size of 50 µm and a lower size measurement limit of 1 µm. In addition to the Coulter Counter measurements, cells were alternatively used by flow cytometry with the following protocol: First, cells were resuspended in dmem+10%FBS+1%P/S. The sample was centrifuged at 1500 rpm for 5 minutes. The supernatant was removed, and the cells were resuspended in 5 mL of PBS into the tube. After this, the cells were counted the cells using a hemocytometer. We

centrifuged 1 mL with 500,000 cells at 1500 rpm for 5 minutes. We proceeded to remove the supernatant and resuspended cells into 500 μL of ice-cold PBS. Afterwards, we added 4.5 mL of ice-cold 70% ethanol in 0.5 mL increments and vortexed in every iteration. This was followed by placing the cells in ice or freezer overnight. After this, we centrifuged again at 1500 rpm for 5 minutes to later remove the supernatant and resuspend cells in 1 mL PBS. To have nuclear signal we pipetted 10 μL of Stock Hoechst 33342 (final Hoechst concentration should be 100 μg/mL) and incubated cells for 60 minutes. Finally, we transferred the mix into a test tube with a Corning Falcon Test Tube with Cell Strainer Snap Cap (i.e. filter) and measured the fluorescence intensity using a SH800S Cell Sorter.

3.2.3 *Cell Size Microfluidic device fabrication*

The microfluidic device fabrication for the device used in this work is the same as described in section 2.2.2.

3.2.4 *Cell Volume Measurements*

Micro-fluidic chambers were exposed to 30s oxygen plasma before being incubated with 50 μg/mL of type I rat-tail collagen (Corning; 354236) for 1 hr at 37 ℃. The chambers were washed with 1X PBS before approximately 50,000 cells were injected into them. The dishes were then immersed in media to prevent evaporation. There is one important difference with the protocol in this work compared to that described in section 2.2.4. Here, cells were seeded with 0.1 μg/mL of Alexa Fluor 488 Dextran (MW 2000 kD; ThermoFisher) which is a heavier dye that was used to slow down endocytosis in long term experiments. Then cells were allowed to adhere in the incubator at 37 ℃ with 5% CO_2 and 90% relative humidity and then imaged within 12 hours. The cells were imaged using a Zeiss Axio Observer inverted, wide-field microscope using a 20x air, 0.8 numerical aperture (NA) objective equipped with an Axiocam 560 mono charged-coupled device (CCD) camera. The microscope was equipped with a CO_2 Module S (Zeiss) and TempModule S (Zeiss) stage-top incubator (Pecon) that was set to 37 ℃ with 5% CO_2 for long-time imaging. Differential interference contrast (DIC) microscopy was used to accurately capture the cell area and shape and Epifluorescent microscopy was used to measure volume. Individual

cells were traced using the same algorithm as in chapter 2 (section 2.2.4). Every experiment on cell volume was repeated at least three times with three technical repeats corresponding to the three individual channels in the microdevice. This was done in order to get a normal distribution for each complete dataset.

3.2.5 *Immunofluorescence*

Immunofluorescence was carried out as described as in (Aifuwa et al, 2015) at single cell density (12,000 cells/cm^2 for all HEK 293A cell lines) for 6 hrs and then fixed. The immunostaining protocol is the same as described in section 2.2.5. Antibodies used included: YAP 63.7 (1:100; ms; SC/101199), Phospho-Myosin Light Chain 2 Thr18/Ser19 (1:100; rb; Cell Signaling Technology #3674), pS6 (1:1000, rb, Cell Signaling Technology #5364). DNA was stained as in section 2.2.5 using 20 ug/mL of Hoechst 33342. In addition, in combination with the Hoechst 33342, we used a succinimidyl ester dye (SE-A647), which reacts with lysil groups reported by Kafri et al. (2013).

Wide-field microscopy using the set-up described above was used to measure the total pMLC, YAP/TAZ, ki67, pS6, DNA content, and total protein content of the cells. To obtain spatial information about pMLC we used a Zeiss LSM 800 confocal microscope equipped with a 63X oil-immersion, 1.2 (NA) objective. A 567nm laser was used to image the stained cells. Images were acquired with a resolution of 1024 x 1024, which gives a field of view of 10485.76 μm^2. We imaged the cells with confocal image stocks of total thickness of 20 μm to cover the entire height of the cells. Confocal image slices were spaced 2 μm apart and the pinhole size was 1 μm. Each fluorescent image was analyzed with the same procedure as described in chapter 2 (section 2.2.5). For confocal *z* stacks, the basal layer of the cell is identified when clear stress fibers are seen (as example shown in Fig. S14b). Fig. S14c shows pMLC are mainly cortical, except for basal layer, where some stress fibers can be seen. Therefore, the pMLC within the cell cytoplasm is very minimal compared to cortical pMLC.

Every experiment was repeated two times with two technical repeats on every experiment. In addition, each technical repeat consisted of at least 100 single cell measurements. The sample size for qIF aimed for at least 200 single cells. This dataset size was targeted in order to get a

normal distribution for each complete dataset. Finally, no single cells were excluded during the analysis of these datasets. The only cells excluded we those forming clusters.

3.2.6 *Cell Protein Synthesis Measurement*

SUnSET method (Schmidt et al, 2009) was applied as a measurement of single cell protein synthesis rate. The HEKs were seeded 20,000 cells/ mL in a 24-well plate for 4 hours in the incubator with DMEM (10% FBS, 1% PS) media, and then treated with 10 μg/mL puromycin (P8833, Sigma Aldrich) diluted in dPBS for 10 minutes in the incubator. Cells were fixed using 4% PFA right after puromycin treatment and stained according to immune-fluorescence protocol described above. Anti-puromycin antibody, clone 12D10 (MABE343 EMD, Millipore) was used in the ratio of 1:1000 in BSA as the primary antibody solution and Mouse Alexa Fluor 488 was used in the ratio of 1:1000 in dPBS as the secondary antibody solution.

3.2.7 *Western Blotting*

Cells were lysed in SDS sample buffer (50mM Tris pH 6.8, 2% SDS, 0.025% bromophenol blue, 10% glycerol, 5% Beta mercaptoethanol), and boiled for 5min. Proteins were separated on 8% to 10% Bis-Tris polyacrylamide gels. Immunoblots were performed as previously described (Meng et al., 2015). Antibodies for Lats1 (#9153) and Lats2 were purchased from Cell Signaling Technology Lats2 (5888). YAP 63.7 (sc-101199) was purchased from Santa Cruz (this antibody recognizes both YAP and TAZ). Vinculin (V9131 was purchased from BD Biosciences).

3.2.8 *Statistical Analysis*

To show significance we used a one-way non-parametric anova (we did not assume gaussian distributions given the shapes of the histograms). We performed the Kruskal-Wallis test. We also performed follow up tests comparing the mean rank of each column with the mean rank of a control column of HEK293A. We performed Dunn's multiple comparisons test and obtained the corresponding P-value. For comparison between two groups such as the birth volume and peak volume in figure 1N, we performed an unpaired non-parametric Mann-Whitney test. For

comparison between protein-expression experiments via qIF, we used a one-way ANOVA analysis with a Brown-Forsythe test.

3.3 Results

We used the fluorescence exclusion method to quantify single cell volume as previously described (Perez Gonzalez, Rochman, Tao et al, 2018). Briefly, we fabricated microchannels coated with collagen I (Fig. 3.1a). Single cells were seeded and allowed to adhere. After cell adhesion, medium was infused with fluorescent FITC-Dextran, which evenly labeled the cell surroundings but remained in the extracellular medium within 5 hours (Fig. 3.1b). The epifluorescence images obtained were then segmented (Fig. 3.1c), and the 3D cell volume was computed as depicted in Fig. 3.1d. and reconstructed (Fig. S10a-c)

$$V_{Cell} = \int \left(\frac{I_{background} - I_{above\ cell}}{I_{background}} \right) \left(\begin{array}{c} Channel \\ Height \end{array} \right) dxdy$$
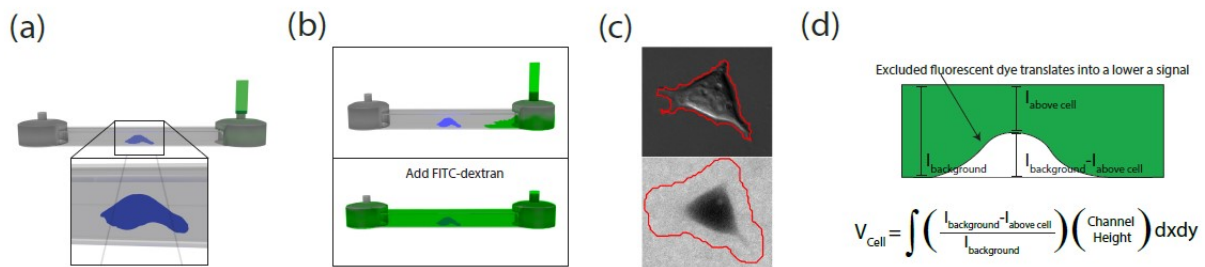
Figure 3.1 Cartoons depicting Fluorescence Exclusion method. (a) Side view of microdevice. In order to estimate the volume for single cells we manufacture long microchannels with an average height of 12μm (b) Fluorescence Exclusion requires addition of fluorescent dye. Cells are seeded in the device before adding the fluorescent dye (top). Once the cells are attached, we flow a combination of media and fluorescent dye. The dye is not permeable through the cell membrane being excluded from the cell interior (bottom). (c) Sample DIC and Fluorescent image for volume calculation. We use the DIC image (top) and the volume channel (bottom) to obtain an accurate segmentation of the cell boundary. Using the theoretical framework, we transform the epifluorescent image to estimate the volume. (d) Theoretical conversion of fluorescence into volume. Side view allows a clear representation of intensity conversion in the images to volumetric units.

3.3.1 YAP/TAZ and the Hippo pathway Regulate Single Cell Volume

Previous work reported positive correlations between the 2D cell adhesion area with cell YAP/TAZ expression (Plouffe et al, 2018), and the 3D cell volume with cell YAP/TAZ activity (defined as nuclear YAP/TAZ content) (Perez Gonzalez, Rochman, Tao et al, 2018). We sought

to further elucidate the relationship between the Hippo pathway and cell volume through the utilization of CRISPR knockouts for Hippo proteins (Fig. 3.2a). Previous studies have shown that in several organisms, the activation of the Hippo pathway is followed by the phosphorylation of YAP/TAZ, leading to inhibition of YAP/TAZ transport into the cell nucleus (Dupont et al, 2011) (Fig. 3.2a). In this pathway, LATS1/2 is responsible for YAP/TAZ phosphorylation and therefore its absence increases YAP/TAZ nuclear import and subsequent activity. Validations of these CRISPR knockouts were performed via quantitative immunofluorescence (qIF) (Fig. 3.2b) and Western Blots (Fig. 3.2c). We found that the average nuclear YAP/TAZ activity increases in the LATS1/2 double knockout (dKO) when compared to the parental HEK 293A, although there is some overlap between the populations. Similarly, in the TAZ KO and the YAP KO, there is a significant decrease in nuclear YAP/TAZ. Finally, qIF for the YAP/TAZ dKO showed low YAP/TAZ activity and low variability, suggesting this corresponds to non-specific binding and is an indication of the level of background noise in our measurement.
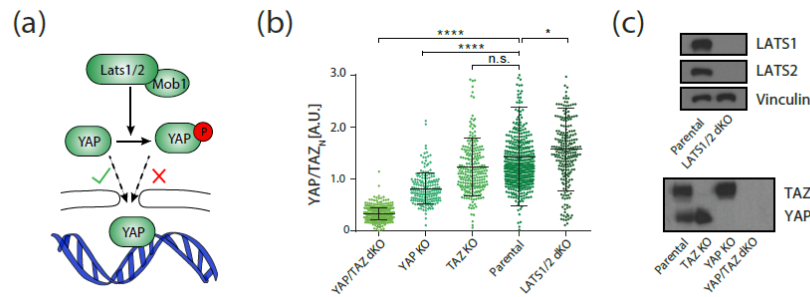
Figure 3.2 Hippo pathway and CRISPR knockouts. (a) Hippo Pathway cartoon. Depiction of key elements of the Hippo pathway. (b) nuclear YAP/TAZ activity by quantitative Immunofluorescence. Hippo pathway activity was assessed by qIF in the parental line and all CRISPR Knockouts ($N_{YAPTAZ\ dKO}$=223, $N_{YAP\ KO}$=156, $N_{TAZ\ KO}$=287, $N_{HEK\ 293A}$=331, $N_{LATS1/2\ dKO}$=207). (c) Hippo pathway Knockout validation. Western Blots were performed to assess Hippo pathway activity in all CRISPR Knockouts.

Across the four CRISPR generated cell lines and the parental HEK 293A, we found that the average amount of nuclear YAP/TAZ strongly correlated with the average cell volume (Fig. 3.3a, b), as seen before for cells growing substrates of varying stiffness (Perez Gonzalez, Rochman, Tao et al, 2018). Accordingly, when comparing volume distributions of all lines (Fig. 3.3a), we found

that YAP/TAZ activity correlates with increasing abundance of larger cells, e.g., LATS1/2 dKO has many large cells and YAP/TAZ dKO has mostly smaller cells. When comparing the average cell volume between populations, we observed an increase of 3.01 % in the LATS1/2 dKO. As YAP/TAZ expression decreased, we observed a volume decrease of 15.8% in the TAZ KO, 18.2% in the YAP KO and 27.2% in the YAP/TAZ dKO (Fig. 3.3b). Additionally, we assessed the cell spreading area, noticing that volume and area are positively correlated with each other, but in some cases a volume change could be observed in the absence of area change (Fig. S1d,e). We also used two more common approaches to assess cell size: Coulter counter (Fig. 3.3d) (Burke et al, 2012; Conlon et al 2001) and flow cytometry (Fig. 3.3c) (Plouffe et al, 2018). Despite requiring the cells to be resuspended, changing their morphology, both the Coulter counter measurements (Fig. 3.3d) and flow cytometry measurements showed similar cell volume trend (Fig. 3.3c).
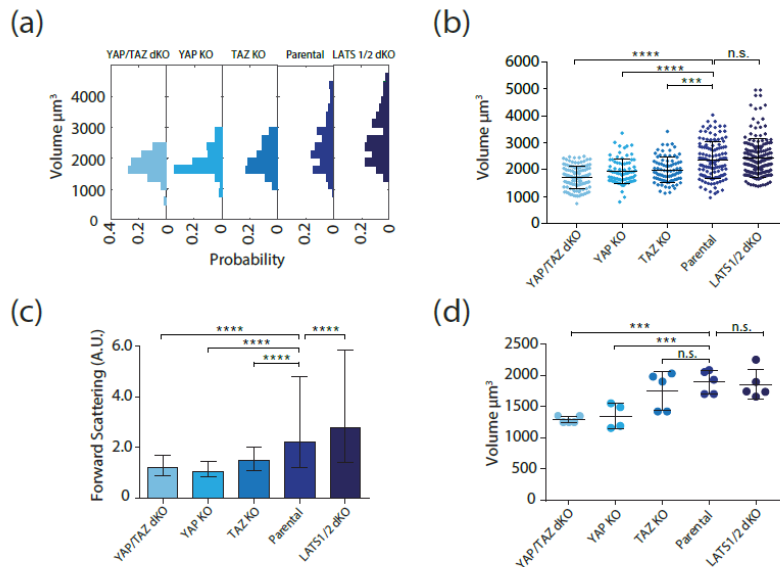
Figure 3.3 Volume measurements across Hippo pathway knockouts (a) Volume measurements of Hippo Pathway Knockouts via FX method. Panel shows the distribution for each cell line ($N_{YAPTAZ\ dKO}=130$, $N_{YAP\ KO}=118$, $N_{TAZ\ KO}=162$, $N_{HEK\ 293A}=135$, $N_{LATS1/2\ dKO}=185$). (b) Volume averages from FX method. Hippo pathway volume averages from figure (a). (c) Volume measurement of Hippo pathway knockouts via Flow Cytometry. (d) Volume measurement of Hippo pathway knockouts via Coulter Counter. ($N_{YAPTAZ\ dKO}=5$, $N_{YAP\ KO}=4$, $N_{TAZ\ KO}=5$, $N_{HEK\ 293A}=5$, $N_{LATS1/2\ dKO}=5$).

In addition to the static cell volume, we examined how the cell volumetric growth rate as well as the volume at the beginning and end of the cell cycle varies with the presence of YAP/TAZ. We tracked single cell volume for five hours within the fabricated microchannels described above

(Fig. 3.4a) and obtained cell growth trajectories (Fig. 3.4b) for each of the five cell lines. A portion of cells undergoing mitosis were observed, for which we measured the volume immediately before and after division (referred to as division and birth volumes onwards). We found that both the cell birth volume and the volume at division increased with the presence of YAP/TAZ (Fig. 3.4c) explicitly confirming that the observed volumetric change corresponds to an intrinsic change in volume within the population.
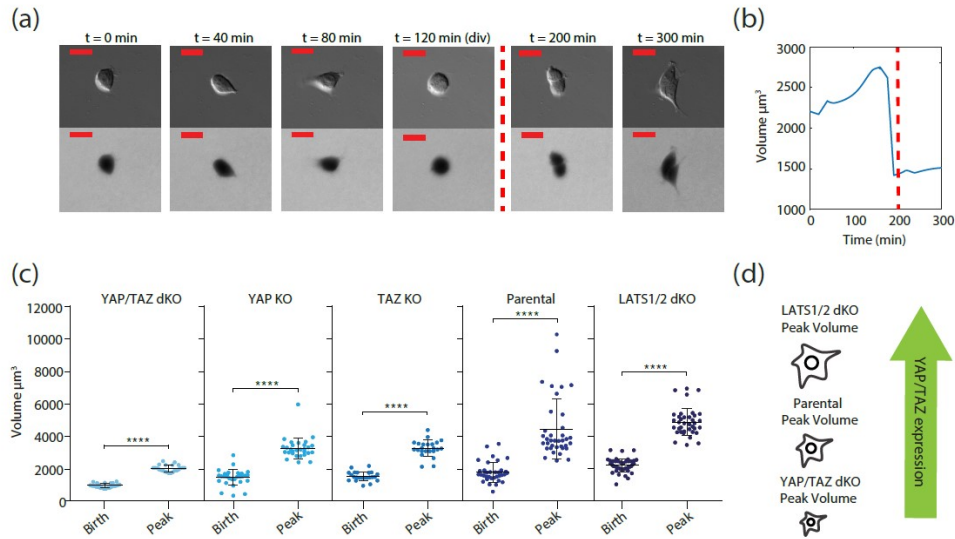
Figure 3.4 Birth and Volume at division are intrinsically changed with varying YAP/TAZ expression. (a) Volume as a function of time. Cells volume was monitored over time for 5 hours. (b) Volume trajectory. Sample trajectory is shown as a function of time for a single cell. (c) Daughter cell volume and volume before division. Averages are presented for the parental cell line and all Hippo pathway KOs. (d) Cartoon illustrating relationship between YAP/TAZ expression and volume.

3.3.2 Single cell growth rate is proportional to cell size and follow a universal growth law

To further understand single cell growth, we quantified added volume per unit time (volumetric growth rate) for many single cells. Fig. 3.5a shows the average cell growth trajectory in blue and the standard deviation as the gray area for each of the 5 cell lines. Fig. 3.5a also displays sample trajectories for each of the cell lines as an inset on the top right of each figure. The degree to which these cell lines display obvious mitotic swelling as previously reported in the literature (Zlotek-Zlotkiewicz et al, 2015) varies with YAP/TAZ activity. The TAZ KO, parental cell line and LATS1/2 dKO display a sharp volume increase and decrease right before division. However, YAP

46

KO and YAP/TAZ dKO show reduced or unresolvable mitotic swelling at the time resolution used in this study.
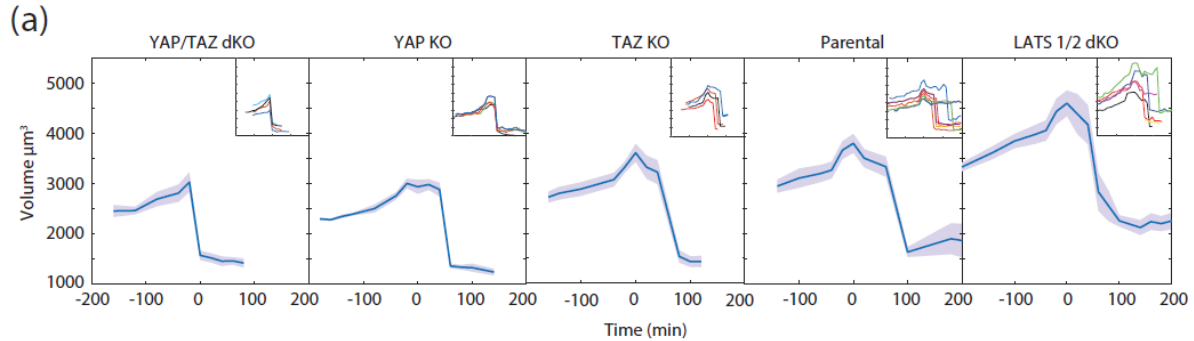
Figure 3.5 Sample and average volume trajectories per cell line. (a) Average trajectory. Average trajectory is shown in blue and the first standard deviation is shown by the gray area. Sample trajectories are displayed in an inset on the top right of every graph to qualitatively show their behavior

To quantify growth trajectories and obtain the growth rate, we fitted an exponential growth law to each trajectory, obtaining dV/dt versus V for each cell (Fig. 3.6a-d). Additionally, we also fitted linear growth curves to the same data (Fig. S11a,b), since it has been noted that it is difficult to distinguish the exponential growth law from the linear growth law (Ginzberg et al, 2015) largely due to the small range of volumes observed within a single cell cycle (roughly a two-fold variation). Indeed, in the next section we discuss that the growth law is unlikely to have a measurable influence on the average cell volume; however, our results show that the volumetric growth rate is proportional to the cell volume across populations. When all growth trajectories for all cells are overlaid (Fig. 3.7a, b), it is apparent that all 5 cell lines follow a similar growth law, i.e., the growth rate $dV/dt \propto V$ regardless of YAP/TAZ activity (and regardless of whether dV/dt for each cell was fitted assuming an exponential or linear dependence on V). The combination of multiple cell lines spanning a much larger range of volumes lends greater confidence to the observation that across populations there is a strong linear dependence of dV/dt on V, indicating an exponential volumetric growth rate with respect to cell volume.
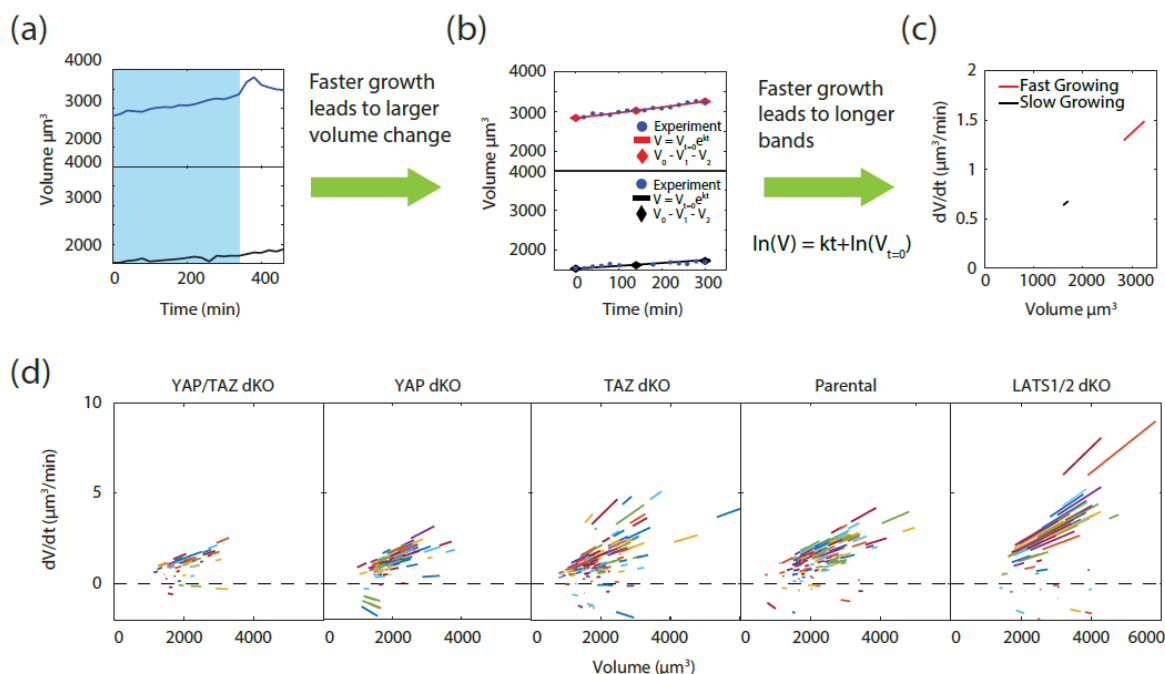
Figure 3.6 Single cell growth rate is proportional to cell size. (a) Description of analysis of volume as a function of time. Two sample volume trajectories are shown, a small cell (bottom panel) and a big cell (top panel). (b) For each cell, we use three points in order to determine the constant for exponential growth. (c) Sample plot of single cell growth rate versus the volume of that cell. (d) Growth rate characterizing volume increase at single cell level. ($N_{YAPTAZ\ dKO}$=130, $N_{YAP\ KO}$=118, $N_{TAZ\ KO}$=162, $N_{HEK\ 293A}$=175, $N_{LATS1/2\ dKO}$=185).

The data shows that the presence of YAP/TAZ seems to be regulating dV/dt with increasing YAP/TAZ activity associated with slightly higher dV/dt. At first glance, this might seem to be the critical observation needed explain how YAP/TAZ and Hippo is regulating cell volume. Thus, it is natural to focus on the regulation of dV/dt. However, average cell volume does not depend only on growth rate, but also the duration of the cell cycle. It can be shown from mathematical considerations that the average cell volume is slightly less than $3/2\tau dV/dt$ (see Perez et al., 2019 in Biorxiv) where τ is the average cell cycle duration. YAP/TAZ has also been shown to regulate the duration of the cell cycle (Pouffle, 2018) (see Fig. 3.8a) with increasing YAP/TAZ activity associated with smaller τ. It is clear that YAP/TAZ is affecting dV/dt and τ in opposite ways (and examining the trend in τ alone is also insufficient to explain volume regulation – see the following section). A larger increase is observed for dV/dt than what would be necessary to compensate for the observed decrease in τ and keep the average volume constant. How YAP/TAZ skews this balance in favor of increased dV/dt remains unclear, and more information regarding the role of

YAP/TAZ in cell cycle regulation may be needed to understand this phenomenon (see Fig. 3.14, 3.15 and 2.16 for more discussion).
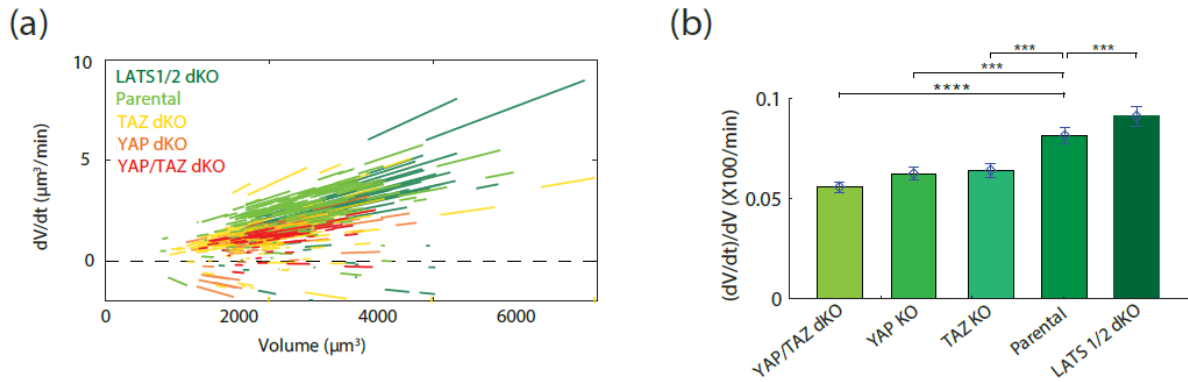
Figure 3.7 Single cell growth rates obey a universal law across Hippo pathway knockouts (a) Growth rate curves overlapped for all Hippo knockouts. (b) Average growth rate per cell line.

Due to endocytosis of FITC-Dextran on longer time scales, we are not able to obtain growth trajectories for the complete cell cycle. Therefore, we are unable to observe correlations between the birth volume and the added volume at the single cell level; however, we do observe a population of cells that exhibit near zero growth over 5 hours, which we interpret as quiescent cells. We observed that cells in quiescence can also transition out of quiescence and grow again. Finally, it is worth noting that growing cells show a continuous and proportional growth rate vs. volume curve, with no visible dependence on cell cycle phase.

3.3.3 Volume differences across Hippo pathway knockouts are not explained by cell cycle duration or volumetric growth law

It is clear how changing the birth and division volumes may affect the average population volume; however, it is also possible that the cell cycle duration, cell cycle phase distribution, and growth rate as a function of volume could impact the mean volume while keeping the birth and division volumes constant. For example, suppose we have a hypothetical cell for which dV/dt is positive during G_1 and zero during S and G_2. Further suppose we can lengthen the duration of G_2 while keeping the birth and division volumes constant. For that cell, lengthening G_2 will increase the

average volume of the population since each cell will spend more time at its maximum volume. We did not observe growth laws of this type in the cell lines utilized for this paper; however, we sought to examine how small variations in the growth law (e.g. comparing the exponential and linear models) may affect average volume. In previous work (Rochman, Popescu and Sun, 2018), we discussed how some conserved quantities may be used to calculate population averages of age-dependent measurements. In particular, volume and DNA distributions for an ensemble may be calculated given the growth trajectory V(t) and DNA content progression DNA(t) (see Perez et al., 2019 in Biorxiv for details). We may compare two cell volume distributions: one obtained with a long cell cycle duration (Fig. 3.8b red curve) and one obtained with a short duration (Fig. 3b black curves). The V(t) curve for the ensemble with the shorter duration will have a steeper rise regardless of whether the growth law is linear or exponential (Fig. 3.8c); however, the resultant volume distributions will be negligibly different (and the difference depends only on whether the growth rate is linear/exponential not on the cell cycle duration) on the scale of variation we observe across the CRISPR knockouts (Fig. 3.8d) see Perez et al. (2019 in Biorxiv) for details. When the ratio of time spent in each cell cycle phase G_1, S, G_2 is conserved, as observed across the CRISPR knockouts (Fig. 3.8f), we also predict the DNA distribution to be independent of cell cycle duration (Fig. 3.8e).
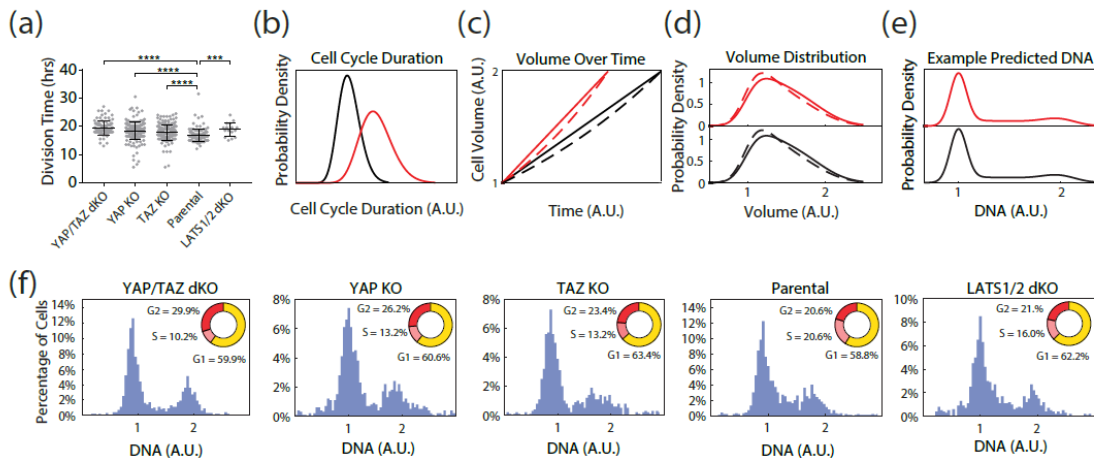
Figure 3.8 Volume difference across Hippo pathway knockouts is independent of aging dynamics (a) YAP/TAZ Decreases Cell Cycle Duration and Bulk Doubling Time. Cell cycle duration and bulk doubling time for the HEK 293A and five KO lines. ($N_{YAPTAZ\ dKO}$=107, $N_{YAP\ KO}$=216, $N_{TAZ\ KO}$=186, $N_{HEK\ 293A}$=122, $N_{LATS1/2\ dKO}$=18). (b) Two population with different cell cycle duration are considered. Long cell cycle duration and short cell cycle duration. (c) Two growth schemes are considered, linear or exponential growth. Further segmentation leads to a solid read line, representing linear growth with short cell cycle duration and a dashed read line, representing exponential growth with

short cell cycle duration. The solid black line, represents linear growth with long cell cycle and a dashed black line, represents an exponential growth with long cell cycle. (d) Volume distributions for each case. $\rho(V)=\int P(V|\varphi)\,\rho(\varphi)d\varphi$. (e) DNA distribution. Predicted from the theoretical framework. (f) YAP/TAZ Does Not Change the Cell Cycle Phase Distribution. A comparison of the DNA distributions across the cell lines examined showed no significant difference (inset cell cycle clock corrected for age see supplemental). ($N_{YAPTAZ\ dKO}$=1137, $N_{YAP\ KO}$=961, $N_{TAZ\ KO}$=774, $N_{HEK\ 293A}$=1202, $N_{LATS1/2\ dKO}$=876).

Thus, cell cycle duration is not predicted to impact the volume distribution, and while modifying the growth law may modestly change the mean cell cycle distribution, only extremely nonlinear trends could replicate the magnitude of variation we observe across the CRISPR knockouts. As we see from Fig. 3.7a, the growth laws for all cell lines are generally similar, and the cell cycle duration for 5 cell lines are also very similar (Fig. 3.8a). Therefore, any impact the Hippo pathway and YAP/TAZ activity may have on the volumetric growth law or cell cycle duration (Fig. 3.8a) alone is unable to explain the volume variation across the CRISPR knockouts.

3.3.4 Volume variations are not explained by cell geometry

In a previous paper **(**Perez Gonzalez, Rochman, Tao et al, 2018**),** we have shown that cell geometry plays a major role cortical force balance and is an important factor in determining cell size. In principle, regulating the spatial distribution of cortical contractility while conserving the osmotic gradient across the cell cortex could result in large changes in cell volume. For example, suppose increasing YAP/TAZ activity decreases cell protrusivity resulting in a more hemispherical cell shape and thus higher curvature. This higher curvature, with the same pMLC expression, leads to a larger contractile force. If the pressure gradient across the cortex were constant, one way to balance that larger contractile force would be to increase cell volume and decrease the curvature while maintaining the same shape. Thus, we sought to examine how cell shape varies with YAP/TAZ activity independently of cell volume and examined the 3D shape where the apical surface was reconstructed from the epifluorescent images used to calculate volume (Fig. 3.9 a, b) and normalized by cell volume (Fig. 3.9c,d). We examined both the raw height profiles (Fig. 3.10a) as a function of the distance from the center of each cell as well as the fitted spherical caps (Fig. S12f). We found that there was no consistent trend in cell shape with increasing YAP/TAZ activity. The YAP/TAZ dKO, YAP KO, TAZ KO, and parental line (HEK293A) were all found to be

remarkably self-scaling. Despite having substantially different volumes, these four cell lines all had similar height profiles. It is interesting to note, however, the LATS1/2 dKO does not exhibit the same shape, spreading more than the others (more "pancake-like"). Thus, the role the Hippo pathway and YAP/TAZ activity may play in cell shape regulation alone cannot explain the variations in volume observed across the CRISPR knockouts.
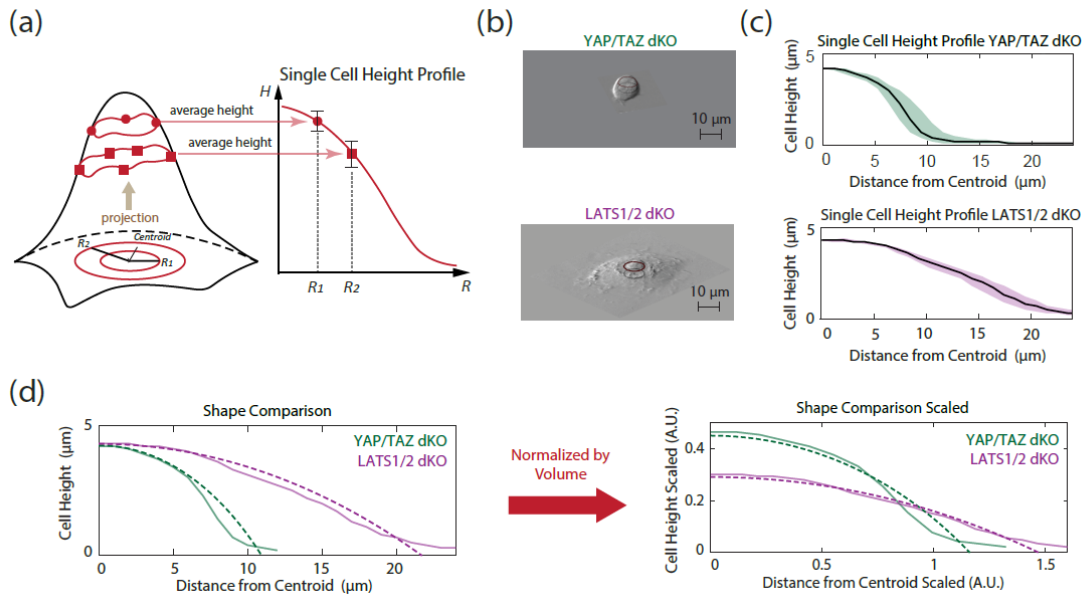
Fig 3.9 Description of analysis of geometry per cell. (a) The Role of YAP/TAZ in 3D Cell Shape – cartoon of analysis. Cartoon depicts single cell profile from volume data (b) 3D rendering. Two sample cells were considered to demonstrate the three-dimensional rendering. Top panel shows the YAP/TAZ dKO and the bottom panel shows the LATS1/2 dKO. (c) Sample profile for two cell lines. Top panel shows YAP/TAZ dKO and bottom panel shows LATS1/2 dKO. (d) Cell shape comparison. Left panel shows the cell height distribution as a function of the radial distance from the cell's center of mass (or volume). Right panel shows the comparison when scaled by volume. The original and volume normalized apical cell shapes with the median height function (solid lines) and best fit spherical cap (dashed lines).
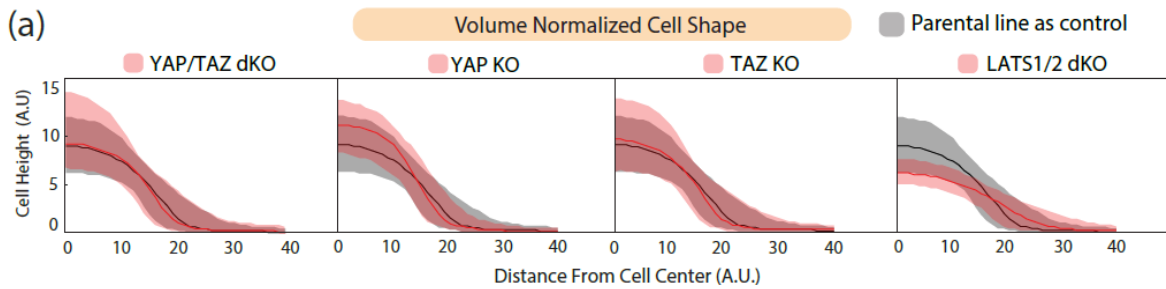
Fig 3.10 Volume difference across Hippo pathway knockouts is independent of geometrical changes. (a) Volume Difference Is Not Explained by Cell Shape. Top panel shows volume normalized median cell height distributions

across each ensemble with the indicated KO in red and HEK293 in gray. Only the LATS1/2 dKO shows a significant difference in 3D apical shape. Bottom panel shows cell spherical cap shape ensemble. The distributions of the best fit spherical caps across each ensemble with the indicated KO in red and HEK293 in gray.

3.3.5 Cell Volume Regulation by YAP/TAZ is independent of mTOR activity

Another possible explanation for the observed cell volume increase with increasing YAP/TAZ activity is from the potential crosstalk between Hippo and mTOR pathways. Hippo pathway has been reported to modulate mTOR pathway in certain conditions. (Tumaneng et al, 2012) showed that in mouse tissue overexpression of YAP leads to the upregulation of AKT through tumor suppressor PTEN, and thus activates mTORC1/2 and downstream components. Over-expression of YAP also increased the level of phosphorylation of both S6K Thr 389 and AKT Ser 473 in tissue.
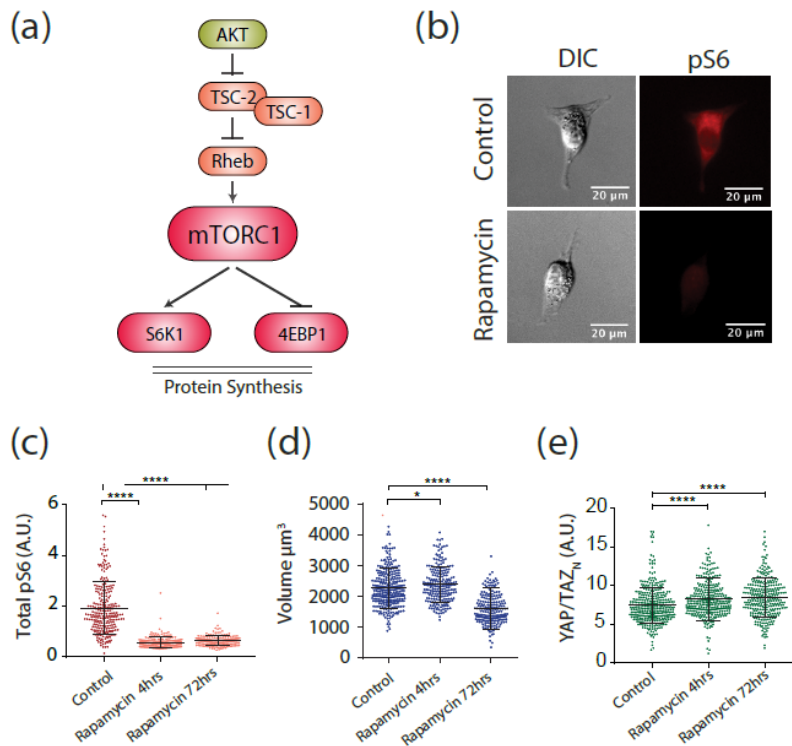
Figure 3.11 Rapamycin decreases volume in parental cell line HEK293A (a) mTOR pathway. Description of the key elements of the pathway. (b) Sample images of control cells and rapamycin treatment. Left two show sample HEK293A cells from control experiment whereas two right images show sample cells from rapamycin treatment (c) Rapamycin inhibition confirmed via qIF. Expression of ribosomal activity reported via qIF of ribosomal protein pS6

($N_{Control}=248$, $N_{Rapamycin-4hours}=196$, $N_{Rapamycin-72hours}=178$). (d) Rapamycin inhibition decreases cell volume at 72 hours of treatment. Volume data for control cells and rapamycin treatment at 4 and 72 hours. ($N_{Control}=314$, $N_{Rapamycin-4hours}=224$, $N_{Rapamycin-72hours}=221$) (e) mTOR inhibition does not affect YAP/TAZ activity. Panel shows nuclear YAP/TAZ expression measured via qIF ($N_{Control}=354$, $N_{Rapamycin-4hours}=326$, $N_{Rapamycin-72hours}=296$)

As mTOR has been described as a major regulator of mammalian cell size due to its relationship with amino acid import and protein synthesis (Fingar et al, 2002; Lloyd, 2013), it is natural to ask whether on the single cell level the regulation of cell volume by Hippo pathway is mediated by the crosstalk between Hippo and mTOR. If YAP/TAZ activity also modulates mTOR activity on the single cell level, the observed cell volume variation in Hippo pathway KOs. In order to explore this potential crosstalk between YAP/TAZ and the mTOR pathway, we first inhibited mTOR using rapamycin and replicated the previously published effect of rapamycin on cell size (Fingar et al, 2002) (Fig. S13a-c). After 4hrs of treatment, mTOR activity is diminished as reported by pS6 expression using qIF (Fig 3.11a, b). However, cell volume did not change significantly after 4 hrs. Instead, a noticeable cell volume decrease of 28.9% occurred after 72 hours, close to the range previously reported (Fingar et al, 2002). In addition, we found that under mTOR inhibition, YAP/TAZ activity remained unchanged, suggesting that mTOR is not an upstream regulator of YAP/TAZ (Fig. S13a, b, d, e).

Next, we sought to characterize mTOR activity (reported to be involved in protein production) in all Hippo pathway KOs, as well as total cell protein content and cell protein synthesis rate. Total cell protein content is measured using the total fluorescence from cells stained with a succinimidyl ester dye (Kafri, 2013). This measurement has already been reported to be well correlated with measurements of dry mass by quantitative phase microscopy (Kafri, 2013). The cell protein synthesis rate is measured using the SUnSET method (Schmidt et al, 2009). By treating cells with low concentration puromycin and staining puromycin labeled pre-mature peptides, we quantified the rate of protein synthesis in single cells by assessing the qIF signal of puromycin labeled peptides within the cytoplasm. We found that although there is major change in YAP/TAZ expression throughout these cell lines (Fig. 3.12b), mTOR activity as measured by total pS6, remained fairly constant (Fig. 3.12a), further ruling out crosstalk between these pathways at the single cell level. We found no change in total cell protein content across 5 cell

lines. The cell protein synthesis rate is also generally constant, with LATS1/2 dKO showing a slight increase.
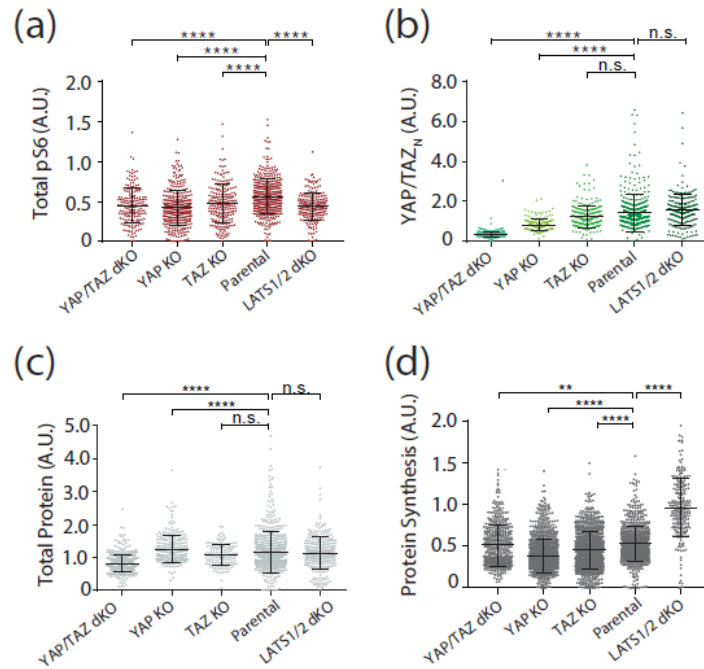
Figure 3.12 Ribosomal activity, total protein and protein synthesis across Hippo pathway knockouts (a) mTOR activity does not change with Hippo pathway knockouts. ($N_{YAPTAZ\ dKO}=177$, $N_{YAP\ KO}=336$, $N_{TAZ\ KO}=218$, $N_{HEK\ 293A}=406$, $N_{LATS1/2\ dKO}=202$). (b) YAP/TAZ activity changes with Hippo pathway knockouts. $N_{YAPTAZ\ dKO}=223$, $N_{YAP\ KO}=156$, $N_{TAZ\ KO}=287$, $N_{HEK\ 293A}=331$, $N_{LATS1/2\ dKO}=207$. (c) Total protein content does not change with Hippo pathway knockouts. $N_{YAPTAZ\ dKO}=664$, $N_{YAP\ KO}=269$, $N_{TAZ\ KO}=150$, $N_{HEK\ 293A}=772$, $N_{LATS1/2\ dKO}=314$). (d) Protein synthesis across Hippo pathway knockouts. ($N_{YAPTAZ\ dKO}=481$, $N_{YAP\ KO}=1027$, $N_{TAZ\ KO}=962$, $N_{HEK\ 293A}=783$, $N_{LATS1/2\ dKO}=219$).

Finally, we asked whether mTOR or Hippo pathways are independent in their regulation of cell volume, and whether they have a synergistic effect. We found that when inhibiting mTOR activity with rapamycin in all Hippo pathway KOs, there was a general trend of obtaining additional volume reduction to what we had already seen in the Hippo KOs (Fig. 3.13a). Only the TAZ KO showed no significant volume reduction after mTOR inhibition. These results suggest that in our conditions, Hippo and mTOR have a synergistic effect in their regulation of cell volume, and act essentially independently (Fig 3.13b).
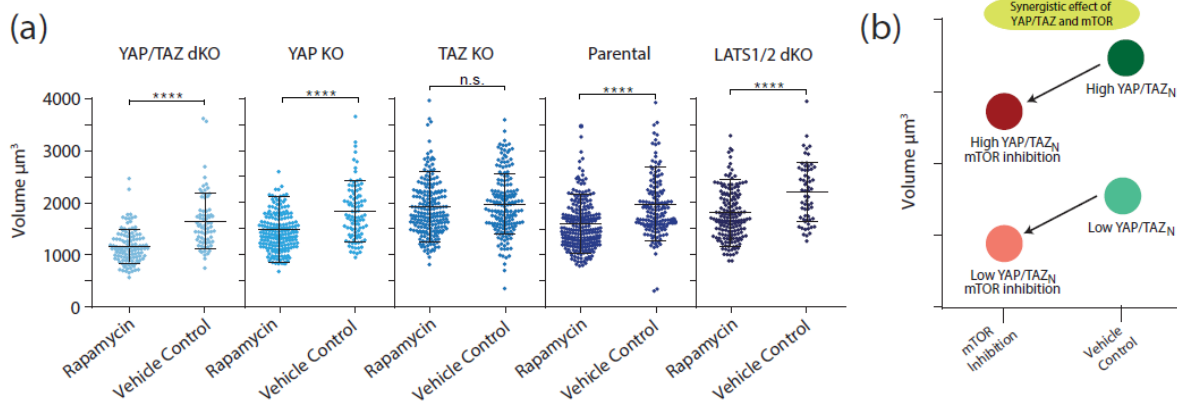
Figure 3.13 Synergistic effect of mTOR pathway and the Hippo pathway (a) Volume measurements on Hippo pathway knockouts and mTOR inhibition. ($N_{YAPTAZ\ dKO\ -\ Control}$ =70, $N_{YAPTAZ\ dKO\ -\ Rapamycin}$=115 , $N_{YAP\ KO\ -\ Control}$= 95, $N_{YAP\ KO\ -\ Rapamycin}$=193, $N_{TAZ\ KO\ -\ Control}$=176, $N_{TAZ\ KO\ -\ Rapamycin}$=206, $N_{HEK\ 293A\ -\ Control}$=154, $N_{HEK\ 293A\ -\ Rapamycin}$=258, $N_{LATS1/2\ dKO\ -\ Control}$=61, $N_{LATS1/2\ dKO\ -\ Rapamycin}$=169) (b) Cartoon of synergistic effect of YAP/TAZ and mTOR volume control.

3.3.6 Tension regulation through G1/S checkpoint could explain cell volume variations.

So far, we have demonstrated that all volume changes observed due to the modulation of YAP/TAZ activity are not explained by the role of YAP/TAZ in the regulation of the volumetric growth rate (Fig. 3.5, 3.6 and 3.7), cell cycle duration (Fig. 3.8), cell geometry (scaled by volume) (Fig. 3.9 and 3.10) or mTOR activity (Fig. 3.11, 3.12 and 3.13). In previous work (Perez Gonzalez, Rochman, Tao et al, 2018), we discussed the relationships between YAP/TAZ, cortical tension, and volume. Here we go a step further to propose that the trend of increasing volume across the CRISPR knockouts might be explained as a consequence of increasing cell tension which in turn increases YAP/TAZ activity (Fig. 3.14a and Fig. 3.15a).
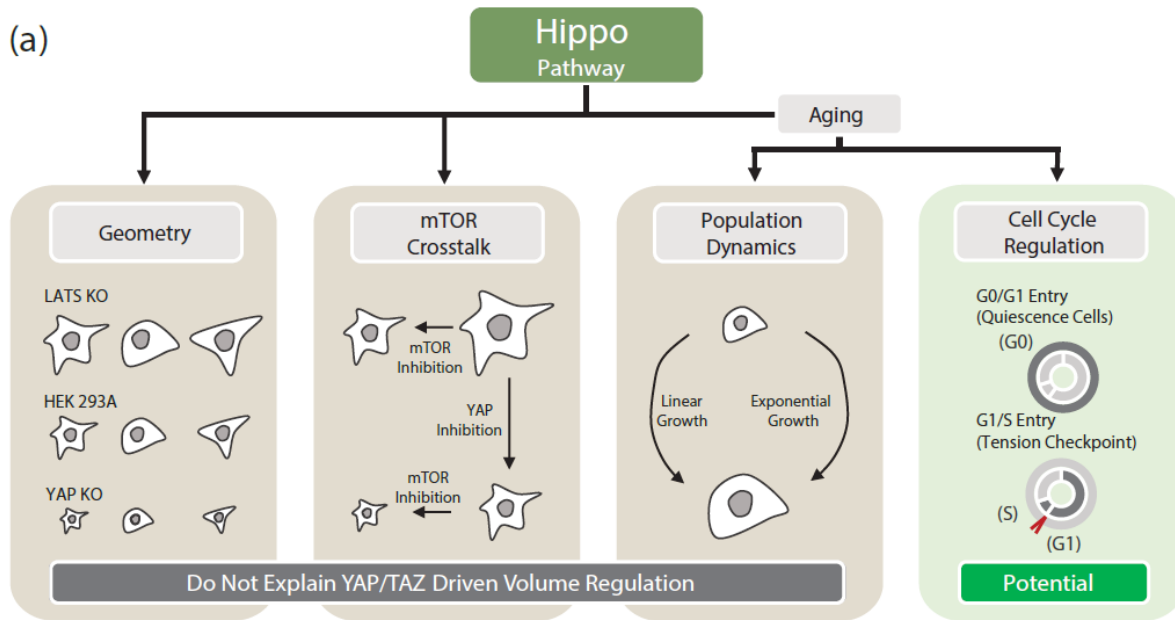
Figure 3.14 Possible pathways that Hippo pathway contributes to cell volume regulation. (a) Hippo pathway is considered to be affecting different properties of the cell and thus regulate cell volume. (i) Hippo pathway affects cell geometry but not in a way to understand cell volume regulation as the cell self-scales its shape when YAP is knocked out. (ii) Hippo pathway cross-talks with mTOR in low amino acid condition whereas the crosstalk fails to explain cell volume regulation in general condition as cell volume regulation of mTOR pathway of Hippo pathway is considered to be in an additive fashion. (iii) Hippo pathway possibly affects cell aging including population dynamics and cell cycle regulation. Potential changes in growth rate caused by perturbing YAP fails to explain cell volume regulation, while cell cycle regulation including G0/G1 checkpoint and G1/S checkpoint might contribute to understanding cell volume regulation.

As previously published, we propose that the distribution of cortical tension maintained through phosphorylated myosin mediated active contraction determines the force balance at the cortex thereby determining the volume of the cell. To validate this framework for the Hippo pathway KOs, we first measured pMLC expression finding that, as expected, it is positively correlated with YAP/TAZ expression and activity (Fig. 3.15c) while its distribution in the cell apical cortices remains fairly constant (Fig. S14a-c). When comparing our measured values for pMLC and volume, we found that pMLC is an excellent proxy for cell volume (Fig. 3.15d). We went on to characterize the pMLC expression for cells identified to be in G_1 by Hoechst labelling for each cell line and found that the G_1 exit value for pMLC (the value bounding 90% of cells in G_1) was again correlated with the average cell volume of the cell line (Fig. S14a). We hypothesize that

YAP/TAZ and pMLC may be influencing an existing G_1/S cell cycle checkpoint. To support the existence of such a checkpoint which has recently been motivated in monolayers (Uroz et al, 2018) for isolated HEK single cells, we measured cell cycle progression in a synchronized population under pMLC inhibition with the ROCK inhibitor Y28632. We took an asynchronous population (Fig. 3.16a,d), performed mitotic shake off detachment to obtain dividing cells, and let this population progress to G_1. We then compared the evolution of this population over time with (Fig. 3.16c,f) and without (Fig. 3.16b,e) the addition of Y27632. We found that with the addition of Y27632, there were significantly fewer cells progressing from G_1 to S. Recently, it was shown that cell cytoskeletal tension impacts the association of SW1/SNF complex with YAP/YAZ, which inhibits transcriptional activity of nuclear YAP/TAZ (Chang, et al. 2018). This result in combination with our observation suggest that pMLC activity and cell tension, together with YAP/TAZ activity are involved in the determination of cell cycle checkpoint.
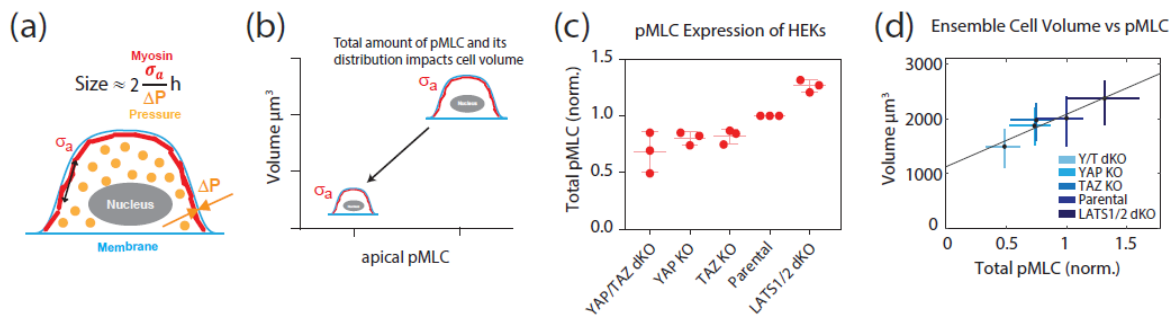
Figure 3.15 Volume and pMLC expression across Hippo pathway knockouts (a) Cartoon depicting volume relationship to cortical tension and pressure difference (b) Cartoon depicting expected apical pMLCs relationship to volume (c) pMLC Expression Changes Among HEKs. Immunofluorescence assay was performed on HEKs to stain phosphorylated myosin light chain (d) Linear Fitting Between Ensemble Cell Volume and Ensemble pMLC. Cell volume and pMLC expression of each cell line as an ensemble was plotted with its mean value and standard deviation. Linear fitting shows the relationship between ensemble cell volume and pMLC.
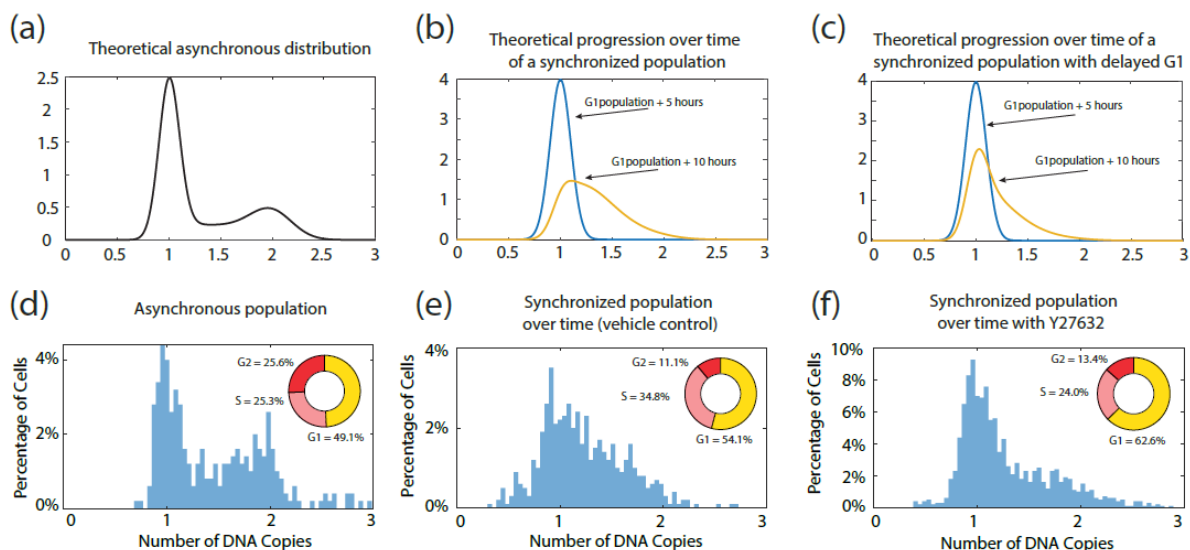
Figure 3.16 Cell cycle progression of synchronized population under Y27632 treatment (a) Theoretical prediction of steady state DNA distribution (b) Progression from G1 synchronization. Synchronized population (blue) versus the population evolving over time (yellow) (c) Theoretical progression from G synchronization (blue) and the population evolving over time when G1 progression is delayed (yellow) (d) asynchronous cell cycle distribution for HEK 293A. (e) Y27632 assay. Panel shows how the cells progress from a synchronized G1 population with vehicle control (DMSO). (f) Y27632 assay. Panel shows how the cells progress from a synchronized G1 population with Y27632.

3.4 Discussion

Our data shows that YAP/TAZ and the Hippo pathway are involved in regulating single cell volume and supports the idea that YAP/TAZ is a mechanosensor. We found birth and division volume to be dependent on YAP/TAZ activity with higher YAP/TAZ activity leading to larger volumes. We validated (Pouffle, 2018) that cell cycle duration decreases with increasing YAP/TAZ activity, and also observed that the volumetric growth rate dV/dt increases with YAP/TAZ activity.

Neither the observed dependence on YAP/TAZ activity for the regulation of cell cycle duration nor any potential modulation of the volumetric growth law were able to explain the volume variation observed. We additionally considered the possibility that this phenomenon is purely mechanical, owing to the potential role of YAP/TAZ in the regulation of cell shape; however, we found four out of five of the cell lines investigated to exhibit self-similar shapes negating this

hypothesis as well. Finally, we sought to establish YAP/TAZ as either directly up or downstream of mTOR, a known regulator of cell volume, in this context and instead found them to act both independently and synergistically.

Having exhausted these more fundamental explanations, we aimed to propose a novel mechanism implicating the role of YAP/TAZ in the regulation of cortical tension and thus cell volume throughout the G1/S checkpoint. We established a strong, positive correlation between YAP/TAZ activity, cell volume, and cell tension and went on to validate the importance of cell tension through the navigation of the G1/S checkpoint in isolated HEK single cells by demonstrating that rho inhibition delays or prohibits exit of G1 and entrance to S. We posit that YAP/TAZ modulates cortical tension, and thus cell volume during this transition, further impacting volume at birth and division.

Chapter 4: Conclusion

4.1 Review of our findings

Throughout the work comprised in this dissertation we have deeply focused in understanding how cells regulate and control cell volume both at the single cell level and at the population level. In order to properly understand how cells determine their volume at the single cell level we had to first develop and characterize a microdevice that could accurately measure volume. Here, we used the Fluorescence eXclusion method to perform such measurements which were also confirmed with other common methods to assess cell size.

In Chapter 2, we used the fluorescence exclusion method to explore the relationship between cell volume and stiffness of the substrate in which the cells are grown. We found that cell volume depends on cell adhesion area and substrate stiffness. Moreover, our data suggests that cells balance forces at the cortex establishing a clear relationship between cortical tension and volume, given a particular adhesion area. Indeed, in a more fundamental level, we have shown that the principle of force balance is well preserved in cells when accounting for pressure difference and cortical contraction. In addition, an interesting feature of our datasets is the fact that the volume trend is rather non-linear as a function of substrate stiffness, leading to a maximum volume for 3T3s and MSCs and a minimum volume for NuFFs at intermediate stiffness. This non-linearity can be explained by our theoretical model where the total amount of cortical tension, here reported as total pMLC per cell, and its distribution in the Z axis play a determinant role on the size of the cell. A more abstract and rather puzzling question is: how do cells transmit these signals? From a physical perspective, the variable of volume is global. It comprises the system as a whole but the variable of cortical tension is a local variable. It is not a variable with a single number across the board but rather a variable that changes at every point in the cell. How can both of these variables be connected. How could the local variable of cortical tension inform the global variable of volume. We considered the literature and found that YAP/TAZ, the downstream effector of the Hippo pathway, had been broadly reported as mechanotransducer that would translocate in the nucleus with changing stiffness. We found that regardless of the non-linearity of the system, for all conditions, bigger cells had higher activity of YAP/TAZ suggesting that this protein is indeed involved in cell volume determination. Finally, we presented measurements of total pMLC for

3T3s, MSCs and NuFFs in different stiffness to show an intriguing trend: when only selecting cells in G1 in the dataset, regardless of the stiffness selected, cells seem to reach similar values of pMLC, suggesting that across conditions, cells in G1 seem to reach a critical tension before progressing to S. This aligns with previous research that suggests the cell cycle is more complex than previously thought and also has complex checkpoints based on mechanical signals.

In Chapter 3, we further sought to demonstrate the role of YAP/TAZ in regulation of cell volume. Here, using the fluorescence exclusion method, we assessed the volume of CRISPR generated knockouts across the Hippo pathway. The goal was simple, to demonstrate that increased expression of YAP/TAZ leads to an increase in volume and vice versa. We found this to be true and pursued a mechanistic explanation of this phenomena. We first analyzed the dynamics of cell volume within each population by analyzing movies in which cells underwent mitosis. By measuring the volume right before division and the volume of the daughter cells we found that the larger cells within each population were increasing in size as a function of YAP/TAZ as well as the daughter cells. This on its own stands and demonstrates that by knocking out YAP/TAZ we have intrinsically changed the volume of the parental cell line. Once this had been demonstrated we considered the most likely options to explain how is this regulation occurring. The first alternative is that the mechanotransducer YAP/TAZ, also regarded as a key regulator of proliferation, changes the cell cycle distribution controlling how many cells are in each phase. This, we reasoned, could potentially lead to a changing weighed average but the experimental data showed otherwise. We found no consistent and significant trend through the 5 cell lines, discarding the role of cell volume regulation driven primarily by cell cycle regulation. A second alternative we considered, is the fact that YAP/TAZ could have induced strong morphological changes in our cell lines. Changes patterned as a function of YAP/TAZ that had become prominent in the LATS1/2 dKO cell line (with the highest expression of YAP/TAZ) and barely prominent in the YAP/TAZ dKO (with no expression of YAP/TAZ). These changes, if existent, could lead to changes in the geometry of the cells at the population level driving the volume changes we found. When performing cross sectional analysis for all 5 cell lines, we found that the parental HEK293A cell line, the YAP KO, the TAZ KO, and the YAP/TAZ dKO we self-scaling. Other than the volume difference, these cells showed similar geometries. The LATS1/2 dKO was an outlier in this analysis, not only increasing in size but also strongly changing its geometry. All considered,

geometrical changes could not be the driving force behind the volume changes across all cell lines. Another alternative to explain these volume changes is the relationship between the Hippo pathway and the mTOR pathway. The mTOR pathway has been broadly regarded as a master regulator of cell size due to its influence in ribosomal synthesis. If we could demonstrate that the Hippo pathway is upstream of the mTOR pathway, we could track the volume variations back to ribosomal synthesis. Surprisingly, we found that when using rapamycin, the YAP/TAZ expression remain unchanged and in the five cell lines the expression of pS6, the total protein content and the protein synthesis remained unchanged, showing that neither pathway has a feedback mechanism into the other one. Moreover, when treating the five cell lines with rapamycin, we saw an additional volume decrease, further demonstrating that both of these forms of volume regulation are independent and that they work together generating a synergistic volume decrease. We finally reported measurements on the cortical contraction of these five cell lines (reported as total pMLC per cell) and found that across the five cell lines, the relationship between pMLC and volume still holds. We performed an assay with Y27632, which suggests that a synchronized population of cells in G1 requires a minimum amount of pMLC to progress through the cell cycle further suggesting the existence of a mechanical checkpoint from G1 to S.

Both of these chapters have described our efforts to understand and determine how cells determine their volume. Some of the main takeaways are that we have proved that a theoretical framework can provide insightful predictions regarding cell shape and cell volume and that we have confirmed that YAP/TAZ is a novel regulator of cell size.

4.2 Future work

On performing these projects, we found that there is a wealth of information to be analyzed and understood when applying biophysical principles to biological environments. By creating a microdevice that address the question of volume in a very precise manner, we were able to obtain data such as the geometrical analysis that has not been previously reported. While attempting to understand how cells regulate their volume we created new tools and analysis. The original idea of measuring volume presented in chapter 2, transformed in the idea of tracking volume over time as shown in chapter 3. This as well motivated new ideas and prospects: (1) We have already done progress with a project in which we analyze how the inhibition of cortical tension translates into

cell volume variations. The tracking of cell volume over time is now allowing us to understand how certain drugs such as the ROCK inhibitor Y27632 might affect cell volume regulation. On a different subject, our lab continues to work on the analysis of cell volume, now attempting to exploit the wealth of data we have collected over the years to create a framework to predict cell volume from DIC images with machine learning tools.

The cornerstone of all of these projects, past and new, is the development of a tool, the cell volume device.

Appendix
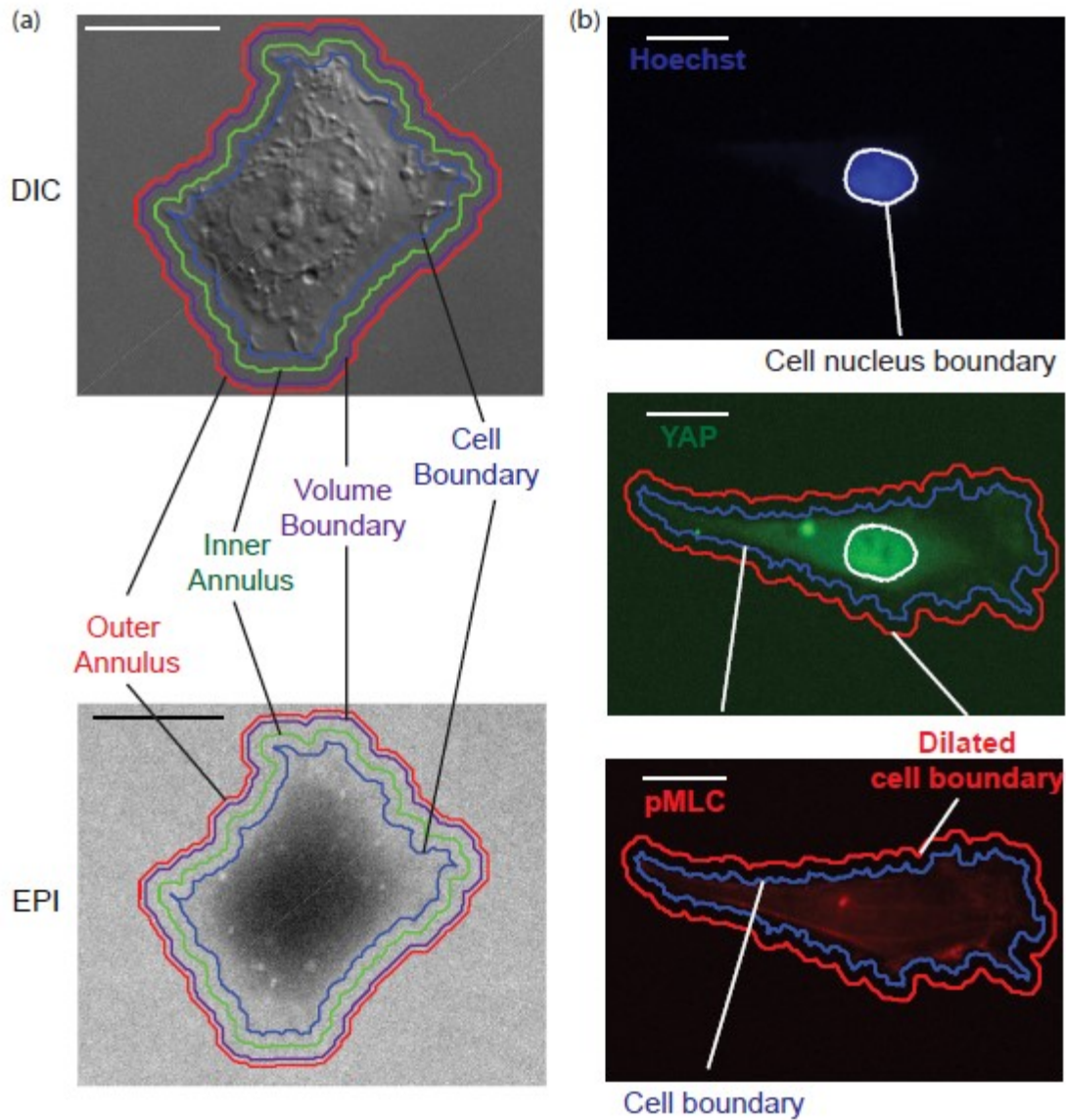
Figure S1 Quantitative immunofluorescence analysis. (a) Examples of cell images in DIC and epifluorescence channels, showing the traced cell boundary (blue), inner (green) and outer (red) annulus, and dilated boundary for volume measurement (purple) (b) Examples of traced cell boundaries from immunofluorescence images. (All scale bars = 10 micrometer.)
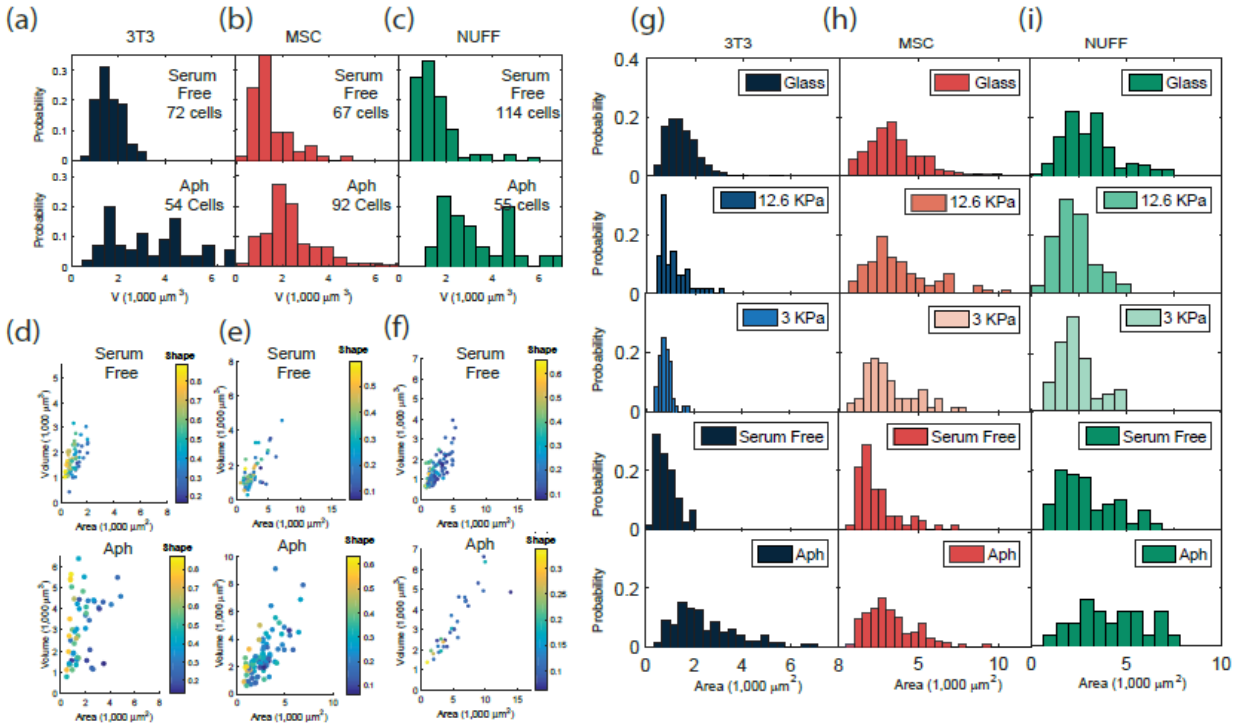
Figure S2 Volume and area for synchronized cells. (a): Cell volume distributions for serum starvation and aphidicolin treatment of 3T3, NuFF and MSC cells seeded on glass. (b) Area vs. volume plots for serum starvation and aphidicolin treatment. (c) Distribution of cell adherent area across all three cell lines. (Number of Cells: 3T3s: N = 72 cells under serum starvation and N = 54 cells treated with Aphidicolin. MSCs: N = 67 cells under serum starvation and N = 92 cells treated with Aphidicolin. NuFFs: N = 114 cells under serum starvation and N = 55 cells treated with Aphidicolin)
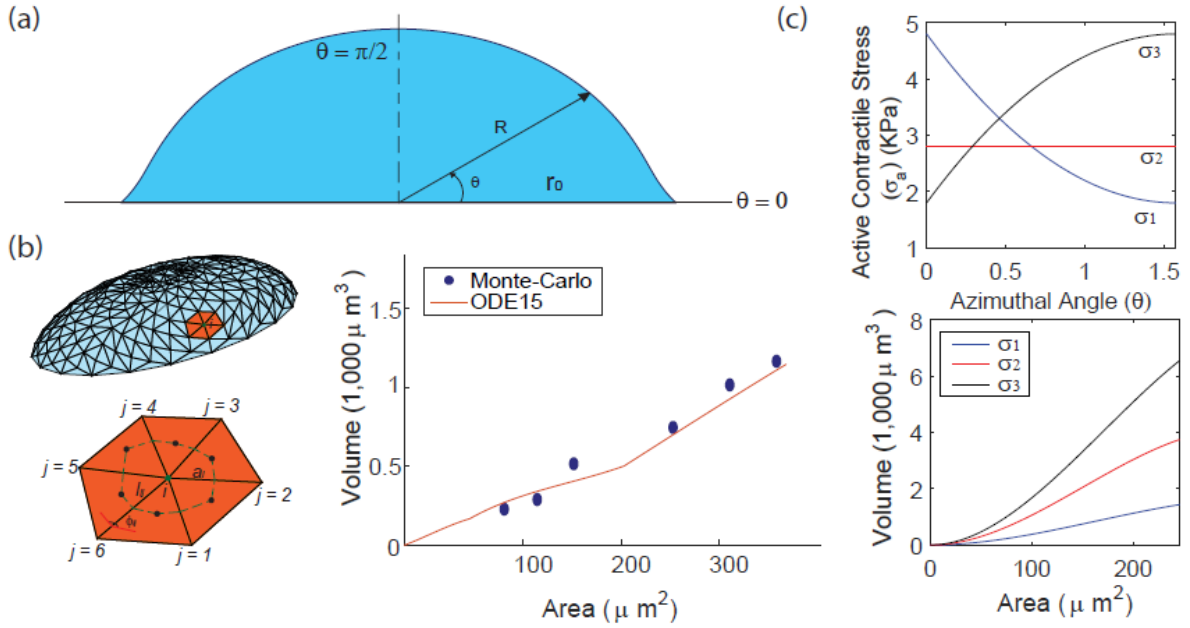
Figure S3 Schematic description of the cell mechanical model (a) Side-view of a cell adherent on a circular pattern. Here, we parametrize the cell apical surface using a spherical coordinate system, defined by local radius R and azimuthal angle θ. The surface is rotationally symmetric about the z-axis. (b) For adhered cells of arbitrary geometry, a triangulated surface in 3D is used to describe the cell apical surface. For each vertex i, j labels vertices that are connected to i; a_i (Eq. (3)) is the area enclosed by the green dash lines, which perpendicularly bisects the edges connecting i and j, connecting the triangle centers (marked as pink dots). We compare cell volume (V) vs, cell adherent area (A) for cells adhered to a circular pattern obtained from solving Eq. S1 using ODE15 (red line) and the 3D Monte-Carlo algorithm (blue dots). Here, $(2\sigma_a/\Delta P)$ h=5μm. (c). Examples of adherent area (A) vs. cell volume (V) for three different σ_a distributions. Cells with active contraction distribution similar to $\sigma_1(\theta)$ (blue line) have high basal contraction; cells with active contraction distribution similar σ_2 (red line) have uniform active contraction; cells with active contraction distribution similar to σ_3 (black line) have high apical contraction.

67
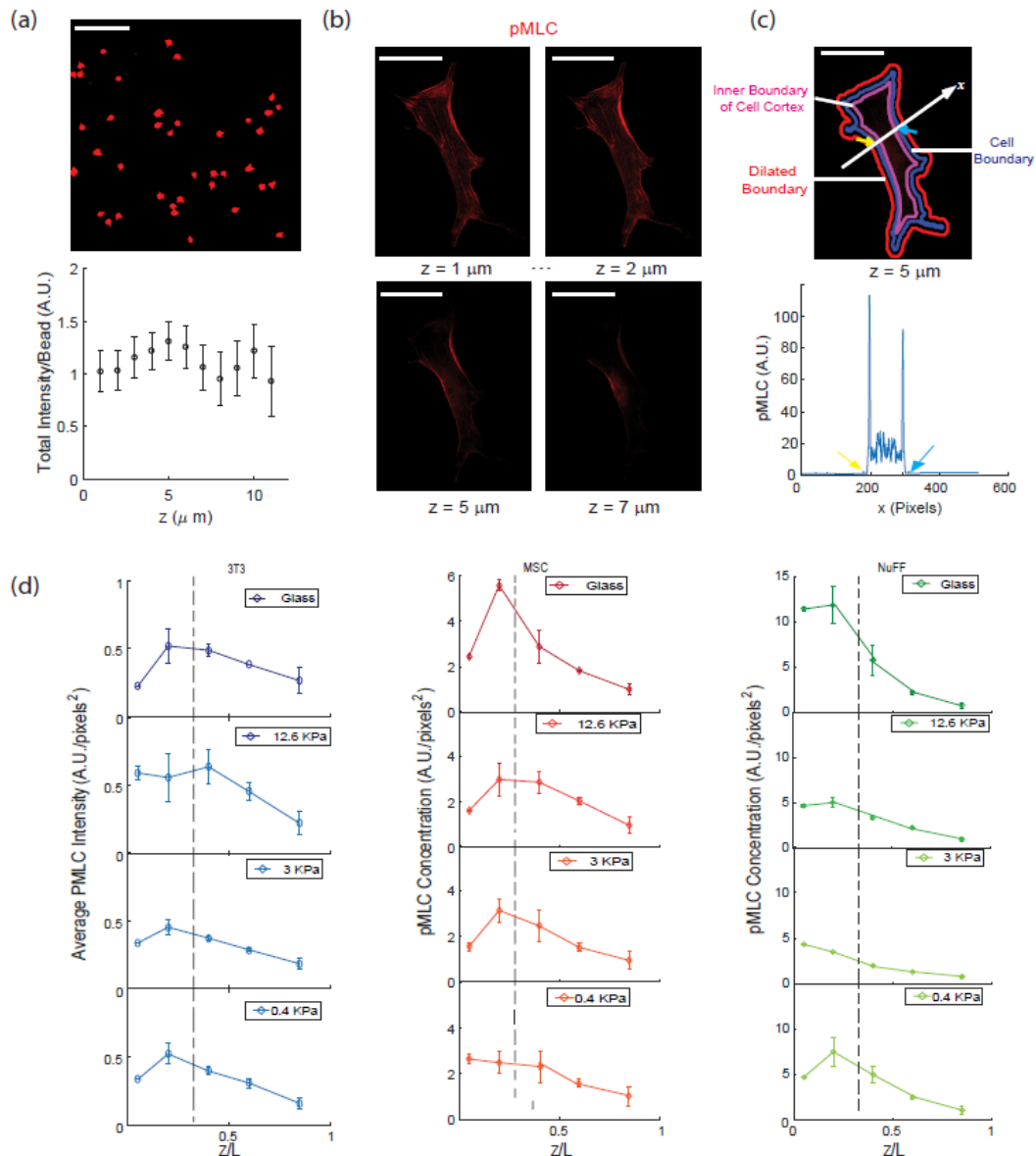
Figure S4 Quantification of spatial distribution of pMLC. (a) An example of a confocal image of fluorescent beads for one z-position. In order to calibrate our confocal intensity measurements, the total intensity per bead is plotted vs. the z position. The measured average intensity per bead remains roughly constant for different z-positions, demonstrating the confocal measurement can be used to quantify intensities at different z-positions. (b) Examples of confocal images of pMLC for NuFF cells on collagen coated glass (63X): Light intensity of pMLC in the cell cortical region is much higher than elsewhere. In addition, clear stress fibers can be seen at cell basal level. (c) Example of a confocal image with the cell boundary traced by computational image analysis: the pink line marks the inner boundary of the cell cortex. The pMLC light intensity is plotted along the x axis (white arrow). The traced cell region is between x = 200 to 310 pixels (marked with yellow and blue arrow, respectively). (d) pMLC intensity (total expression per united area) as a function of z-position for all three cell lines, which shows roughly the same trend as the total cortical pMLC intensity in Fig. 3 in the main text. (scale bar = 20 micrometer. All error bars represent standard error)
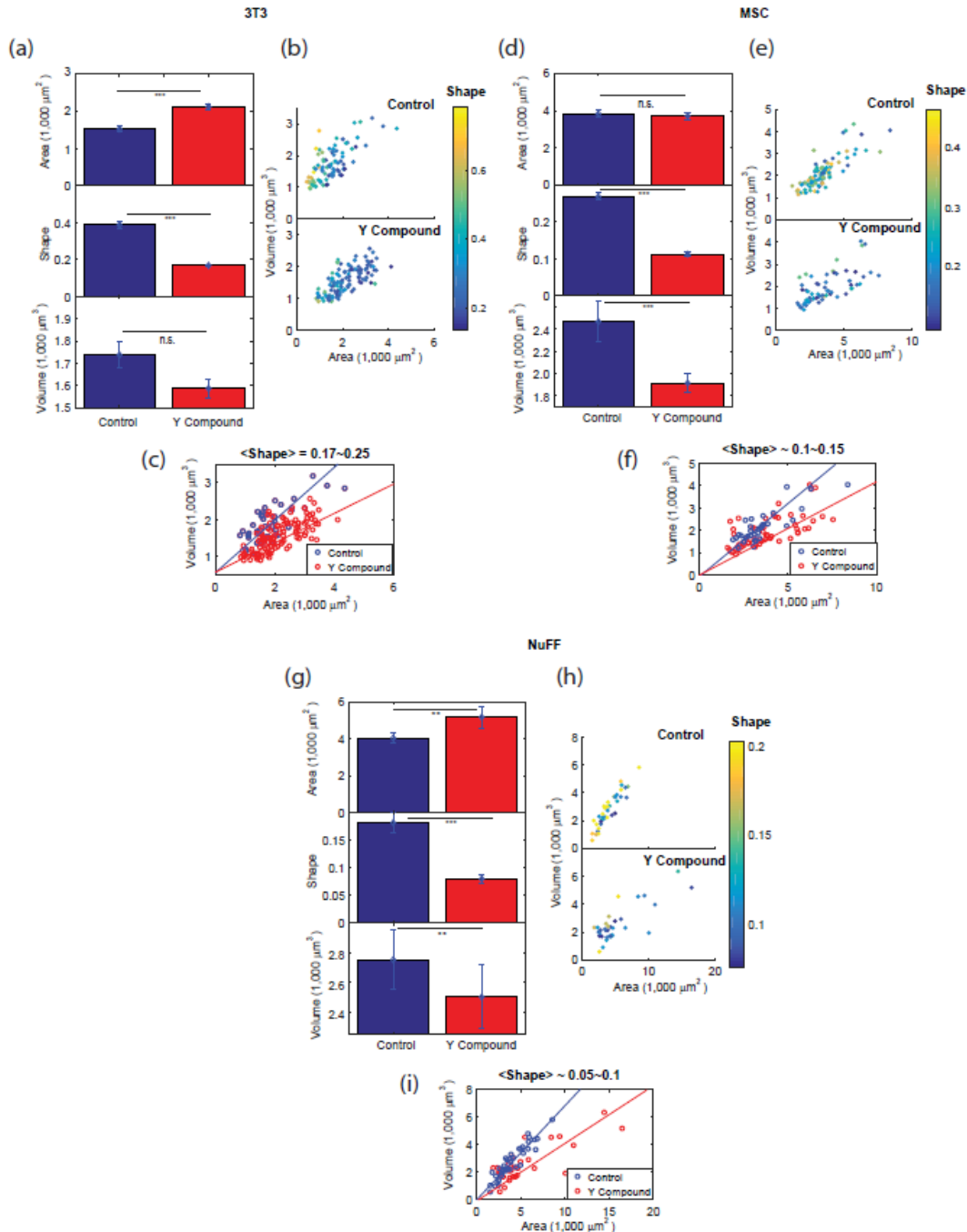
Figure S5 Cell volume after cells are exposed to ROCK inhibitor Y27632 cultured on stiff glass substrate. (a), (d), and (g): cell adhesion area, shape and volume comparison between control and Y-compound treatment of 3T3 cells (a), MSC cells(d) and NuFF cells (f). (b), (e) and (h): cell adhesion area and volume plot of control and cells treated with Y27632 for 3T3s (b), MSCs, and NuFF cells (h); (c) (f) and (i): Comparison of area vs. volume plot between control and cells treated with Y27632. The comparison is done between the cells with similar shape factor. (For 3T3s: N = 94 cells for control and N = 61 cells for Y27632 treatment; For MSCs: N = 83 for control and N = 118 for Y27632 treatment; For NuFF: N = 117 for control and N = 78 for Y27632 treatment. Statistical significance; n.s. p>0.05; ** p<10^{-3} ; *** p<10^{-6})
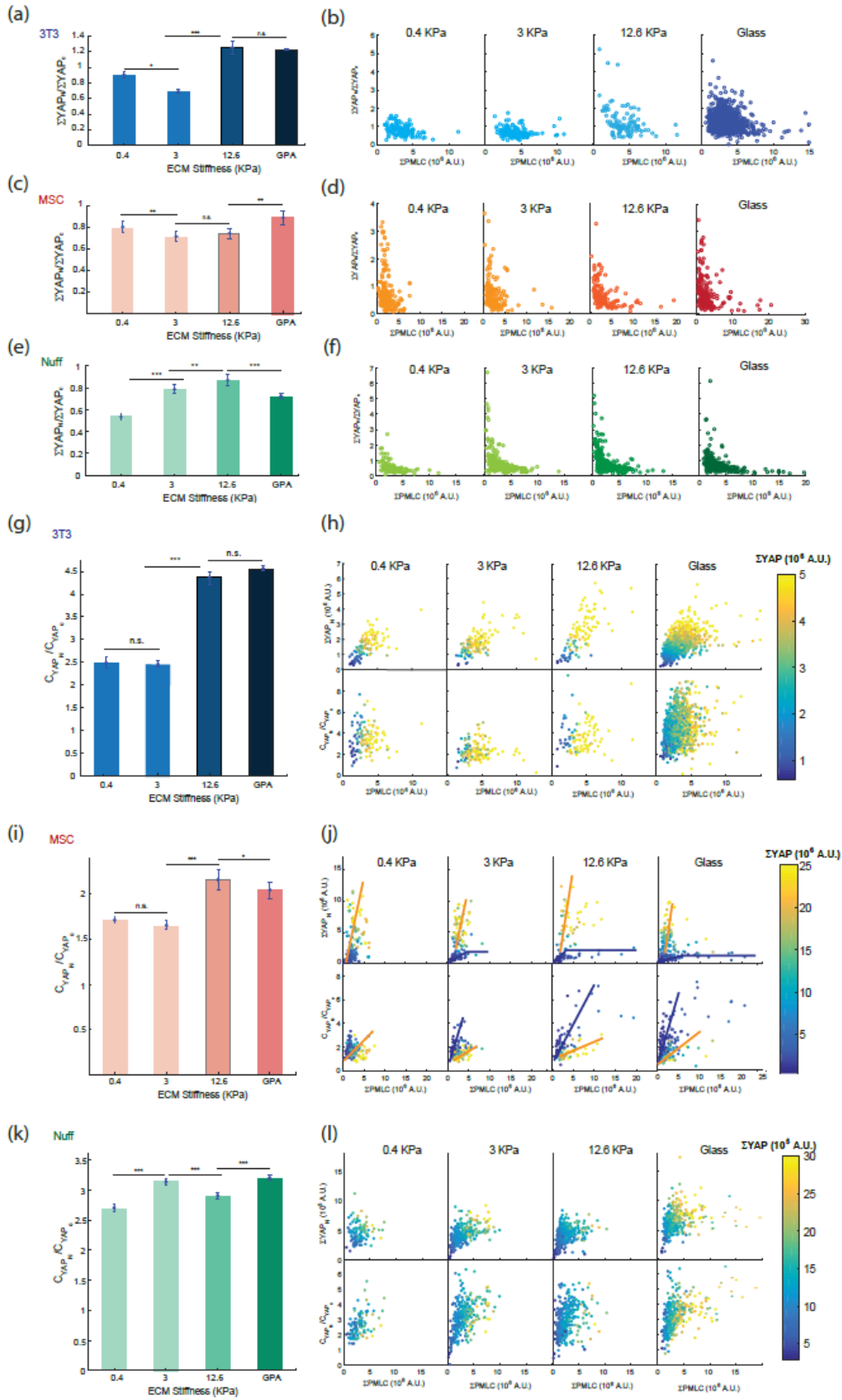
Figure S6 Quantification of YAP distribution and pMLC from epifluorescence images. (a-f) Total pMLC intensity per cell versus the ratio between total nuclear YAP expression and total cytoplasmic YAP expression for all three cell lines. These plots show that there is no obvious correlation between pMLC and YAP ratios (a,c,e) show average value per stiffness and (b,d,f) explicitly display single cell measurements. (g-l) Correlation between total pMLC expression per cell and total nuclear YAP expression, and the correlation between total pMLC per cell and the ratio between YAP nuclear intensity and cytoplasmic intensity. (g,i,k) displays average concentration ratio per ECM stiffness and (h,j,l) Data points are color coded by the total YAP expression per cell. We find that the concentration ratio follows the trend we found between total pMLC intensity and total nuclear YAP expression. But for the MSC cells, the appearance of separate branches in the correlation is less obvious in the pMLC vs. intensity plot. Cells belong to the upper branch have high overall YAP per cell, but low nuclear to cytoplasmic YAP intensity/concentration ratio. (All error bar represent standard error. Statistical significance: *** $p<10^{-6}$, **$p<10^{-3}$, *$p<0.01$)
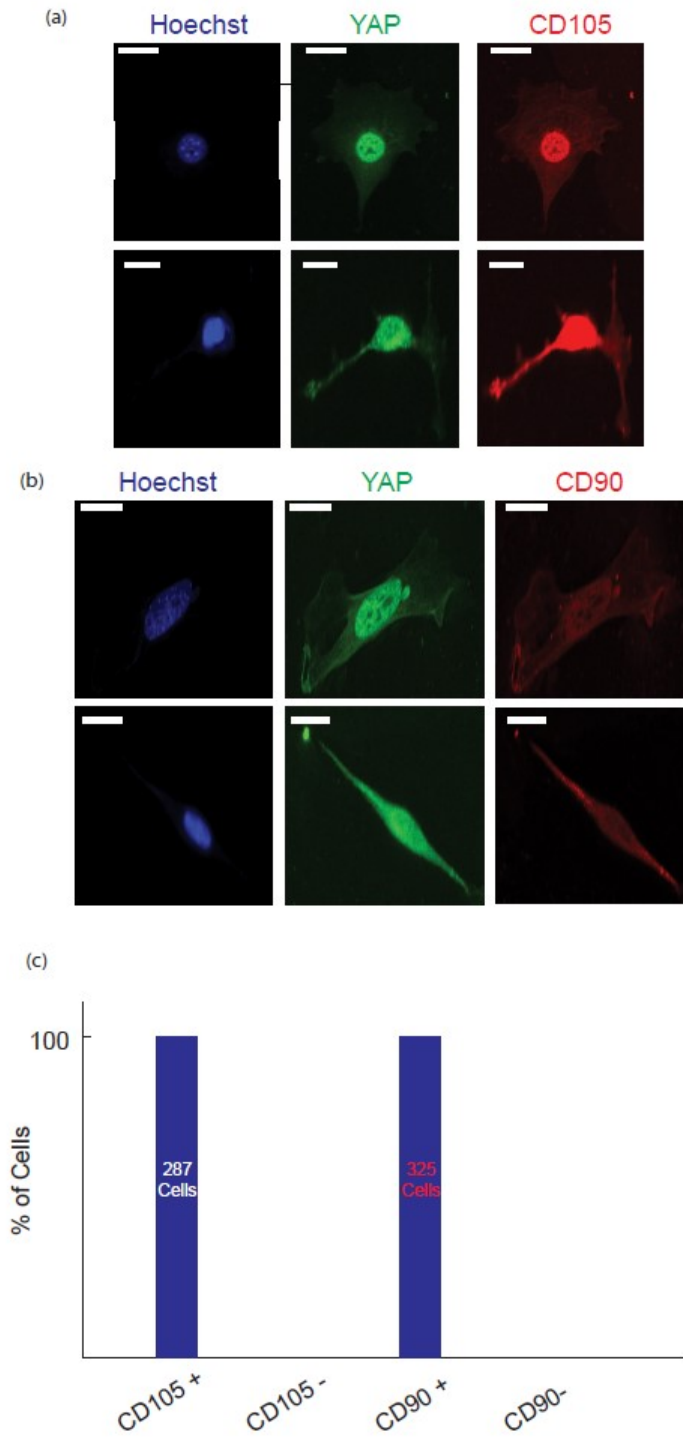
Figure S7 MSC cells expressing differential marker CD105 and CD90. All MSC cells positively express these markers.

73
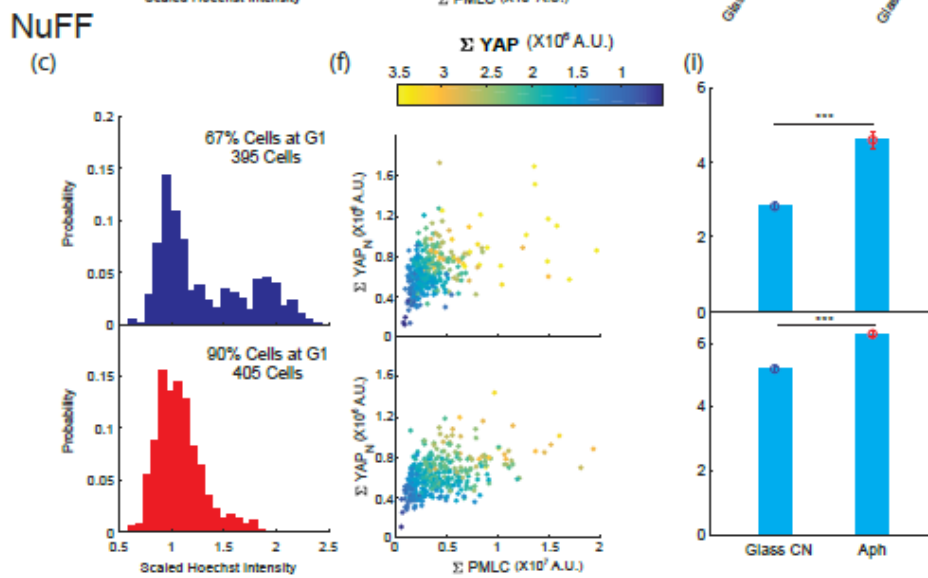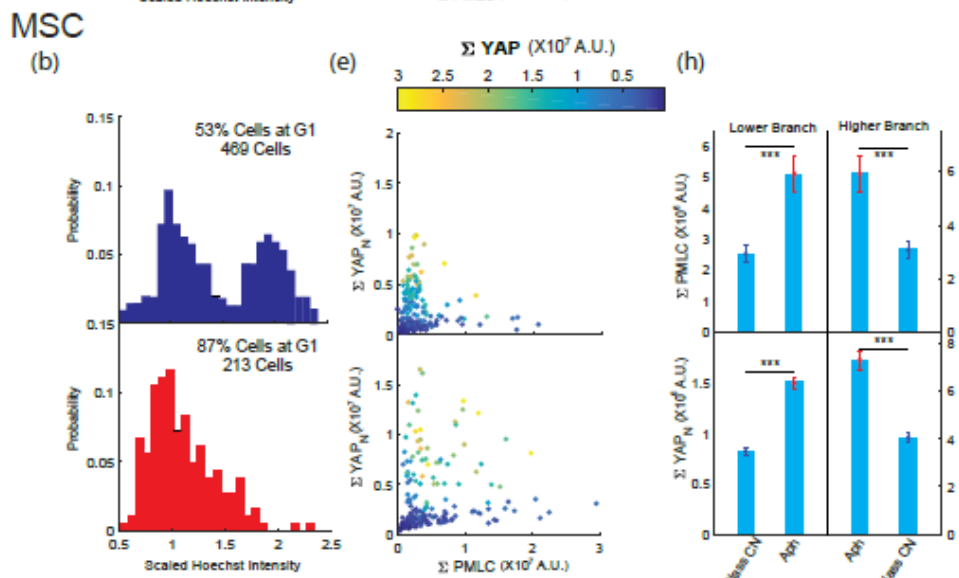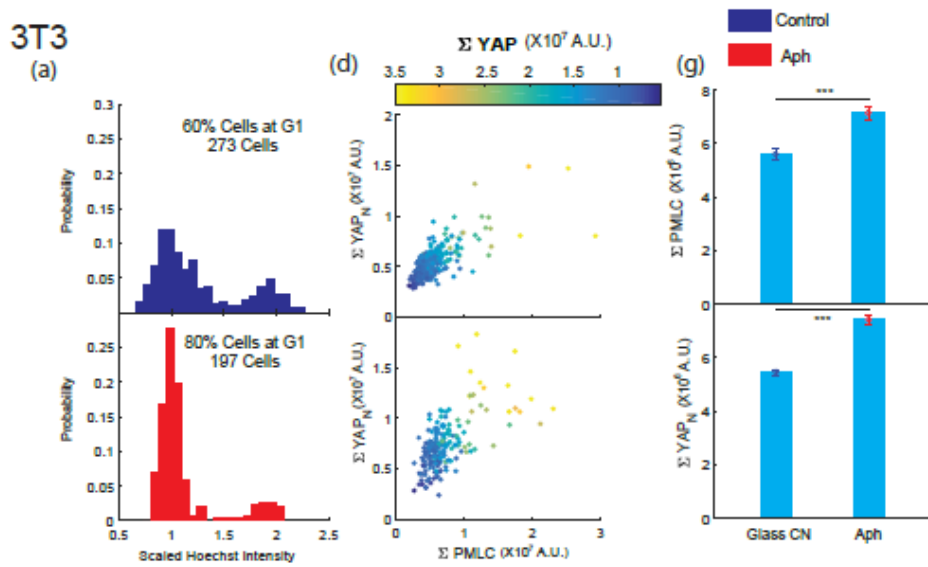
Figure S8 Comparisons between cells treated with aphidicolin and control for all three cell lines. (a)~(c) DNA distribution for 3T3s (a), MSCs(b), and NuFFs(c). In general, cells treated with aphidicolin are mostly in G1. (d)~(f), PMLC and YAPN plot for 3T3 (d), MSC(e) and NuFF(f) cells. (g)~(i), Comparison of mean PMLC and YAPN for 3T3 (g), MSC (h), and NuFF(i). Cells treated with aphidicolin have higher expression of pMLC and nucleus YAP. (Number of cells: 3T3s: N = 273 cells for the control and N = 197 cells treated with Aphidicolin; MSCs: N = 469 cells for the control and N = 213 cells treated with Aphidicolin. NuFFs: N = 395 cells for the control and N = 405 cells treated with Aphidicolin. *** $p < 10^{-6}$).

3T3

(a)

60% Cells at G1
695 Cells

96% Cells at G1
594 Cells

(d)

Σ YAP (X10⁶ A.U.)

MSC

(b)

52% Cells at G1
573 Cells

80% Cells at G1
352 Cells

(e)

Σ YAP (X10⁶ A.U.)

NuFF

(c)

70% Cells at G1
340Cells

90% Cells at G1
276Cells

(f)

Σ YAP (X10⁶ A.U.)

(g)

Control
Serum Free

(h)

Lower Branch   Higher Branch

(i)

75
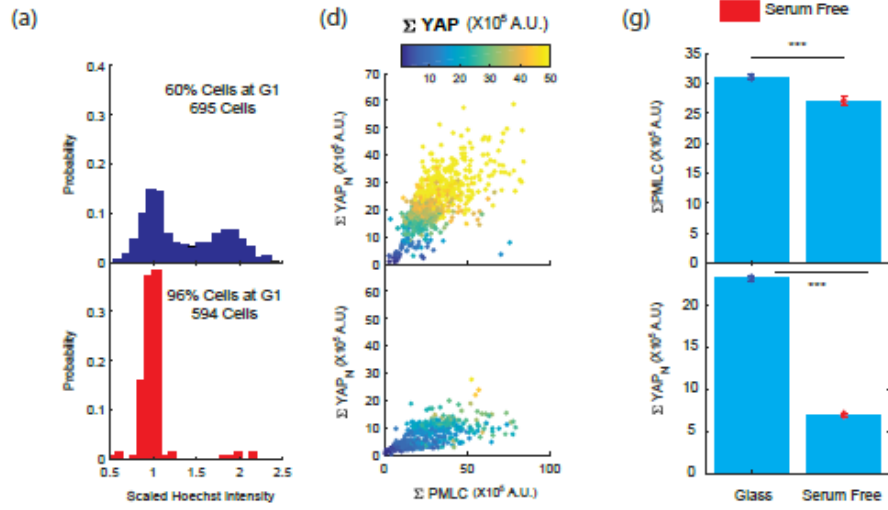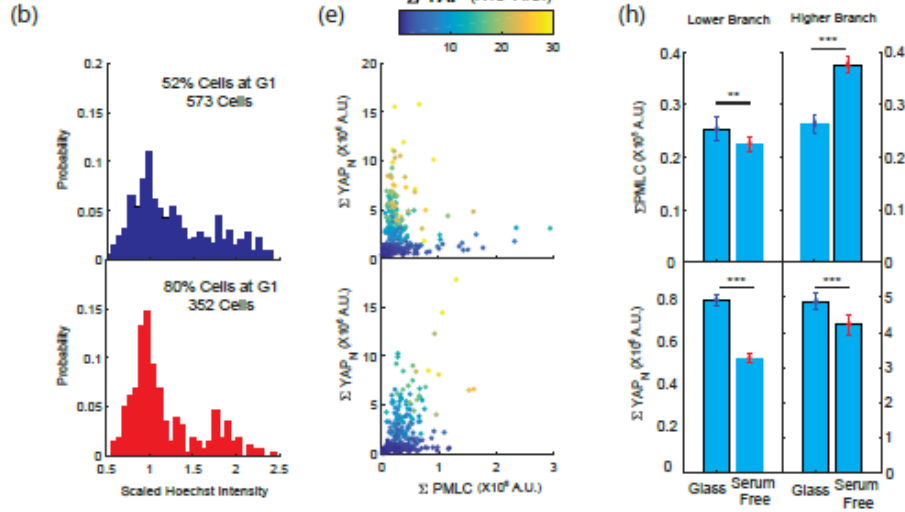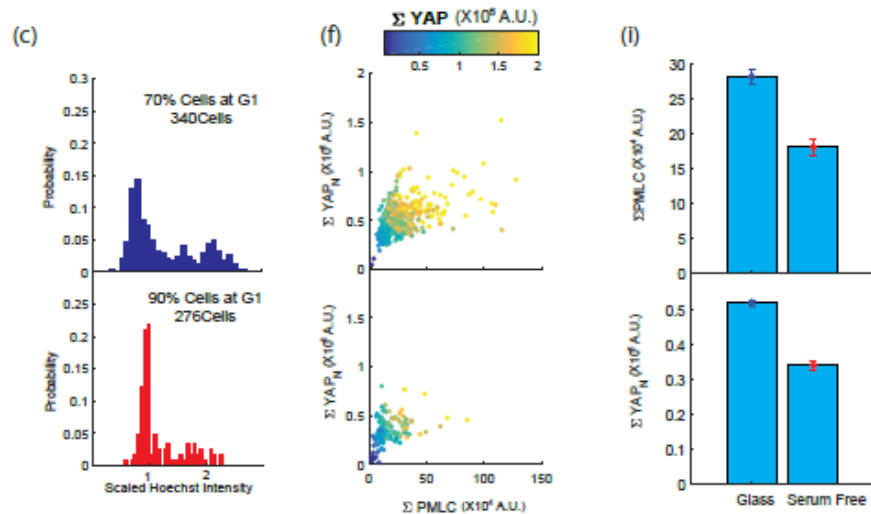
Figure S9 Comparison between cells under serum free condition and control for all three cell lines. (a)~(c) DNA distribution for 3T3s (a), MSCs(b), and NuFFs(c). In general, cells cultured under serum free condition are mostly in G1. (d)~(f), PMLC and YAP_N plot for 3T3 (d), MSC(e) and NuFF(f) cells. (g)~(i), Comparison of mean PMLC and YAP_N for 3T3 (g), MSC (h), and NuFF(i). In general, cells cultured under serum free condition have lower pMLC and nucleus YAP, except for the higher branch of MSCs, where there are higher percentage of cells at upper branch when treated with serum free condition (Number of cells: 3T3s: N = 695 cells for the control and N = 594 cells cultured under serum free condition; MSCs: N = 573cells for the control and N = 352 cells cultured under serum free condition. NuFFs: N = 340 cells for the control and N = 276 cells cultured under serum free condition. *** $p < 10^{-6}$; ** $p <= 0.001$)

(a) (b) (c)

(d)

YAP/TAZ dKO   YAP KO   TAZ KO   Parental   LATS1/2 dKO

Volume μm³

Area μm²

(e)
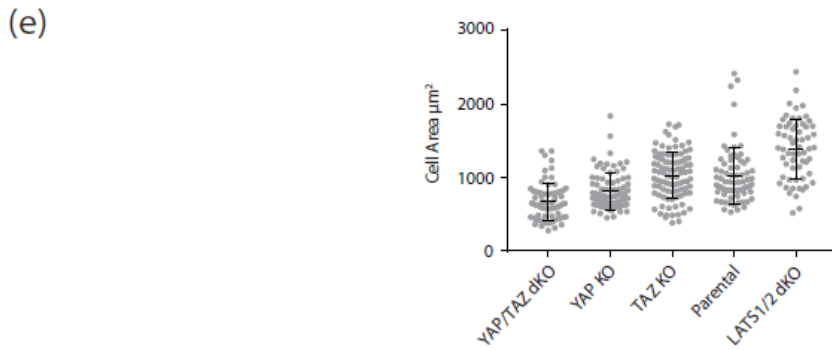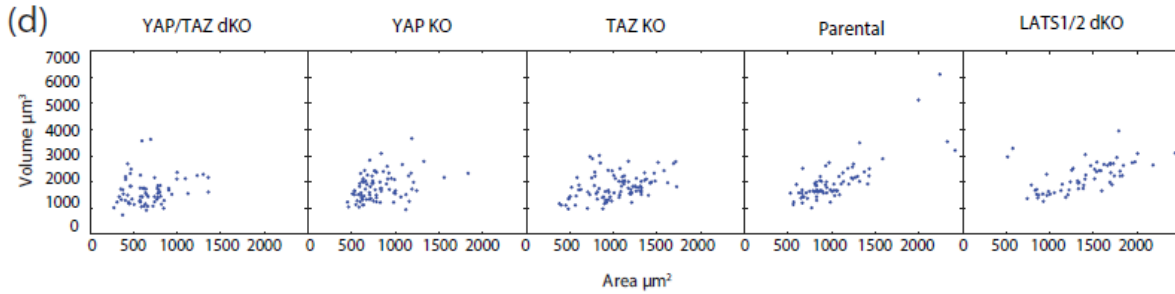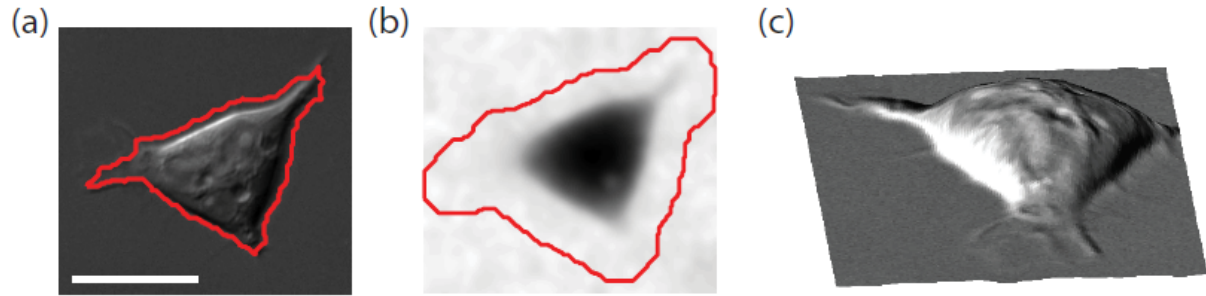
Cell Area μm²

	YAP/TAZ dKO	YAP KO	TAZ KO	Parental	LATS1/2 dKO
Average Area ± error	671.6 ± 29.9μm²	811.3 ± 27.4 μm²	1028 ± 32.7 μm²	1018 ± 44.2 μm²	1386 ± 52.4 μm²

Table 1. Statistics of Cell Area across the Hippo Pathway knockouts. Average Value + SEM.

	YAP/TAZ dKO	YAP KO	TAZ KO	Parental	LATS1/2 dKO
Average Volume ± error	1725 ± 38.4μm³	1931 ± 51.5 μm³	1986 ± 52.2 μm³	2362 ± 60.9 μm³	2437 ± 53.5 μm³

Table 2. Statistics of Cell Volume across the Hippo Pathway knockouts. Average Value + SEM.

Figure S10. Volume and area analysis for all cell lines. (a) DIC image overlaid with cell boundary used for calculating morphological properties. (b) Epifluorescent volume image overlaid with the boundary used to segment the region integrated to yield volume as described in the main text. The volume boundary is dilated 20 pixels out from the cell boundary. The annulus used to calculate the background intensity is constructed from boundaries dilated 10 and 25 pixels from the cell boundary (not shown). (c) Three-dimensional reconstruction of the cell. The heights are derived from the epifluorescent volume image as described in the main text and colorized with the intensity map defined by the DIC image. (d) Volume versus area for each one of the five cell lines including the CRISPR knockouts. ($N_{YAPTAZ\ dKO}$=70, $N_{YAP\ KO}$=81, $N_{TAZ\ KO}$=95, $N_{HEK\ 293A}$=74, $N_{LATS1/2\ dKO}$=61). (e) Shows the distribution for cell area for each cell line from the previous figure S10e. Table 1. Average area. Table 2. Average volume.
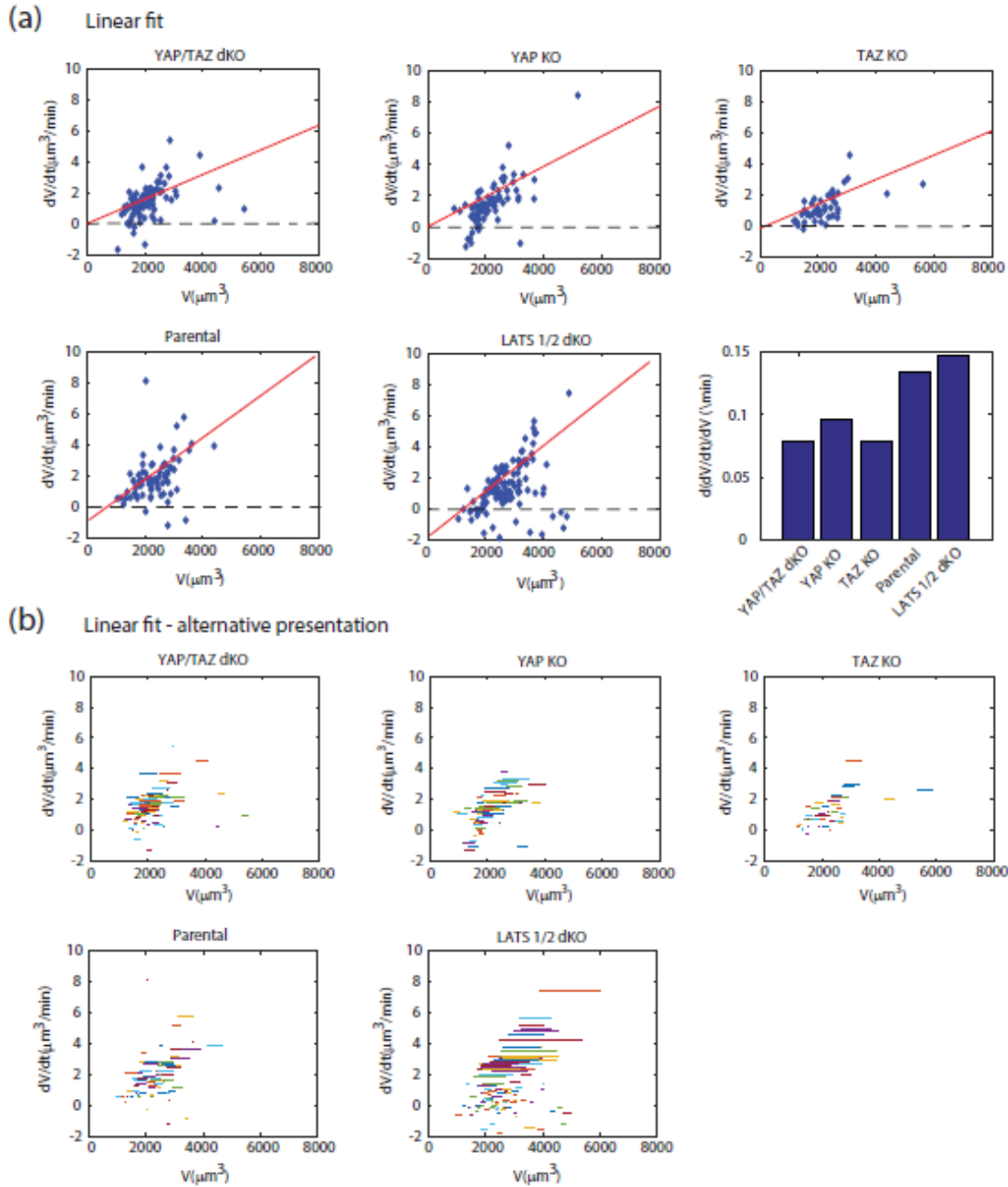
Figure S11 Growth analysis assuming linear behavior (a) Growth rate characterizing volume increase at single cell level by using a linear fitting to each individual curve. The first five panels show the individual cell growth versus their associated initial volume. The last panel shows the slope of the fitting for all five cell lines ($N_{YAPTAZ\ dKO}$=130, $N_{YAP\ KO}$=118, $N_{TAZ\ KO}$=162, $N_{HEK\ 293A}$=175, $N_{LATS1/2\ dKO}$=185). (b) Growth rate characterizing volume increase at single cell level with an alternative representation. The five panels show the individual cell growth versus their volume over time ($N_{YAPTAZ\ dKO}$=130, $N_{YAP\ KO}$=118, $N_{TAZ\ KO}$=162, $N_{HEK\ 293A}$=175, $N_{LATS1/2\ dKO}$=185).
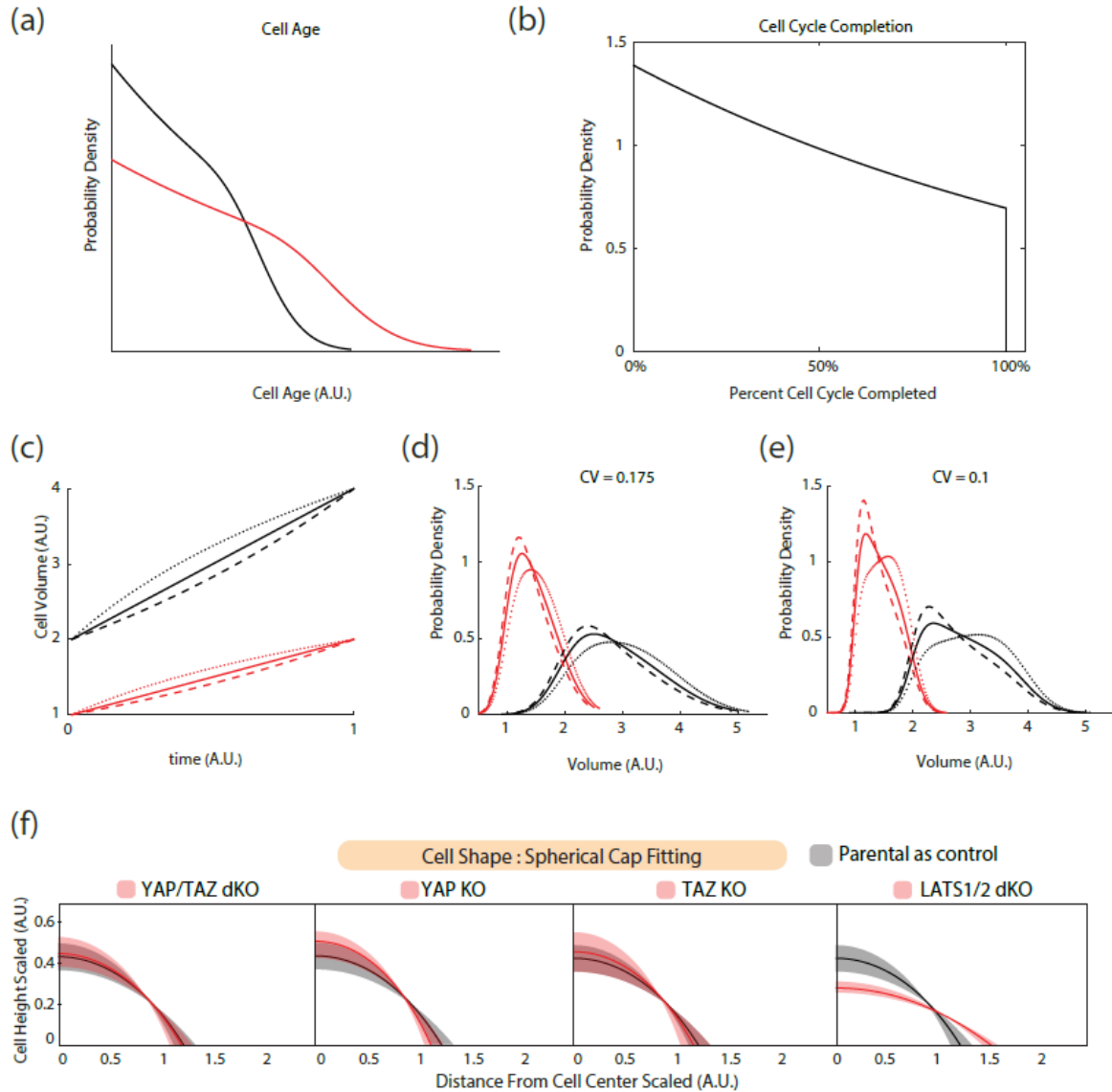
Figure S12 Cell cycle change impact on volume and geometrical differences among cell lines. (a) Example cell age distributions for cells with a long cell cycle duration (red line) and a short cell cycle duration (black line). (b) The cell cycle completion distribution well conserved for a variety of cell cycle distributions. (c) Growth trajectories for cells obeying a hypothetical logarithmic growth law (dotted lines), linear growth law (solid line), and exponential growth law (dashed line). Small cells ranging in volume from one to two arbitrary units (red curves) and large cells ranging in volume from two to four arbitrary units (black curves) are displayed. (d) Resultant volume distributions where the conditional probability has a large CV. All growth laws produce similar volume distributions. (e) Resultant volume distributions where the conditional probability has a small CV. The resulting volume distributions are clearly distinguishable. (f) The fitted spherical cap distributions for the Hippo knockouts (red) in comparison to control HEK 293A (gray). The shaded band represents the median 50% of the population. The only cell line with a significant shape difference is the LATS1/2 dKO.
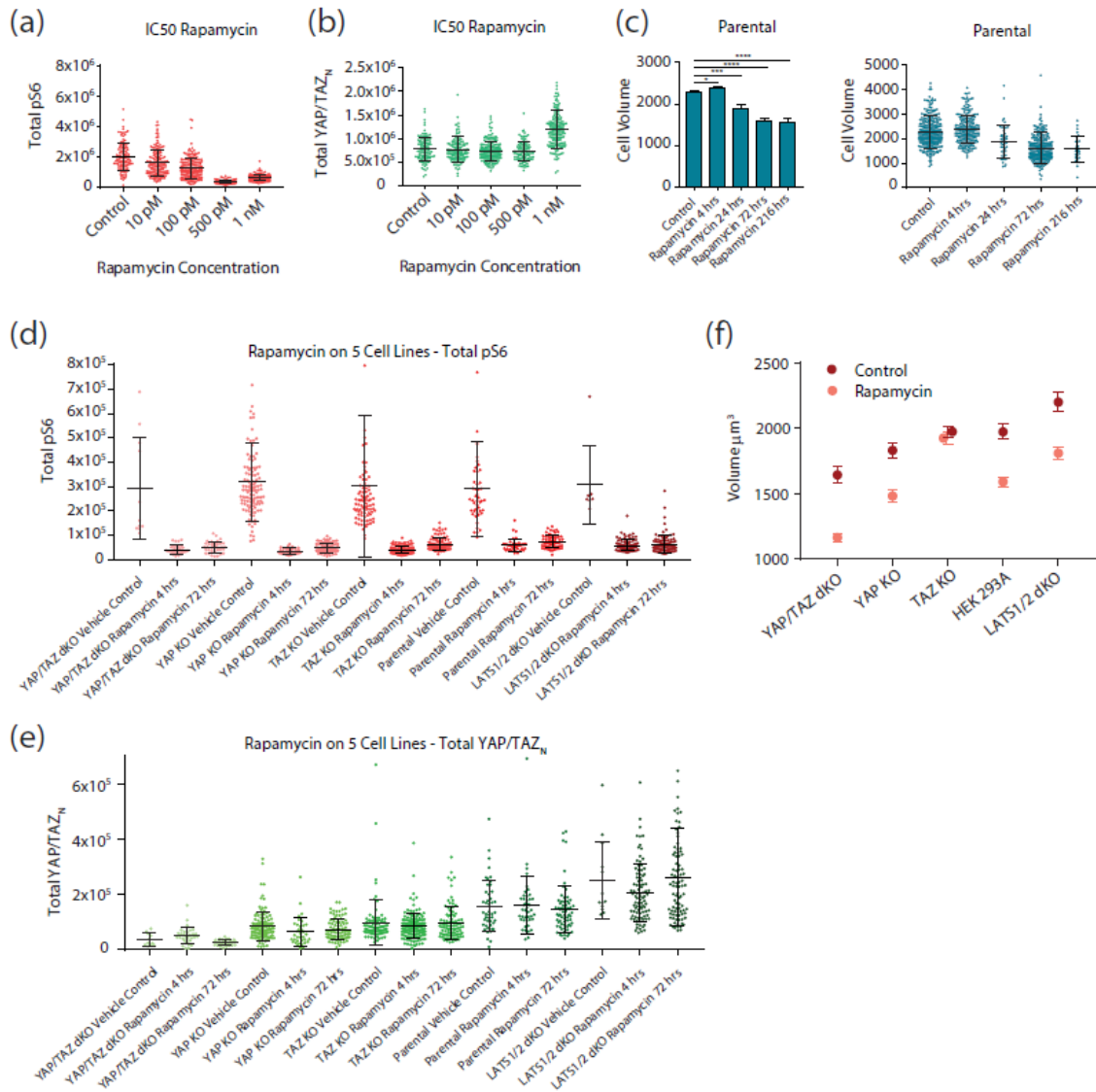
Figure S13 mTOR effect on cell volume (a) IC50 curve for rapamycin exposure on the parental cell line. mTOR activity as measured by total pS6 decreases as the concentration of rapamycin is increase ($N_{Control}$ =111, $N_{10 pM}$ =150, $N_{100 pM}$=198, $N_{500 pM}$=116, $N_{1 nM}$ =178). (b) IC50 curve for rapamycin exposure on the parental line. YAP/TAZ expression remains roughly constant through exposure to rapamycin. (c) Effect of rapamycin on cell volume at 4 hours, 24 hours, 72 hours and 216 hours. Left shows average statistics while left shows all data. ($N_{Control}$ =314, $N_{Rapamycin 4 hrs}$ =224, $N_{Rapamycin 24 hrs}$ =46, $N_{Rapamycin 72 hrs}$ =289, $N_{Rapamycin 216 hrs}$ =28). (d) Effect on mTOR activity by rapamycin for all 5 cell lines at 4 hrs and 72 hrs. ($N_{YAP/TAZ dKO Control}$ =11, $N_{YAP/TAZ dKO Rapa 4hrs}$ =33, $N_{YAP/TAZ dKO Rapa 72 hrs}$ =38, $N_{YAP KO Control}$ =117, $N_{YAP KO Rapa 4hrs}$ =36, $N_{YAP KO Rapa 72 hrs}$ =85, $N_{TAZ KO Control}$ =90, $N_{TAZ KO Rapa 4hrs}$ =157, $N_{TAZ KO Rapa 72 hrs}$ =93, $N_{Parental Control}$ =46, $N_{Parental Rapa 4hrs}$ =43, $N_{Parental Rapa 72 hrs}$ =68, $N_{LATS1/2 dKO Control}$ =7, $N_{LATS1/2 dKO Rapa 4hrs}$ =92, $N_{LATS1/2 dKO Rapa 72 hrs}$ =90). (e) YAP/TAZ expression in the 5 cell lines with rapamycin treatment. (f) Average volume of the five cell lines in the Hippo pathway (red) and average volume of the five cell lines with rapamycin treatment (pink).

	YAP/TAZ	YAP	TAZ	HEK 293A	LATS1/2
Vehicle Control Average Volume (DMSO)	1644 μm^3	1832 μm^3	1974 μm^3	1973 μm^3	2201 μm^3
Vehicle Control Standard deviation (DMSO)	64 μm^3	60 μm^3	43 μm^3	57 μm^3	73 μm^3
1nM Rapamycin Average Volume	1165 μm^3	1483 μm^3	1925 μm^3	1592 μm^3	1810 μm^3
1nM Rapamycin Standard deviation	29.96 μm^3	45 μm^3	47.25 μm^3	35.29 μm^3	49 μm^3

Table 3. Statistics of Cell Volume across the Hippo Pathway knockouts and its respective treatment with Rapamycin.
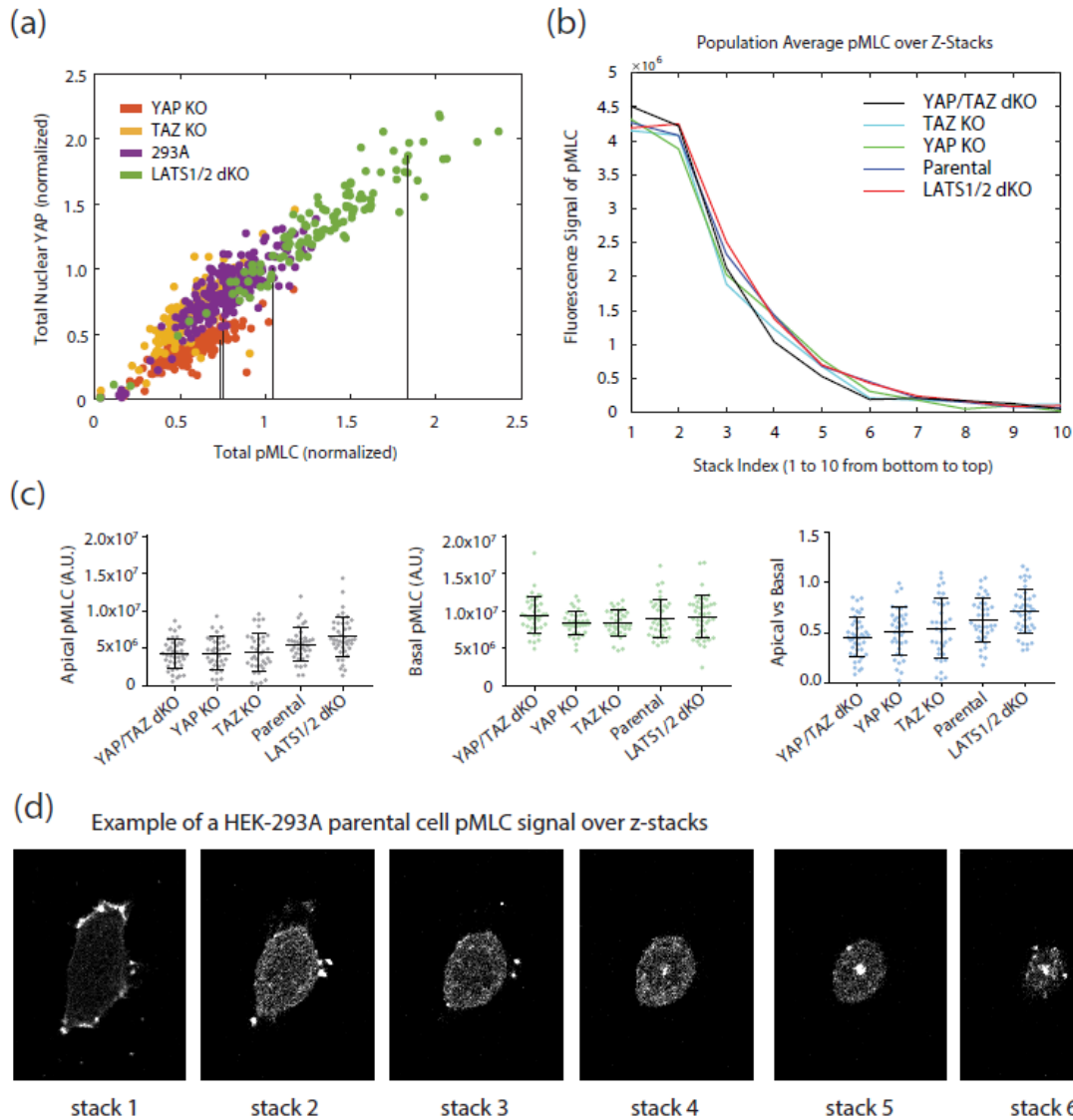
Figure S14 pMLC analysis on all Hippo pathway knockouts (a) Average pMLC expression across population of HEKs over 10 z-stacks. Each stack is 1 um interval. The bottom stack (stack #1) is manually chosen and focused to qualitatively match the maximum radius of the adherent surface of a cell. (b) Apical and basal pMLC expression across HEKs. The top-left panel shows the apical pMLC expression for the single cells of HEKS. The top-right panel shows the basal pMLC expression for the single cells of HEKs. The bottom panel shows the Apical/Basal ratio of pMLC expression for the single cells of HEKs. The bottom 2 stacks are counted as the basal stacks and the top 8 stacks are counted as apical stacks. The summation of the fluorescence signals of the corresponding stacks are counted as the expression of pMLC of apical or basal. ($N_{YAPTAZ\ dKO}$=40, $N_{YAP\ KO}$=36, $N_{TAZ\ KO}$=36, $N_{HEK\ 293A}$=37, $N_{LATS1/2\ dKO}$=43). (c) Example of the pMLC signal over different z-stacks. A HEK-293A parental cell was investigated and the pMLC confocal fluorescence images over 6 z-stacks from the bottom of this cell were shown.

References

1. Aifuwa, Ivie, et al. "Senescent stromal cells induce cancer cell migration via inhibition of RhoA/ROCK/myosin-based cell contractility." *Oncotarget* 6.31 (2015): 30516.

2. Amir, A. Cell Size Regulation in Bacteria. Phys. Rev. Lett. 112, 208102 (2014).

3. Bergert, Martin, et al. "Confocal reference free traction force microscopy." *Nature Communications* 7 (2016): 12814.

4. Bottier C, Gabella C, Vianay B, Buscemi L, Sbalzarini IF, Meiser J-J, Verkhovsky AB (2011). Dynamic measurement of the height and volume of migrating cells by a novel fluorescence microscopy technique. Lab Chip 11, 2855–3863.

5. Brooks RF, Shields R (1985). Cell Growth, cell division and cell size homeostasis in Swiss 3T3 cells. Exp Cell Res 156, 1-6.

6. Burke, C.W., Jung Soo Suk, Kim, A. J., Hsiang Y. J., Klibanov, A. L., Hanes, J., and Price, R. J. "Markedly enhanced skeletal muscle transfection achieved by the ultrasound-targeted delivery of non-viral gene nanocarriers with microbubbles." *Journal of controlled release* 162, no. 2 (2012): 414-421.

7. Cadart C, Zlotek-Zlotkiewicz E, Venkova L, Thouvenin O, Racine V, Le Berre M, Monnier S, Piel M (2017). Fluorescence eXclusion measurement of volume in live cells. Methods Cell Biol 139, 103–120.

8. Cadart, C., Monnier, S., Grilli, J., Sáez, P.J., Srivastava, N., Attia, R., Terriac, E., Baum, B., Cosentino-Lagomarsino, M. and Piel, M., 2018. Size control in mammalian cells involves modulation of both growth rate and cell cycle duration. *Nature communications*, *9*(1), p.3275.

9. Campos, M. et al. A Constant Size Extension Drives Bacterial Cell Size Homeostasis. Cell 159, 1433–1446 (2014).

10. Codelia VA, Sun G, Irvine KD (2014). Regulation of YAP by mechanical strain through Jnk and Hippo signaling. Curr Biol 24, 2012–2017.

11. Conlon, I., and Raff, M. (1999). Size control in animal development. Cell 96, 235–244.

12. Conlon, I. J., Dunn, G. A., Mudge, A. W. and Raff, M. C. (2001) "Extracellular control of cell size." *Nature cell biology* 3, no. 10: 918.

13. Conlon I, Raff M (2003). Differences in the way a mammalian cell and yeast cells coordinate cell growth and cell-cycle progression. J Biol 2, 7.

14. Cukierman, E., Pankov, R., Stevens, D.R. and Yamada, K.M., Taking cell-matrix adhesions to the third dimension. Science. 2001. 294.

15. Dannhauser, D., Rossi, D., Ripaldi, M., Netti, P.A., and Causa, F. "Single-cell screening of multiple biophysical properties in leukemia diagnosis from peripheral blood by pure light scattering." *Scientific reports* 7, no. 1 (2017): 12666.

16. Di Talia, S., Skotheim, J.M., Bean, J.M., Siggia, E.D., and Cross, F.R. (2007). The effects of molecular noise and size control on variability in the budding yeast cell cycle. Nature 448, 947–951.

17. Discher, D.E., Janmey, P. and Wang, Y.L., 2005. Tissue cells feel and respond to the stiffness of their substrate. *Science*, *310* (5751), pp.1139-1143.

18. Dong J, Feldmann G, Huang J, Wu S, Zhang N, Comerford SA, Gayyed MF, Anders RA, Maitra A, Pan D (2007). Elucidation of a universal size-control mechanism in Drosophila and mammals. Cell 130, 1120-1133.

19. Dolznig, H., Grebien, F., Sauer, T., Beug, H. & Müllner, E. W. Evidence for a size-sensing mechanism in animal cells. Nat. Cell Biol. 6, 899–905 (2004)

20. Dupont S, Morsut L, Aragona M, Enzo E, Giulitti S, Cordenonsi M, Zanconato F, Le Digabel J, Forcato M, Bicciato S, *et al.* (2011). Role of YAP/TAZ in mechanotransduction. Nature 474, 179–183.

21. Edgar, B.A. (2006). How flies get their size: genetics meets physiology. Nat. Rev. Genet. 7, 907–916.

22. Elliott H, Fischer RS, Myers KA, Desai RA, Gao L, Chen CS, Adelstein RS, Waterman CM, Danuser G (2015). Myosin II controls cellular branching morphogenesis and migration in three dimensions by minimizing cell surface curvature. Nat Cell Biol 17, 137–147.

23. Elosegui-Artola A, Oria R, Chen Y, Kosmalska A, Perez-Gonzalez C, Castro N, Zhu C, Trepat X, Roca-Cusachs P (2016). Mechanical regulation of a molecular clutch defines force transmission and transduction in response to matrix rigidity. Nat Cell Biol 18, 540–548.

24. Elosegui-Artola, A., Andreu, I., Beedle, A.E.M., Lezamiz, A., Uroz, M., Kosmalska,

A.J., Oria, R., Kechagia, J.Z., Rico-Lastres, P., Le Roux, A., Shanahan, C.M., Trepat, X., Navajas, D., Garcia-Manyes, S., Roca-Cusachs, P. Force Triggers YAP Nuclear Entry by Regulating Transport across Nuclear Pores. *Cell* **171**, 1397–1410.e1314 (2017).

25. Engler AJ, Sen S, Sweeney HL, Discher D (2006). Matrix elasticity directs stem cell lineage specification. Cell 126, 677-689.

26. Fantes, P. A. Control of cell size and cycle time in Schizosaccharomyces pombe. J. Cell. Sci. 24, 51–67 (1977).

27. Fernandez-Gonzalez R, Zallen JA (2009). Cell mechanics and feedback regulation of actomyosin networks. Sci Signal 2, pe78.

28. Fingar, D. C., Salama, S., Christina Tsou, E. D. Harlow, and John Blenis. "Mammalian cell size is controlled by mTOR and its downstream targets S6K1 and 4EBP1/eIF4E." *Genes & development* 16, no. 12 (2002): 1472-1487.

29. Fox TO, Pardee AB (1970). Animal cells: noncorrelation of length of G1 phase with size after mitosis. Science 167, 80-82.

30. Franklin, J.L., and Johnson, E.M. (1998). Control of neuronal size homeostasis by trophic factor-mediated coupling of protein degradation to protein synthesis. J. Cell Biol. 142, 1313–1324.

31. Geiger B, Spatz JP, Bershadsky AD (2009). Environmental sensing through focal adhesions. Nat Rev Mol Cell Biol 10, 21–23.

32. Ginzberg MB, Kafri R, and Kirschner M (2015). On being the right (cell) size. Science 348, 1245075.

33. Ginzberg, M. B. et al. Cell size sensing in animal cells coordinates anabolic growth rates and cell cycle progression to maintain cell size uniformity. eLife 7, pii: e26957 (2018).

34. Godin M, Delgado FF, Son S, Grover WH, Bryan AK, Tzur A, Jorgensen P, Payer K, Grossman AD, Krischner MW, Manalis SR (2010). Using buoyant mass to measure the growth of single cells. Nat Methods 7, 387-390.

35. Grewal, S.S., Li, L., Orian, A., Eisenman, R.N., and Edgar, B.A. (2005). Myc dependent regulation of ribosomal RNA synthesis during Drosophila development. Nat. Cell Biol. 7, 295–302.

36. Guo M, Pegoraro AF, Mao A, Zhou EH, Arany PR, Han Y, Mackintosh FC (2017). Cell volume change through water efflux impacts cell stiffness and stem cell fate. Proc Natl Acad Sci USA 113, E8618–E8627.

37. Gutierrez, Edgar, et al. "High refractive index silicone gels for simultaneous total internal reflection fluorescence and traction force microscopy of adherent cells." *PLoS One* 6.9 (2011): e23807.

38. Han SJ, Bielawski KS, Ting LH, Rodriguez ML, Sniadecki NJ (2012). Decoupling substrate stiffness, spread area, micropost density: a close spatial relationship between traction forces and focal adhesions. Biophys J 103, 640–648.

39. He L, Tao J, Maity D, Si F, Wu Y, Wu T, Sun SX (2018). Role of membrane- tension gated Ca flux in cell mechanosensation. J Cell Sci jcs-208470.

40. Hecht, V.C., Sullivan, L.B., Kimmerling, R.J., Kim, D.H., Hosios, A.M., Stockslager, M.A., Stevens, M.M., Kang, J.H., Wirtz, D., Vander Heiden, M.G. and Manalis, S.R. Biophysical changes reduce energetic demand in growth factor–deprived lymphocytes. *J Cell Biol*, (2016), *212*(4), pp.439-447.

41. Hola M, Riley PA (1987). The relative significance of growth rate and interdivision time in the size control of culture mammalian epithelial cells. J Cell Sci 88, 73-80.

42. Hurley J (1970). Sizing particles with a Coulter counter. Biophys J 10, 74–79.

43. Johnston GC, Pringle JR, Hartwell LH. 1977. Coordination of growth with cell division in the yeast Saccharomyces cerevisiae. Experimental Cell Research 105:79–98.

44. Kafri, Ran, Jason Levy, Miriam B. Ginzberg, Seungeun Oh, Galit Lahav, and Marc W. Kirschner. "Dynamics extracted from fixed cells reveal feedback linking cell growth to cell cycle." *Nature* 494, no. 7438 (2013): 480.

45. Killander D, Zetterberg A (1965a). Quantitative cytochemical studies on Interphase growth. I. Determination of dna, rna and mass content of age determined mouse fibroblasts in vitro and of intercellular variation in generation time.

46. Killander D, Zetterberg A (1965b). A quantitative cytochemical investigation of the relationship between cell mass and initiation of DNA synthesis in mouse fibroblasts in vitro. Exp Cell Res 40, 12-20.

47. Krokan H, Wist E, Krokan RH (1981). Aphidicolin inhibits DNA synthesis by DNA polymerase alpha and isolated nuclei by a similar mechanism. Nucleic Acids Res 9, 4709–4710.

48. Kozma, S.C., and Thomas, G. "Regulation of cell size in growth, development and human disease: PI3K, PKB and S6K." *Bioessays* 24, no. 1 (2002): 65-71.

49. Kwon, C.H., Zhu, X., Zhang, J., Knoop, L.L., Tharp, R., Smeyne, R.J., Eberhart, C.G., Burger, P.C., and Baker, S.J. (2001). Pten regulates neuronal soma size: a mouse model of Lhermitte-Duclos disease. Nat. Genet. 29, 404–411.

50. Laplante, M., and Sabatini, D.M. (2012). mTOR signaling in growth control and disease. Cell 149, 274–293.

51. Liu, S. et al. Size uniformity of animal cells is actively maintained by a p38 MAPK-dependent regulation of G1-length. eLife 7, e26947 (2018).

52. Lloyd AC (2013). The regulation of cell size. Cell 154, 1194-1205.

53. Low BC, Pan CQ, Shivashankar GV, Bershadsky A, Sudol M, Sheetz M (2014). YAP/TAZ as mechanosensors and mechanotransducers in regulating organ size and tumor growth. FEBS Lett 588, 2663–2670.

54. Meng, Z., Moroishi, T., Mottier-Pavie, V., Plouffe, S.W., Hansen, C. G., Hong, A. W., Park, H. W. et al. "MAP4K family kinases act in parallel to MST1/2 to activate LATS1/2 in the Hippo pathway." *Nature communications* 6 (2015): 8357.

55. Mittnacht, Sibylle, and Robert A. Weinberg. "G1/S phosphorylation of the retinoblastoma protein is associated with an altered affinity for the nuclear compartment." *Cell* 65.3 (1991): 381-393.

56. Montagne, J., Stewart, M.J., Stocker, H., Hafen, E., Kozma, S.C., and Thomas, G. 1999. Drosophila S6 kinase: A regulator of cell size. Science 285: 2126–2129.

57. Mohri, Z., Hernandez, A.D.R. and Krams, R., 2017. The emerging role of YAP/TAZ in mechanotransduction. *Journal of thoracic disease*, *9*(5), p.E507.

58. Nardella, C., Carracedo, A., Alimonti, A., Hobbs, R.M., Clohessy, J.G., Chen, Z., Egia, A., Fornari, A., Fiorentino, M., Loda, M., et al. (2009). Differential requirement of mTOR in postmitotic tissues and tumorigenesis. Sci. Signal. 2, ra2.

59. Neto-Silva, R.M., de Beco, S. and Johnston, L.A., 2010. Evidence for a growth-stabilizing regulatory feedback mechanism between Myc and Yorkie, the Drosophila homolog of Yap. *Developmental cell*, *19*(4), pp.507-520.

60. Nurse, P. and Thuriaux, P. (1977). Controls over the timing of DNA replication during the cell cycle of fission yeast. Exp. Cell Res. 107, 365-375i

61. Oldham, S. and Hafen, E., 2003. Insulin/IGF and target of rapamycin signaling: a TOR de force in growth control. *Trends in cell biology*, *13*(2), pp.79-85.

62. Pan, K. Z., Saunders, T. E., Flor-Parra, I., Howard, M. & Chang, F. Cortical regulation of cell size by a sizer cdr2p. eLife 2014, e02040 (2014).

63. Perez-Gonzalez, N., Tao, J., Rochman, N. D., Vig, D., Wirtz, D., & Sun, S. X. (2018). Cell Tension and Mechanical Regulation of Cell Volume. *Molecular biology of the cell*, mbc-E18.

64. Piccolo S, Dupont S, Cordenonsi M. (2014). The biology of YAP/TAZ: Hippo signaling and beyond. Physiol Rev 94, 1287–1312.

65. Plouffe, S.W., Lin, K.C., Moore, J.L., Tan, F.E., Ma, S., Ye, Z., Qiu, Y., Ren, B. and Guan, K.L., (2018). The Hippo pathway effector proteins YAP and TAZ have both distinct and overlapping functions in the cell. *Journal of Biological Chemistry*, pp.jbc-RA118.

66. Rehfeldt F, Brown AEX, Raab M, Cai S, Zajac AL, Zemel A, Discher DE (2012). Hyaluronic acid matrices show matrix stiffness in 2D and 3D dictates cytoskeletal order and myosin-II phosphorylation within stem cells. Integ Biol 4, 422–430.

67. Rochman, Nash D., Popescu, D.M., and Sun., S. X. "Ergodicity, hidden bias and the growth rate gain." Physical biology 15.3 (2018): 036006.

68. Sakaue-Sawano, A., Kurokawa, H., Morimura, T., Hanyu, A., Hama, H., Osawa, H., Kashiwagi, S., Fukami, K., Miyata, T., Miyoshi, H. and Imamura, T., 2008. Visualizing spatiotemporal dynamics of multicellular cell-cycle progression. *Cell*, *132*(3), pp.487-498.

69. Saucedo, L.J., and Edgar, B.A. (2002). Why size matters: altering cell size. Curr. Opin. Genet. Dev. 12, 565–571.

70. Saucedo LJ, Edgar BA (2007). Filling out the Hippo pathway. Nat Mol Cell Biol 8, 613, 253-262.

71. Savage, V. M., Allen, A. P., Brown, J. H., Gillooly, J. F., Herman, A. B., Woodruff, W. H., & West, G. B. (2007). Scaling of number, size, and metabolic rate of cells with body size in mammals. *Proceedings of the National Academy of Sciences*, *104*(11), 4718-4723.

72. Schmelzle T, Hall MN (2000). TOR, a central controller of cell growth. Cell 103, 253-262.

73. Schmidt, E. K., Clavarino, G., Ceppi, M., and Pierre, P. "SUnSET, a nonradioactive method to monitor protein synthesis." *Nature methods* 6, no. 4 (2009): 275.

74. Shen Z, Stanger BZ (2015). YAP regulates S-phase entry in endothelial cells. PLoS One 10, e0117522.

75. Smith Q, Stukalin E, Kusuma S, Gerecht S, Sun SX (2015). Stochasticity and spatial interaction govern stem cell differentiation dynamics. Sci Rep 5, 12617.

76. Smith, A.S., Nowak, R.B., Zhou, S., Giannetto, M., Gokhin, D.S., Papoin, J., Ghiran, I.C., Blanc, L., Wan, J. and Fowler, V.M., 2018. Myosin IIA interacts with the spectrin-actin membrane skeleton to control red blood cell membrane curvature and deformability. *Proceedings of the National Academy of Sciences*, p.201718285.

77. Soifer, I., Robert, L. & Amir, A. Single-cell analysis of growth in budding yeast and bacteria reveals a common size regulation strategy. Curr. Biol. 26, 356–361 (2016).

78. Son, S. et al. Direct observation of mammalian cell growth and size regulation. Nat. Methods 9, 910–2 (2012).

79. Son S, Kang JH, Oh S, Kirschner MW, Mitchison TJ, Manalis S (2015). Resonant microchannel volume and mass measurements show that suspended cells swell during mitosis. J Cell Biol 211, 757–763.

80. Son S, Tzur A, Weng Y, Jorgensen P, Kim J, Kirschner MW, Manalis SR (2012). Direct observation of mammalian cell growth and size regulation. Nat Methods 9, 910-912.

81. Stocker, H. and Hafen, E. 2000. Genetic control of cell size. Curr. Opin. Genet. Dev. 10: 529–535.

82. Stukalin EB, Aifuwa I, Kim JS, Wirtz D, Sun SX (2013). Age-dependent stochastic models for understanding population fluctuations in continuously cultured cells. J R Soc Interface 10, 20130325.

83. Style, Robert W., et al. "Traction force microscopy in physics and biology." *Soft matter* 10.23 (2014): 4047-4055.

84. Sun, H., Tu, X. and Baserga, R., 2006. A mechanism for cell size regulation by the insulin and insulin-like growth factor-I receptors. *Cancer research*, *66*(23), pp.11106-11109.

85. Sung Y, Tzur A, Oh S, Choi W, Li V, Dasari RR, Yaqoob Z, Kirschner MW (2013). Size homeostasis in adherent cells studied by synthetic phase microscopy. Proc Natl Acad Sci USA 110, 16687–16692.

86. Sveiczer, A., Novak, B. and Mitchison, J.M., 1996. The size control of fission yeast revisited. *Journal of cell science*, *109*(12), pp.2947-2957.

87. Tao J, Li Y, Vig DK, Sun SX (2017). Cell mechanics: a dialogue. Rep Prog Phys 80, 036601.

88. Tao J, Sun SX (2015). Active biochemical regulation of cell volume and a simple model of cell tension response. Biophys J 109, 1541–1550.

89. Tojkander S, Gateva G, Lappalainen P (2012). Actin stress fibers-assembly, dynamics and biological roles. J Cell Sci 125, 1855–1864.

90. Tzur A, Kafri R, LeBleu VS, Lahav G, Kirschner MW (2009). Cell growth and size homeostasis in proliferating animal cells. Science 325, 167–171.

91. Tumaneng, K., Russell, R.C., and Guan, K.L. (2012a). Organ size control by Hippo and TOR pathways. Curr. Biol. 22, R368–R379.

92. Tumaneng, K., Schlegelmilch, K., Russell, R.C., Yimlamai, D., Basnet, H., Mahadevan, N., Fitamant, J., Bardeesy, N., Camargo, F.D., and Guan, K.L. (2012b). YAP mediates crosstalk between the Hippo and PI(3)K–TOR pathways by suppressing PTEN via miR-29. Nat. Cell Biol. 14, 1322–1329.

93. Uroz M, Wistorf S, Serra-Picamal X, Conte V, Sales-Pardo M, Roca-Cusachs P, Guimera R, Trepat X (2018). Regulation of cell cycle progression by cell–cell and cell–matrix forces. Nat Cell Biol 20, 646.

94. Varsano G, Wang Y, Wu M (2017). Probing mammalian cell size homeostasis by channel-assisted cell shaping. Cell Rep 20, 397–410.

95. Wang M, Chai N, Sha B, Guo M, Zhuang J, Xu F, Li F (2018). The effect of substrate stiffness on cancer cell volume homeostasis. J Cell Physiol 233, 1414–1423.

96. Yen A, Fried J, Kitahara T, Stride A, Clarkson BD (1975). The kinetic significance of cell size, I. Variation of cell cycle parameters with size measured at mitosis. Exp Cell Res 95, 295-302.

97. Yu FX, Zhao B, Guan KL (2015). Hippo pathway in organ size control, tissue homeostasis and cancer. Cell 163, 811-828.

98. Zhao B, Tumaneng K, Guan KL (2011). The Hippo pathway in organ size control, tissue regeneration and stem cell self-renewal. Nat Cell Biol 13, 877-881.

99. Zhao B, Ye X, Yu J, Li L, Li W, Li S, Yu J, Lin JD, Wang CY, Chinnaiyan AM, *et al.* (2008). TEAD mediates YAP-dependent gene induction and growth control. Genes Dev 22, 1962–1971.

100. Zhao XH, Laschinger C, Arora P, Szaszi K, Kapus A, McCulloch CA (2007). Force activates smooth muscle a-actin promoter activity through the Rho signaling pathway. J Cell Sci 120, 1801–1809.

101. Zlotek-Zlotkiewicz E, Monnier S, Cappello G, Le Berre M, Piel M (2015). Optical volume and mass measurements show that mammalian cells swell during mitosis. J Cell Biol 211, 765–774.

Curriculum Vitae

Nicolas Andres Perez Gonzalez

Baltimore, USA

+1 (443) 326 7508 – nrperez@jhu.edu

EDUCATION

Johns Hopkins University	2018-2019
Ph.D. in Chemical and Biomolecular Engineering	(Baltimore, USA)
Pontificia Universidad Catolica de Chile	2013 – 2014
M.Sc. in Engineering	(Santiago, Chile)
Pontificia Universidad Catolica de Chile	2008 – 2012
B.S. in Physics	(Santiago, Chile)

WORK EXPERIENCE

University of Bern and Alveolix AG   June – September 2018
Developed a machine learning based software to improve quality control in manufacturing of organ-on-chip technologies

(Bern, Switzerland)

RESEARCH EXPERIENCE

Johns Hopkins University – Institute for Nanobiotechnology   August 2014 – February 2019
Research on Biophysics of Cancer – Wirtz lab / Sun lab   (Baltimore, USA)

Pontificia Universidad Catolica de Chile – Master's research   2012 – 2014
Computational Modeling on Cell Mechanics   (Santiago, Chile)

Pontificia Universidad Catolica de Chile   December 2010 – January 2011
Summer Research Assistant - Studies on Feynman Diagrams   (Santiago, Chile)

Pontificia Universidad Catolica de Chile   December 2011 – January 2012
Summer Research Assistant - CP violation in neutral heavy mesons   (Santiago, Chile)

LEADERSHIP

President Student's Center of Physics   October 2010 – October 2011
Pontificia Universidad Catolica de Chile   (Santiago, Chile)

Academic Advisor of Physics Faculty   October 2011 – October 2012
Pontificia Universidad Catolica de Chile   (Santiago, Chile)

CONFERENCES

INBT symposium – Advanced Biomanufacturing JHU	April 2018
Presenting work on the role of YAP/TAZ is cell volume regulation	(Baltimore, USA)
EMBO-ASCB	December 2017
Presenting work on the role of tension in cell volume regulation	(Philadelphia, USA)
EMBO Hippo signaling pathway	October 2017
Mechanical regulation of cell volume through the Hippo pathway	(Rome, Italy)
Genome Engineering	May 2017
CRISPR conference at Broad Institute	(Boston, USA)

AWARDS

Scholarship "Becas Chile"	2014 – 2018
Johns Hopkins University	(Baltimore, USA)
Fellowship awarded by Chile's government	
Scholarship "Technology Fellowship"	2016 – 2017
Johns Hopkins University	(Baltimore, USA)
Fellowship awarded to develop innovative material for engineering department at JHU	
Scholarship "Hijos de Profesionales de la educación"	March 2008 – June 2012
Pontificia Universidad Catolica de Chile	(Santiago, Chile)
Scholarship for students with parents in the field of education – Partial tuition	
Scholarship "Matricula de Honor"	2008 – 2010
Pontificia Universidad Catolica de Chile	(Santiago, Chile)
Scholarship for the student with the highest GPA in the physics class – 50% tuition	

ARTICLES

Modelling Toxoplasma gondii infection in a 3D cell culture system in vitro. J Danielson, N. Perez Gonzalez, J. Romano, I. Coppens

Dorsoventral polarity directs cell responses to migration track geometries. P. Mistriotis, E. Wisniewski, R.A. Law, K. Bera, Y. Li, S. Tuntithavornwat, N. Perez Gonzalez, A. Afthinos, R.A. Surcel, E.S. Schiffhauer, D.G. Thomas, D.N. Robinson, P. Kalab, S.X.Sun and K. Konstantopoulos. (In review at Nature Cell Biology)

Cell Tension and Mechanical Regulation of Cell Volume. N. Perez Gonzalez, J. Tao, N.D. Rochman, D. Vig, E.Y. Chiu, D. Wirtz, S.X. Sun. MBoC.

Going with the Flow: Water Flux and Cell Shape during Cytokinesis. Y. Li, L. He, N. Perez Gonzalez, J. Graham, C. Wolgemuth, D. Wirtz, S.X. Sun. Biophysical Journal 113(11), 2387-2495
Poroelastic model of the nucleus. N. Perez Gonzalez, D. Wirtz, D. Hurtado. (Submitted at Biophysical Journal)

SKILLS AND INTERESTS

Laboratory Techniques	Cell Culture, Immunofluorescence, PCR, Bacterial work, Transfection, Virus production, CRISPR-Cas9 knockout, western blot, microfabrication.
Computer languages	Python, Java, MATLAB, Latex
Programs	Maple, COMSOL, GNUPlot, Graphpad, Adobe Illustrator
Languages Native	Spanish speaker, Proficient English, Intermediate German